NRL Report 7105

# Instabilities Observed in Lower-E-Layer Alkali-Plasma-Cloud Releases and Their Implications Regarding Sporadic E

JOHN R. DAVIS

*Radar Techniques Branch*
*Radar Division*

July 28, 1970

NAVAL RESEARCH LABORATORY
Washington, D.C.

This document has been approved for public release and sale; its distribution is unlimited.

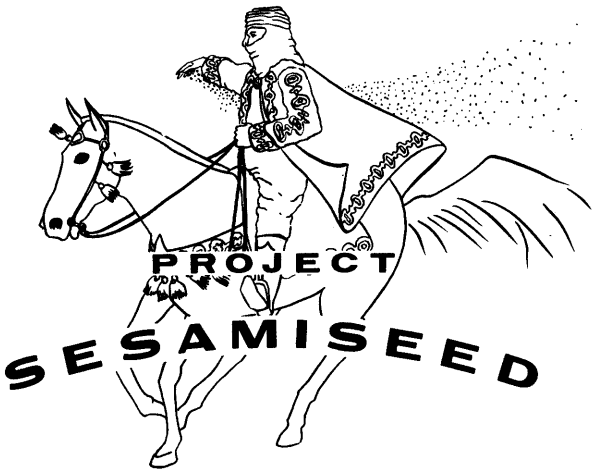
PROJECT
SESAMISEED

CONTENTS


Abstract iii
Problem Status iv
Authorization iv

PART I. INTRODUCTION AND DESCRIPTION OF THE EXPERIMENT 1

INTRODUCTION 1

Purpose of the Experiment 1
Organization of This Report 3

SPORADIC E: A HISTORICAL SKETCH OF RESEARCH DIRECTED TOWARD ITS EXPLANATION 4

Introduction 4
Certain Observed Characteristics of Sporadic E 4
Elementary Wind-Shear Theory of Sporadic E 5
Observations and Criticisms Relevant to the Elementary Wind-Shear Theory of Sporadic E 6
Refined Wind-Shear Theory of Sporadic E 7
Observations and Criticisms Relevant to the Refined Wind-Shear Theory of Sporadic E 8
Alternatives to the Wind-Shear Theory of Sporadic E 9

SOME CONSIDERATIONS OF CHEMISTRY 10

Normal E Layer 10
Metallic Ions and Sporadic E 12
Chemistry of an Explosive Cesium Release 13

PART II. RESULTS OF THE EXPERIMENT 15

EXPERIMENTAL DATA AND ANALYSIS 15

Introduction 15
Some General Features of the Data 17
Phase II: Ordered or Stable Diffusion 19
Phase III: Irregular Motion 21
Phase IV: Sporadic-E Formation 25

PLASMA CLOUD RADAR ECHO STATISTICS 32

Scattering Entity 32
Effects of Atmospheric Fluid Properties 33
Lognormal Statistics and an Analogy 34

PART III. PLASMA DIAGNOSTICS AND INTERPRETATION OF THE RESULTS 35

DYNAMICS OF THE MOTION AND A SURVEY OF POSSIBLE INSTABILITY MECHANISMS 35

Fluid Environment 35
Equations of Motion 37
Instability Mechanisms Related to the Thermodynamics of the Blast Wave 39
Instability Mechanisms Which Require Anisotropy in the Velocity Distribution 44
Instability Mechanisms Dependent Upon Plasma Inhomogeneity 46

APPLICATION OF THE $\mathbf{E} \times \mathbf{B}$ INSTABILITY 49

$\mathbf{E} \times \mathbf{B}$ Instability Applied to Phase III in Plasma Cloud Evolution 49
A Possible Interpretation of Phase IV Behavior in Terms of the Nonlinear $\mathbf{E} \times \mathbf{B}$ Instability, and Implications for Sporadic E 57

CONCLUSIONS AND RECOMMENDATIONS 61

Behavior of Plasma Clouds in the Lower E Layer 61
$\mathbf{E} \times \mathbf{B}$ Instability 61
Recommendations for Further Investigations 62

ACKNOWLEDGMENTS 63

REFERENCES 64

APPENDIX — Additional Plasma Cloud Data 72

## ABSTRACT

This report describes a study of gun- and rocket-emplaced alkali plasma clouds in the 85-105 km altitude region of the ionosphere. The object of the investigation is to study the small-scale (tens-of-meters), short-term (fractions-of-seconds) irregular motion of the magnetofluid in the lower E layer. Motions on this spatial and temporal scale are known to be responsible for radiofrequency scattering at E-layer heights, and it has been suspected that they are important in the appearance and evolution of the sporadic-E layer. The resolution which is necessary to discern motions on the scale indicated was afforded by decameter- and meter-wavelength coherent-pulse-doppler radar.

As it is the object of this report to associate the results of the investigation with sporadic E (and, indeed, to postulate an alternative to the popular, but deficient, wind-shear theory of sporadic E), an effort is made to describe the origins, evolution, successes, and failures of this theory. It is found that the wind-shear theory is capable of explaining the transport of metallic ions from high in the E layer down to the 90-110 km region where sporadic E most frequently is found, but is not capable of explaining the mechanism by which sporadic-E layers are formed in this altitude interval. A description of lower-E-layer chemistry and the thermochemistry of an alkali plasma cloud is also presented.

A description of a plasma cloud's evolution, drawn from experimental data, indicates that four phases of development ensue:

1. Phase I is a blast-wave expansion phase in which the plasma cloud is formed as an ellipsoidal bubble, oriented along the geomagnetic field, which expands rapidly to a radius of several hundred meters.

2. Phase II is a period termed ordered diffusion in which the plasma cloud retains a regular shape, and hence appears to the radar as a single scatterer.

3. Phase III is a period termed irregular motion in which spectrally discrete echoes from seemingly coherent, short-lived, scattering entities appear sporadically, superimposed upon the otherwise diffuse plasma cloud radar echo. (The large apparent size and spectral discreteness of the echoes indicate that they represent collective scattering from a wave-like density structure, hence the term coherent, encompassing nominally the entire plasma cloud.)

4. Phase IV is a period in which, in some cases, the plasma cloud is formed into a sporadic-E-like reflecting layer (this phase is characterized by undulations in spectral dispersion and signal amplitude with a period of tens to hundreds of seconds, corresponding to motion which is symmetric relative to the geomagnetic field direction).

A survey of possible instability mechanisms which can explain the spatial and temporal scales of the irregular motion observed in Phase III of plasma cloud evolution leads to the conclusion that a dissipative instability involving crossed electric and magnetic fields in the presence of a properly oriented plasma density gradient is the most likely candidate. It is found that the observed tens-of-meters instability wavelengths and tenths-of-seconds growth times are predicted by this

mechanism, and curves of these parameters are presented for various altitudes, electrostatic field intensities, and wavelengths. A more sophisticated, two-dimensional, nonlinear instability analysis predicts a cyclic growth-and-decay process for the instability in the lower E layer and is in remarkable agreement with the Phase IV plasma cloud behavior. This circumstance is interpreted as strong evidence that the instability is instrumental in the formation of temperate-latitude nonblanketing sporadic E.

## PROBLEM STATUS

This is an interim report on one phase of a continuing problem. Work is proceeding on this phase and on other allied subjects.

## AUTHORIZATION

NRL Problem R02-23.501
Project FB 2835-70-X-0014

Manuscript submitted March 23, 1970.

# INSTABILITIES OBSERVED IN LOWER-E-LAYER ALKALI-PLASMA-CLOUD RELEASES AND THEIR IMPLICATIONS REGARDING SPORADIC E

## PART I. INTRODUCTION AND DESCRIPTION OF THE EXPERIMENT

### INTRODUCTION

#### Purpose of the Experiment

The presence of the sporadic-E layer has been a source of frustration to radio communicators since the advent of high-frequency skywave communications networks. The adjective *sporadic* refers to the pattern of behavior which distinguishes sporadic E: sudden and unpredictable appearance, unpredictable duration, and equally unpredictable, and sudden, disappearance. Its morphology is at least partially understood. Sporadic E appears as layers of intense ionization, often with plasma frequencies as high as 10 MHz, at altitudes from 90 to 140 km. These layers normally are quite thin, with a width of a few kilometers in the vertical dimension. They may be extensive in horizontal dimensions, covering many thousands of square kilometers (termed "blanketing"), or may be patchy, consisting of several layerlets of much smaller dimensions (termed "diffuse").

Sporadic E occurs in the lowest portion of what is traditionally considered to be the ionosphere. (The D layer, which falls between 60 and 90 km, is of importance primarily for kilometer-wavelength radiowaves and was discovered more recently.) It was first associated with blanketing of skywave communications when it appeared, with no apparent cause, on ionosonde records used by communicators to evaluate their transmission paths. These records simply display the time which elapses between the transmission of a pulsed high-frequency (decameter-wavelength) radio wave and its reception after being reflected from an ionospheric layer. Sporadic E manifests itself on these records as intense reflections, from altitudes of 90 to 140 km, which often extend to such a high radio frequency that no energy is able to penetrate to the 200 to 400-km region which normally is used for skywave communications.

The effects which sporadic E can have upon communications can be devastating or beneficial. Its blanketing effects can restrict shortwave broadcasts, which normally serve large geographical regions at ranges of 2000 to 4000 mi, to effective maximum ranges of a few hundred miles. Due to its highly intense character, however, sporadic E can also be used to provide meter-wave communications (which normally are ineffective for skywave propagation because meter wavelengths are not reflected by the normal ionospheric layers) over short skywave distances of a few hundred miles. This service is unreliable, however, due to the unpredictable nature of sporadic E.

Research in sporadic E has yielded the result that this layer is most likely composed of metallic ions of meteoric origin, which are transported by some means to regions which are favorable for their concentration into the pancake-like features which constitute sporadic E. Three types of theories compete for prominence as the mechanism

---

Note: This report is substantially the same as the Ph.D. dissertation submitted in May 1970 by the author to the Department of Physics, The Catholic University of America, Washington, D.C.

by which these layers are formed: (a) the wind-shear theory in which there is invoked a neutral-wind-associated plasma transport governed by the geomagnetic field; (b) fluid turbulence theories in which hydrodynamic forces, which operate only in certain conditions in a shear flow, are invoked; and (c) plasma instability theories in which magnetohydrodynamic forces, which depend both on the geomagnetic field and on the electrostatic field in the lower ionosphere, are invoked. Each of these theories has achieved some success, although only the wind-shear theory has received detailed theoretical and experimental attention. As will be shown below, this theory is capable of explaining the transport of metallic ions from high in the E layer (140 to 160 km) to the 110 to 120 km region. It is not capable of explaining the formation of sporadic E in the 90 to 110 km region where most persistent sporadic E is found. This investigation is directed toward this most important lower altitude extreme.

It is the object of this report to describe the results of an experiment which demonstrates that plasma instabilities do occur in the E layer, to present a theoretical analysis of a plasma instability which can explain the experimental results, and to associate these findings with evidence that this plasma instability is instrumental in the formation of sporadic E. The experiment involves the use of alkali plasma clouds emplaced in the lower E layer to study the magnetofluid motions which are of importance for the formation of temperate-latitude sporadic E. The experimental tools are (a) a 7-in. extended barrel gun, developed and operated by the U.S. Army Ballistic Research Laboratory, which is capable of launching 2-kg payloads to altitudes as high as 100 km (1); (b) Nike-Cajun rockets which are capable of conveying 18-kg payloads to altitudes above 100 km; and (c) high-power, coherent-pulse-doppler, decameter- and meter-wavelength radars which are used for observation of the plasma clouds.

The concept upon which this investigation is based is derived from the circumstance that the behavior of an irregularly flowing fluid is described by its velocity spectrum. Inasmuch as the lower E layer is known to exhibit highly irregular behavior, and its most important feature is the motion of its charged constituents (i.e., its ions and electrons), an attractive investigation is one in which the velocity spectrum displayed by the motion of these charged constituents is measured. In the investigation described here, this purpose is served by using decameter- and meter-wavelength radar to observe the velocity spectrum of internal motions in highly ionized cesium "seed" or "tracer" clouds emplaced in the 85-105 km altitude region.

Other chemical-release programs are directed at somewhat different purposes. Project Firefly (2-15), which is the direct ancestor of this investigation, was conceived as an effort to study the physics and chemistry of charged and uncharged gas molecules liberated explosively in the upper atmosphere, including blast-wave, turbulent diffusion, chemical consumption, and radiofrequency reflection effects. However, the instrumentation which was available in the late 1950's and early 1960's was incapable of resolving small-scale internal motions of the plasma cloud, and very little information on physical processes at spatial scales of less than a few hundred meters, and temporal scales of less than several seconds, was acquired. Project Firefly was of great value for studying neutral-gas blast-wave behavior (13), for assessing the degree of thermal and subsequent solar ionization of the release products (5,7), and for obtaining initial information regarding plasma cloud persistence (10,11). The optical data were excellent for studying those motions in the neutral atmosphere associated with hundreds-of-meters spatial scale and tens-of-seconds temporal scale (14). The radiofrequency instrumentation showed gross agreement with the optical results regarding cloud size and movement and suggested that the charged constituents were indeed influenced by the magnetic field, and hence expanded anisotropically (10,11).

Most subsequent chemical release programs in the lower E layer have been directed at investigating the neutral winds and their correlation with sporadic E* and have continued to concentrate on the hundreds-of-meters, and larger, scale of E-layer motions. The investigation reported here differs from its predecessors principally in that the advanced decameter-wavelength radar which has been used as the primary instrumentation is capable of resolving motions of tens-of-meters scale structure in the plasma clouds at speeds of a few meters per second and less.

## Organization of This Report

Part I of this report is of an introductory nature. The "Introduction," which ends with this section, seeks only to establish the barest foundation for the work to be reported in subsequent sections and to indicate the order in which each topic of discussion appears. This action is taken because, by virtue of the phenomenologically complex nature of the lower E layer and sporadic E, it is believed that the introduction of each of the several topics to be treated should be deferred until that topic is discussed in detail. The next section on "Sporadic E . . ." is a description of both the theoretical and experimental research regarding sporadic E, most of which has been concentrated in the last decade. The description is undertaken in a chronological manner, with a stress upon (a) the particular observed characteristics of sporadic E which exhibit temporal and spatial scales comparable to those studied in this investigation, (b) the development and refinement of theories of sporadic-E formation which seek to explain these, and larger, scale characteristics, and (c) the deficiencies of these theories and the aspects of sporadic E which require further explanation. The section titled "Some Considerations of Chemistry" is a description of the chemistry of the undisturbed E layer and of sporadic E, together with an explanation of the thermochemistry of an explosively injected cesium plasma cloud in the lower E layer. This latter section is intended to establish the validity for interpreting the results of this investigation in terms of normal-E-layer processes.

Part II contains a description of the experimental data and their interpretation. The section on "Experimental Data and Analysis" is arranged so as to incorporate a presentation of examples of the experimental data in various stages of plasma cloud evolution into a phenomenological model of plasma cloud behavior. The section on "Plasma Cloud Radar Echo Statistics" presents a discussion of certain statistical properties of the radar data which are of importance for their interpretation in terms of collective behavior in the plasma cloud.

Part III contains a diagnosis of the instability mechanisms which are possible in the plasma cloud and an analytical application of the most attractive candidate mechanism to the conditions under which the experiment is conducted. The section titled "Dynamics of the Motion . . ." contains a description of this environment, a development of the equations of motion, and a survey of instability mechanisms which are possible in each phase of plasma cloud evolution. The next section on "Application of the $\mathbf{E} \times \mathbf{B}$ Instability" contains a development of the dispersion relation for the selected instability mechanism, and also the results of several numerical computations of growth rates and wavelengths appropriate to the altitude interval between 85 and 110 km. These results are compared with the decameter radar data. It is concluded, on the basis of the favorable comparison between theory and observations, that the selected instability mechanism is responsible for the behavior of cesium plasma clouds. A possible explanation of sporadic-E formation in terms of this instability is presented. The last section of Part III contains conclusions which may be drawn from this investigation and recommendations for future study.

*The next section on "Sporadic E . . ." and Refs. 16-68 describe these programs.

## SPORADIC E: A HISTORICAL SKETCH OF RESEARCH DIRECTED TOWARD ITS EXPLANATION

### Introduction

It is the purpose of this section to describe only one particular type of sporadic E and, indeed, to consider only those aspects of this type which bear upon the investigation at hand.

It has been recognized since Stewart's (16) studies in the nineteenth century that intense currents flow in the earth's upper atmosphere. The aptly-named dynamo region in which these currents flow is the altitude region around 100 km in which sporadic E appears, and sporadic E has been historically associated with the dynamo currents. The intense, somewhat predictable, equatorial- and auroral-zone sporadic E have been associated with charged particle fluxes and the dynamo current, and they no longer represent a scientific challenge. Midlatitude sporadic E has not been satisfactorily explained despite some ten years of concentrated effort, and it is this type (which can be further subdivided into blanketing and nonblanketing, or diffuse, species) which is the object of this investigation.

Since the late 1950's, theoretical and experimental research into midlatitude sporadic E has centered on attempts to evaluate and refine a theory of sporadic-E behavior in which neutral-gas winds act as a driving force for ions and, in conjunction with the geomagnetic field, force them, and the free electrons tied to them by space charge, to converge into high-charge-density layers. This theory is designated as the wind-shear theory of sporadic E. It has evolved through a series of theoretical developments and experimental tests into a highly refined chemical-hydrodynamic-electromagnetic model. In the following sections there appears a historical description of this theory, together with examples of its successes and failures (of which many of the latter stand unresolved), and a description of competing theories.

### Certain Observed Characteristics of Sporadic E

Sporadic E displays certain characteristics of importance for this investigation which are not unique to a specific model or theory of behavior. These characteristics will now be delineated to provide a background knowledge.

Rocket-carried magnetometers have confirmed the expectation that, even at midlatitudes, a substantial sheet current flows in the lower E layer. Typical data indicate that the total magnetic induction changes by as much as 20 gammas within a narrow layer between 105 and 120 km altitude, and normally no more than about 6 to 10 km thick (17,18). This result is consistent with the expected dynamo current intensity.

Rocket-carried Langmuir probes have found that charged particle densities within this region display a spatial fine structure, with a characteristic thickness of some tens to hundreds of meters, in which finger-like charge-density lamina are bounded by steep gradients and are clustered irregularly in layers of a few kilometers thickness (19,20). These layers nearly always are found to occur very near an altitude of 100 km with such regularity that one author (19) speculates that a characteristic peculiar to that height is responsible for triggering an "avalanche" process of electron production. These rocket flights indicate a tendency for sporadic-E layers, or lamina of relatively high charge density which may not be dense enough to be called sporadic-E layers, to appear in pairs with a separation of 5 to 10 km. They also confirm that substantial E-layer ionization persists after sunset, when the cessation of photoionization by direct sunlight would suggest a rapid disappearance of the predominant daytime ion species.

Decameter-wavelength radar backscatter from sporadic E indicates that field-aligned irregularities are common (21), and a theory of sporadic-E scattering by turbulent irregularities, developed by Booker (22,23) before the advent of the wind-shear theory, is consistent with these data if the scattering irregularities are considered to have a characteristic scale of 80 to 570 m. Tao (24) developed a similar theory, in which the turbulence might be a result of high shearing winds, and found that irregularities of 50 m on a vertical scale should be common. Thus far, then, the rocket and radiowave measurements of charge-density fine structure are consistent with a theory of scattering from turbulent irregularities. However, Austin and Manson (25) in some recent radio-frequency partial-reflection experiments found that irregularities of tens of meters at an altitude of 90 km can best be explained by scattering from a limited number of discrete irregularities. These discrete scatterers are supposed to be sharply bounded, with a change in electron density of 10% to 40% in a few tens of meters at the boundary, and to be horizontally stratified.

In summary, measurements of charge-density fine structure and sporadic E in the dynamo region indicate that scale sizes of tens of meters are common. Although a theory of turbulent continuum scattering can be fit to some data, more recent results indicate that this scattering results from a limited number of discrete horizontally stratified irregularities. This circumstance is of concern here because (as will be explained more thoroughly below) certain failures of the wind-shear theory make an alternative theory based on some form of neutral or magnetohydrodynamic turbulence attractive. Some workers dispute even that turbulent flow can occur in the dynamo region, except under very rare and extreme conditions of wind-shear; this matter also will be treated below.

## Elementary Wind-Shear Theory of Sporadic E

The wind-shear theory has undergone a decade of development. It began with a primitive argument by Dungey (26) in which he pointed out that since charged particle motion is affected by a magnetic field, then an effect of a wind in the neutral gas blowing obliquely across the geomagnetic field would be to drive the charged constituents along the direction of the magnetic field at a speed in proportion to the component of the wind velocity which is parallel to the field. Dungey concluded that north-south wind shears can produce layers of enhanced electron density at an altitude of about 110 km with enhancements of 5% over the undisturbed density.

The elementary wind-shear theory of sporadic E actually originated with Whitehead (27) and Axford (28) who pointed out that due to the high ion-neutral collision frequency (three to twenty times the ion gyrofrequency in the lower E region), it is actually the component of neutral wind *transverse* to the geomagnetic field (i.e., east-west rather than north-south) which is of importance in causing the ion convergence mechanism. In a region where the electron-neutral collision frequency is much lower than the electron gyrofrequency, while the ions enjoy the opposite circumstance, a neutral wind blowing across the magnetic field forces the ions to move with it, but leaves the electrons tied to the field lines. The ion motion constitutes a current perpendicular to the magnetic field, which is then subject to a $\mathbf{j} \times \mathbf{B}$ force perpendicular to both the magnetic field and the neutral wind. For an east-west wind moving ions through the geomagnetic field, the ions are forced in a vertical direction, form a space-charge field, and draw the electrons along the magnetic field obliquely with the ions. A shearing wind can create a charge-density layer by this means.

Whitehead and Axford treated a horizontal east-west wind profile in which the wind vector changed from east-directed to west-directed with altitude in a sinusoidal profile.* Vertical winds were ignored, and currents in all directions were prohibited. Only a single, positively charged, ionic species was allowed. Production and loss of ion-electron pairs were ignored. The result of the elementary wind-shear theory was that ion convergence due to east-west wind shear would lead to an enhancement of electron density at a point near the wind-shear null where the shear is at its highest value. An electron-density enhancement by a factor of ten or more above the ambient density would be permitted in layers which typically would have gradually sloped boundaries. The electron density in regions immediately adjacent to the enhanced layers would be depleted.

A second feature of the elementary theory, and possibly its most successful one, was the recognition by its proponents that the type of wind profile required for sporadic-E formation would be common in the upper atmosphere due to the internal gravity wave influence described by Hines (29), and that the behavior of this type of profile would be expected to have a pronounced influence on the formation and vertical motion of sporadic-E layers. Axford (30) noted that motion of the neutral wind profile in a downward direction would result from the gravity wave influence, and that ionization thus should be expected to move gradually downward, in layers, to a lower limit estimated to be at about 110 km. He noted also that standing waves can occur in the gravity wave spectrum, and that sporadic-E layers would under these conditions remain stationary.

## Observations and Criticisms Relevant to the Elementary Wind-Shear Theory of Sporadic E

Rocket-emitted chemiluminescent trail releases immediately verified one aspect vital to the elementary wind-shear theory: the neutral-wind velocity profile above about 105 km altitude displays an oscillatory behavior, with a two to four scale-height wavelength, and a downward phase velocity of about one wavelength per 12 hr (31-34). The behavior below 105 km is less regular.

Most other measurements yielded mixed or contrary results. An attempt by Heisler and Whitehead (35) to associate certain characteristic parameters of sporadic E with tilts in the reflecting layers, and then to associate these tilts with the horizontal component of the geomagnetic field, met with some success. However, this result is two steps removed from demonstrating the association of wind shear with sporadic E (and, indeed, it would tend to corroborate any theory of sporadic E which would give rise to a layer tilted upward at its leading edge). Other workers (36,37) used a direct comparison of the probability of sporadic E occurrence with the horizontal component of the earth's magnetic field and found that there is a correlation favorable to the elementary wind-shear theory, on the average, for only 7 hr each day. Indeed, these workers found that some indicators showed no systematic relationship at all to the magnetic field.

Several combined observations of wind shear (using chemical trails deposited by rockets) and sporadic E (using ionosondes and Langmuir probes) gave mixed, but partially confirmatory, results (38,39). In most of these cases, as well as in a few others (19,40), the wind profiles displayed properly oriented wind-shear nulls and sporadic E within a few kilometers of these points, but almost invariably above an altitude of 110 km. In most cases the sporadic E was found to form at an altitude of 120 to 140 km, and then to descend at the same rate of descent as the wind profiles to an altitude between 110 and 120 km. At that altitude, all correlation between wind profile and sporadic-E-layer

*Whitehead's treatment suffered from a sign error which resulted in an oppositely directed shear being required for ion convergence, but his results are otherwise correct.

height disappeared, although the sporadic-E layers themselves often remained for several hours longer. In many of these cases, sporadic-E layers appeared in the 90-100 km region which were either randomly placed relative to the wind profile, or which appeared at points of nominally unfavorable shear direction (19,41-44). Consistent with these indications, some wind measurements indicated that the east-west wind component obeys the gravity-wave-associated oscillatory altitude dependence and downward motion only above about 120 km (43,45).

Finally, there are some examples of measurements which yield precisely the contrary result from those cited above. Bowen et al. (46) and Murphy et al. (47) report observations in which the predominance of data *above* 110 km showed sporadic-E layers at shearing nulls of the nominally unfavorable sense, and data *below* 100 km showed sporadic-E layers in nominally favored positions.

In summary, there seems to be a slight weight of evidence to indicate that sporadic E can often be associated with properly oriented shearing nulls at altitudes above 110 to 120 km, and that when these conditions exist, the layers of enhanced ionization move downward with the wind profile to an altitude of about 110 km. There are exceptions to this behavior. In some cases, sporadic E forms at a nominally unfavored altitude, and in some cases its motion is not systematically downward (43). Below 110 km, where most sporadic E is found, there seems to be no discernible association with wind profile. It can be concluded, however, that the bare fact that ionization normally is driven downward, in layers, from higher in the E layer is indicative of the means by which a continuing supply of ionization is transported to the 90-110 km altitude region. The means by which it is formed into layers is not yet understood.

Layzer (48) formulated a generalization of the elementary wind-shear theory in which he pointed out several characteristics of observed sporadic E which were at variance with those permitted by theory. In particular, Layzer noted that (a) the elementary theory predicted layers of variable thickness, with thickness inversely proportional to the square of maximum density, and (b) the elementary theory predicted that electron density would be reduced in the region immediately adjacent to the layer. Observations indicated that sporadic E layers are nearly always of a kilometer or so thickness, with a wide variation in peak electron density, and are not surrounded by a depleted region. Layzer also took note of the fact that the elementary theory requires sporadic-E layers to form at points of high shear, which is contradicted by some observations, and that the elementary theory permits a smaller fractional enhancement of electron density in a layer than is commonly observed.

Layzer also took theoretical umbrage at inadequacies in certain of the assumptions upon which the elementary theory was based, notably the failure to include possible vertically varying, horizontal, electric polarization fields. (This point, together with the additional uncertainty introduced by vertical motion of the entire wind profile, would make it difficult to predict exactly where the sporadic-E layer should appear relative to the wind profile, and hence complicates what previously had been thought to be a readily verifiable theory.)

## Refined Wind-Shear Theory of Sporadic E

Over the few years following Layzer's provocative critique of the elementary theory, a great deal of further development took place. In particular, a two-ion theory, in which a mixture of long-lived and short-lived ions was considered to be present in the E layer, permitted the peak achievable electron density to be greatly increased (49-51). The theory also answered Layzer's criticism regarding the predicted depletion of regions adjacent to sporadic-E layers, in that the rapidly recombining (and, presumably, rapidly

photoionizing) species would keep these regions supplied while the long-lived ions were transported toward the regions of high convergence. During their growth phase, layers predicted from the two-ion theory would display a flat-topped electron density distribution with altitude, and hence would not be subject to the elementary theory's rule of thickness inversely proportional to maximum density. The sharply bounded character of observed sporadic-E layers was allowed in the refined theory by permitting the electron temperature in the boundaries to be elevated over ambient temperature by several tens of degrees Kelvin (52-54). This elevation in temperature would arise from electron drift in an electrostatic field parallel to the geomagnetic field. If the effective recombination coefficient varied in inverse proportion to electron temperature, it would be decreased in the layer boundaries, and the electron density thus would be increased. The effect of this increase in electron density in the layer boundaries would be a steepened density gradient.

Further refinements stressed that the effects of electrostatic fields and vertical winds in the ambient medium, together with the superposition of steady horizontal wind components upon the wind-shear profile, would all tend to displace the predicted position of sporadic-E layer formation from the position of maximum favorable shear (55,56). MacLeod (57) presented many characteristics of the refined theory in extensive detail and illustrated his argument with several experimental observations. In MacLeod's data, the "successfully-predicted" sporadic-E layers fell within 2 km of the point of maximum east-west shear, and hence these examples demonstrated that the influences which would tend to displace the ion convergence maxima from this point were ineffective. (It is amusing to note that while the proponents of the wind-shear theory accept the appearance of sporadic E at or near the wind-shear maximum as evidence for their theory, they also discard contrary evidence by stating that many possible unmeasured influences can explain displacement from this position.) MacLeod conceded that it is not possible to assert conclusively at present whether the refined wind-shear theory properly describes the mechanism by which sporadic E is actually formed; he simply stated that this mechanism is *capable* of forming such layers.

## Observations and Criticisms Relevant to the Refined Wind-Shear Theory of Sporadic E

Rocketborne mass spectrometers confirmed that sporadic-E layers can be composed of long-lived metallic ions, and hence validated the two-ion refinement to the wind-shear theory.*

Measurements of electron temperature in the E layer have also been carried out by rocket instrumentation, and their results are perhaps more mystifying than illuminating. Daytime electron temperatures at altitudes between 90 and 120 km have been found to be about three times the value predicted by the neutral-gas model, whereas analytical considerations indicate that they should be very nearly the same as the neutral-gas temperature (58). Electron temperatures measured in sporadic-E layers have been found to be greater than the neutral-gas temperature as well, but there is no consistent evidence for either an overall elevation of the electron temperature in sporadic E relative to the ambient electron temperature, or for a depression of the midlayer electron temperature below that in the boundaries. Examples exist which tend both to confirm and to negate the former (59).

*A description of the chemical composition of sporadic E is presented in the section titled "Some Considerations of Chemistry" which contains references to the mass-spectrometer experiments.

A recent series of rocket measurements has provided what is probably the strongest evidence against all current versions of the wind-shear theory. Dorling et al. (60) have measured positive ion density and horizontal wind profiles through sporadic-E layers and have found a layer at 108-km altitude which was located very near the *unfavored* wind-shear maximum for ion convergence. Ionosonde data have confirmed the location of a sporadic-E layer at that altitude. This result is of importance because it argues against the possibility that the wind-shear mechanism is effective in creating sporadic E above 100 km. (It has already been concluded that wind-shear is ineffective below this level.)

## Alternatives to the Wind-Shear Theory of Sporadic E

A brief reference has been made above to theories of scattering by turbulent irregularities in sporadic E. Some experimental evidence exists which tends to confirm these theories, and hence to suggest a role for turbulence in the formation of sporadic E. Evidence to the contrary also exists but does not dispute the important circumstance for this investigation that some type of irregular structure (turbulent or otherwise) with characteristic scale sizes of tens to hundreds of meters does indeed exist in the E layer.

As will be discussed in the section titled "Plasma Cloud Radar Echo Statistics" in Part II below, in connection with an interpretation of the radar echo statistics of the cesium plasma cloud data gathered in this investigation, there is a large body of experimental evidence which indicates that irregularity scales of tens to hundreds of meters in the lower E region are characteristic of an inertial turbulent regime of fluid motion in the E layer. Because motions of the neutral gas are of importance in this region, the effect upon charged constituents of any such turbulence must be considered in the formation of sporadic E. An obvious possibility is that eddy currents in the ionic components, caused by neutral-fluid vortex motion, may create space-charge electric fields of small scale which can give rise to drift motions and, possibly, to plasma instabilities.

Some workers dispute even the possibility that turbulence exists in the E region, except for extremely rare conditions of exceptionally high shearing winds (61,62).

A criterion may be determined for establishing the stability of plane parallel fluid flow against shear-dependent turbulence. A Richardson number is defined by

$$R_i = \frac{\frac{g}{T}\left(\frac{dT}{dz} + \Gamma\right)}{\left(\frac{dv}{dz}\right)^2}$$

where $g$ is the acceleration of gravity, $T$ is the temperature, $dT/dz$ is the atmospheric temperature gradient, $dv/dz$ is the vertical shear of horizontal neutral winds, and $\Gamma$ is the adiabatic lapse rate. The atmospheric temperature in the E layer is an increasing function of altitude. The parameter $\Gamma$ is greater than zero. Shear-dependent turbulence occurs when $R_i$ is sufficiently small, or negative, and hence (since all quantities are positive) must occur only for sufficiently large values of the shear. It is contended by these authors (61,62) that the magnitude of shear necessary to satisfy the Richardson criterion at 100 km altitude is at least 0.1 $sec^{-1}$. This value is seldom achieved (33). It should be noted, however, that the critical Richardson number for turbulence in shear flow is a subjective quantity and may be appropriate only to within an order of magnitude. There may exist sufficient latitude within this uncertainty to allow turbulence more frequently than is estimated by these workers.

Of principal concern for this investigation is the fact that even if turbulent motion as defined in conventional hydrodynamics does not occur in the lower E region, there is no dispute that irregularities of tens- to hundreds-of-meters scale size do indeed exist.

Some observers report that, although the occurrence of sporadic E appears to bear no relation to the positions of nulls in the wind velocity profile and to the positions of maxima in the vertical gradient of horizontal wind velocity, it bears a strong relation to the rate of change with altitude of the latter quantity. That is, sporadic-E layers occur at or near positions in which either the direction of the horizontal wind gradient changes radically over a small interval of altitude, or its magnitude changes discontinuously in a small interval of altitude (12,61-66). Typical wind direction changes of 90° to 180° occur over altitude intervals as small as 100 m and are found most frequently in the 100-110 km region where sporadic E is concentrated (61). Based upon these indications, Bedinger et al. (65) postulate that sporadic E is associated with nonlinear laminar flow in which discontinuities occur in gravity-wave phase fronts analogous to compression shocks in acoustic waves. The points at which sporadic-E layers form (by some unspecified mechanism which depends upon the jump in density and temperature at the gravity shock) are the surfaces of physical discontinuity prescribed by the nonlinear motion.

Kato (67) also concentrates on the points at which the wind direction changes suddenly with altitude. Postulating that (contrary to the theory described above) hydrodynamic turbulence is induced at these positions, he analyzes the effect of the geomagnetic field upon the resultant currents and predicts the formation of sporadic-E layers by this mechanism.

Gershman et al. (68) describe an instability, dependent upon the existence of shearing winds, which can occur in the period of formation of a sporadic-E layer and which can lead to the appearance of irregularities of hundreds-of-meters scale size within growth periods of about 100 sec. This type of irregularity would lead to fine structure of hundreds-of-meters scale within sporadic-E layers.

Probably the most prominent alternative to the wind-shear theory as a mechanism for sporadic-E layer formation is a drift-dissipative plasma instability which will be described in detail in the first two sections of Part III. This mechanism depends upon the existence of a plasma density gradient in a particular geometrical relationship to ambient electrostatic and magnetic fields and can occur as a consequence of the wind-vector discontinuities which are described above, whether or not the irregularities produced by them are properly described by turbulence in the hydrodynamic sense. It requires plasma-density gradient scales of tens to hundreds of meters and an electrostatic field of thousandths to hundredths of a volt per meter. These conditions are entirely within reason in the dynamo region. In addition, they will be seen below to be consistent with the physical parameters which characterize the cesium plasma clouds upon which this investigation is based.

Further amplification of this subject is deferred to later sections; it is sufficient to note here that the mechanism treated in this investigation is a strong contender for the explanation of ionospheric sporadic E, in competition with the wind-shear theory and others described in this section.

## SOME CONSIDERATIONS OF CHEMISTRY

### Normal E Layer

The E layer is conventionally considered to be bounded from below by the mesopause at 80-85 km altitude, where a temperature minimum of about 180°K is reached. Up to

this level, the atmospheric constituents are in nearly the same proportions as at ground level and are ionized to only a very small extent. In the lower E layer these same proportions are represented in the neutral constituents, although at altitudes above about 110 km monatomic oxygen begins to be present in increasing amounts. Nitric oxide, although it is a minor constituent of the neutral atmosphere, is of importance in the E layer because of its low ionization potential.

The processes of photodissociation and photoionization are primary causes for the ionization in this region of the atmosphere and depend on solar radiation in the far ultraviolet and shorter wavelengths. Table 1 lists the wavelengths of importance for dissociation and ionization of the most important molecular constituents.

Table 1
Ionization Threshold Wavelengths for E-Layer Constituents

| Constituent | Process | Threshold Wavelength (Å) | Constituent | Process | Threshold Wavelength (Å) |
|---|---|---|---|---|---|
| $O_2$ | Dissociation | 2400 | $O_2$ | Ionization | 1026 |
| NO | Ionization | 1340 | O | Ionization | 910 |

Of particular importance in these processes are the intense solar emission components of hydrogen Lyman-$\alpha$ (1216 Å), hydrogen Lyman-$\beta$ (1026 Å), and the hydrogen Lyman continuum (911 to 840 Å). Hard x rays of wavelengths from 4 Å to 50 Å also penetrate to 90-110 km altitude and are important for ionization of $O_2$, $N_2$, and O. Wavelengths of the intervening region (nominally 50 Å to 850 Å) do not penetrate to the lower E layer.

The principal ionic constituents which emerge from these processes are the diatomic oxygen and nitric oxide ions. Nitrogen, although abundant among the neutral constituents, is not an important ionic species. It is believed that molecular nitrogen ions either undergo charge-exchange reactions with molecular oxygen to form molecular oxygen ions, or combine with oxygen to form ionic nitric oxide. In the daytime E region, nitric oxide and molecular oxygen ions are present in nearly equal proportion. At night, however, there is strong evidence (69-71) that the proportion of nitric oxide ions to molecular oxygen ions is quite high, indicating that molecular oxygen recombines more rapidly than nitric oxide after sunset. The relative persistence of nitric oxide ions after sunset might be explained by the presence of nightglow ultraviolet (69) of which hydrogen Lyman-$\alpha$ is a strong constituent.

The limiting process for E-layer ionization formation is generally conceded to be dissociative recombination (69,72) in which an electron encounters a molecular ion and combines with it to form an unstable neutral molecule, which then splits into two neutral atoms. This process is believed to be dominant for both molecular oxygen and nitric oxide ions. Electron attachment to molecular oxygen is considered to be negligible by comparison. A great deal of work has been done in the laboratory to measure the dissociative recombination coefficients of common molecular ions (73,74) and some results are presented in Table 2.

Table 2
Dissociative Recombination Rate Coefficients for Molecular Ions*

| Ion | Rate Coefficient ($10^{-7}$ $cm^3/sec$) |
|---|---|
| $O_2^+$ | $1.7 \pm 1$ |
| $N_2^+$ | $2.9 \pm 0.2$ |
| $NO^+$ | $5 \pm 1$ |

*See Ref. 73.

If it is considered that average electron densities of no more than $10^5$ $cm^{-3}$ are common in the lower E layer under sunlit conditions, than an e-folding time for decay after sunset of about 100 sec would be expected. In fact, however, substantial E-layer ionization persists throughout the night, and the extent of nightglow ionization of nitric oxide is inadequate (69) to account for this persistence.

It is now believed that long-lived metallic ions are responsible for the nighttime persistence of the E layer (70). Such constituents would not only explain the large electron densities observed in this region at night, but would provide a source for the oxygen and nitric oxide ions found in darkness. Charge exchange reactions of metallic ions with these molecules would permit continuous production of molecular ions, and hence they would be detected throughout the night regardless of their loss rates.

## Metallic Ions and Sporadic E

Rocket probes launched into the E region have shown that metallic atoms and ions exist there in substantial quantities. This circumstance has been found to hold both during periods when sporadic-E layers have existed (75) and when they have not (76). The metallic constituents have been found to be principally iron, magnesium, sodium, silicon, calcium, and aluminum (in order of abundance), and they have been present in the approximate proportions in which they occur in meteors (77). This fact supports the thesis that metallic atoms and ions in the ionosphere are ablated from meteors. They may be ionized readily by solar ultraviolet and may also participate in charge exchange reactions with nitric oxide and oxygen ions. This latter process is particularly likely because several experiments (75,76) have shown that nitric oxide and oxygen ion distributions display density minima at the same altitudes at which the metallic ions display peaks.

Sporadic-E layers have often been found to consist largely of metallic ions, and it is generally accepted that temperate-latitude sporadic E is nearly always so composed. The atomic metal ions are long-lived, as opposed to molecular ions which are subject to dissociative recombination. Indeed, it has been postulated that the ultimate consumption of metallic ions is made possible only after a slow intervening reaction with ozone (76) in which a metallic oxide ion is formed, which is then susceptible to dissociative recombination.

Others (78) have suggested that the consumption of metallic ions in the E layer, and in particular of those in sporadic E, cannot be explained by any known chemical process. The reaction between the metallic ion and ozone, they argue, is followed rapidly by a reaction of the metallic oxide ion with monatomic oxygen which reforms the metal ion and molecular oxygen. These authors maintain that chemistry is of very little consequence for deionization in the E layer and that only diffusion need be considered. It might be added that the alkali metals are even less susceptible to reactions with other molecular constituents, including ozone, than are the alkaline earths, in particular, and the other elements whose ions have partially filled valence shells. The cesium ion, which is of interest for the plasma cloud study, and other alkali metal ions have full outer shells, and hence do not readily form valence bonds with oxygen atoms, for example. Thus even the first step of the ion-ozone reaction postulated above is unlikely for alkali metal ions.

It can thus be seen that the cesium plasma cloud study bears a direct chemical relation to the behavior of sporadic E. The cesium ions are metallic and monatomic, as are, it is believed, the constituents of sporadic E. The cesium ions formed in a plasma cloud are at least as long-lived as the metallic ions which constitute sporadic E and are subject to the same influences. In addition, the demonstrated long lifetime of metallic ions in the E layer in daytime makes it possible to ignore chemical processes, such as dissociative recombination, as being important in the consumption of the cesium ions, and permits diffusion to be considered as the primary mechanism for dissipation.

## Chemistry of an Explosive Cesium Release

To a large extent, the thermochemistry of the cesium plasma cloud is determined by the energy imposed upon its constituents during the detonation phase of the release. The mixture of ingredients which has been used in all cesium releases in this program is one which was developed as a result of Project Firefly in the late 1950's and early 1960's. This mixture, a melt-cast combination of 34% cesium nitrate, 21% granulated aluminum, 26% trinitrotoluene (TNT), and 19% cyclonite (RDX), has been found (79) to yield almost complete vaporization of the cesium, which composes approximately 6% of the mixture. Radar data indicate that approximately 0.16% of the cesium is ionized in the detonation wave, with a resultant net degree of ionization of $10^{-4}$ of the total gaseous explosion products. Other components of the detonation-produced gases are carbon monoxide, and nitrogen and hydrogen in molecular form. The aluminum oxide is emitted in condensed form.

That thermal processes are responsible for this initial ionization is evident, and so some consideration of the thermochemistry of the detonation is of importance. Groves (13) has adapted Brode's (80) treatment of blast waves in air to the circumstances which obtain in the lower ionosphere.

Groves' treatment indicates that three phases of motion occur in the detonation. At first, the gaseous explosion products expand rapidly until they sweep up enough ambient air into a thin enough shell for a shock wave to be formed. This event occurs when the ratio of density within the shock to that in the ambient is about 8.8:1 and the pressure ratio is about 400. During this phase, the gases do work in accelerating and heating the ambient air. There then begins a second phase in which expansion continues with no change in shock density or pressure until the density and pressure of the gaseous explosion products behind the shock equal those in the shock itself. At this point, approximately 63% of the total explosive energy has been transformed into kinetic energy. The final phase involves return of this energy into internal energy of the explosion products and ambient air.

Some simple thermodynamic considerations permit temperatures, which are of importance for determining the degree of ionization of the cesium vapor, to be estimated. The explosion releases approximately $5 \times 10^{13}$ ergs/kg of energy. Assuming that this energy is initially in the form of internal energy, the initial temperature in the explosion products is 4000°K. After expansion to ambient pressure $P_{amb}$, Brode's numerical solution indicates that the radius $r_{exp}$ of the cloud is given by

$$r^3_{exp} = 8 \times 10^{-3} \frac{E_{oo}}{P_{amb}}$$

in terms of the initial energy $E_{oo}$. By use of the perfect gas law, there results a mean temperature in the expanded cloud of about 680°K.

The general picture which emerges is that of a hot bubble of initial temperature 4000°K, which expands behind a shock of about 400 atmospheres overpressure until most of the initial energy is converted into energy of motion. The decay which then follows results in a decrease of bubble temperature to about 680°K. Since this temperature is more than three times that of the ambient air, the bubble is at this point less dense than its surroundings.

For thermal ionization of alkali metals, Pressman et al. (5) have determined the degree of ionization in terms of temperature and ionization potential. For cesium, the most easily ionized of all metallic atoms, the ionization potential is 3.9 eV. Assuming the reactions of importance to be

$$3Al + CsNO_3 \longrightarrow Cs\uparrow + Al_2O_3 + AlN + Q_1$$

$$2Al + CsNO_3 \longrightarrow Cs\uparrow + Al_2O_3 + \frac{1}{2} N_2 + Q_2$$

With $Q_1$ = 381 kcal and $Q_2$ = 224 kcal, these authors find that the temperature in the reaction zone even for a deflagrative release (in which no explosive is mixed with the cesium nitrate and aluminum) is about 3500°K. The principal difference between their low-energy release and the explosive releases treated here is the chemical yield, which in their case seemed to be only about 10%. Assuming, as seems reasonable from Groves' analysis, that most of the explosive energy is expended in physical displacement of the explosion products and, ultimately, in heating the ambient air, the reaction zone temperature of 3500°K and pressure of 500 atmospheres treated by Pressman et al. are appropriate to the case of interest here. Their result — an estimate that $10^{-3}$ of the cesium atoms would be thermally ionized — compares with the value of $1.6\times10^{-3}$ cited above as indicated by radar data. For the 2-kg payloads of concern here, a total of about $3\times10^{21}$ electrons results, and these electrons are concentrated within volumes between $10^6$ and $3\times10^7$ m$^3$ depending on altitude. Initial electron densities of $10^8$ to $3\times10^9$ cm$^{-3}$ thus are expected.

After the detonation phase, several processes begin to act simultaneously. Cesium is photoionized by solar radiation of wavelength shorter than 3200 Å and has a photoionization probability in sunlight of $3\times10^{-4}$ sec$^{-1}$ (81) to $6.5\times10^{-4}$ sec$^{-1}$ (3). Hence, daylight releases would be expected to provide ionization continuously for many hundreds of seconds. Calculation of the loss rates, both by chemical consumption and diffusion, is difficult. The considerations in the preceding subsection of this report indicate that diffusion is the most important process in daytime when the continuous photoionization process competes with, and probably overwhelms, the chemical loss mechanisms.

At night, however, the situation is not nearly so clear cut. Not only is photoionization absent as a continuous source of new electrons, but a second mechanism of loss may exist which is not important during daytime. Narcisi (76) and Donahue (82) have both discussed measurements regarding sodium in the lower ionosphere. This element would be expected to obey chemistry similar to cesium, since both are alkali metals, and hence these measurements are of importance here. It is believed (82) that two serial processes are important in governing the abundance of neutral and ionized sodium:

$$Na + O_3 \longrightarrow NaO + O_2$$

followed by

$$NaO + O \longrightarrow Na + O_2 ,$$

and

$$Na^+ + O_3 \longrightarrow NaO^+ + O_2$$

followed by

$$NaO^+ + e \longrightarrow Na + O \text{ (dissociative recombination).}$$

This pair of reactions gives rise to an altitude dependence, with a ratio of sodium atom to sodium ion concentration of 50:1 at 93 km, declining to unity at 110 km. Reaction rates have been estimated for these processes, based upon measurements and upon the postulated existence of a dust layer in the lower E layer to act as a sodium source. These reaction rates, together with the rate at which cesium is photoionized by sunlight, indicate that these loss processes would not be effective in daylight. At night, however, these consumption mechanisms must be considered of importance. In addition, it is noted that monatomic oxygen is converted to ozone after sunset, and hence the sodium (or, in this investigation, cesium) ion-ozone reaction would be expected to be even faster than in daylight.

It may be concluded that for releases in daylight, chemical consumption processes play a minor part, and dissipation of a cesium plasma cloud can be considered to be a result of diffusion. Sunlit cesium plasma clouds are probably an accurate simulation of the source for sporadic E of the metallic-ion type. For releases in darkness, however, the rapidity of the expected chemical consumption processes, and the absence of photoionization for replenishment, is likely to result in short plasma cloud lifetimes. Nighttime sporadic E probably occurs only when a massive aerosol layer provides continuous replenishment of the metallic ions by duffusion, and the relatively small cesium plasma clouds probably do not persist long enough to permit the behavior of nighttime sporadic E to be studied.

# PART II. RESULTS OF THE EXPERIMENT

## EXPERIMENTAL DATA AND ANALYSIS

### Introduction

Most of the experimental data were acquired with the use of a high-power, coherent-pulse-doppler, decameter-wavelength radar located at the Naval Research Laboratory's Chesapeake Bay Division. Similar meter-wavelength data were also acquired for many of the releases, but in all cases (except one) data ceased immediately after the blast-wave phase and are thus of no interest in this investigation. The outstanding feature of the type of data which was acquired is the extremely narrow frequency resolution which is possible. Doppler shifts of the effective scattering elements (associated, in this investigation, with the phase velocities of the plasma irregularities) can be measured to a precision limited only by their lifetimes. A typical scattering entity (defined here as a large, persistent, monochromatic signal) in this investigation has a $1/e$ lifetime of 1 to 10 sec, and hence its phase velocity and spectral content may be measured to a precision of 0.1 to 1.0 Hz in the frequency domain, or to a precision of a few meters per second in velocity at a typical radar wavelength of 20 m. This resolution capability is based upon the phase-coherent character of the radar signal; its significance for this investigation is that the radar pulse spectrum is generated in a manner which preserves phase continuity among pulses and permits received data to be processed as though they consist of segments of a continuous wave (with certain limitations, which are of little importance in this investigation). The range or time-delay resolution which is afforded by pulsing the radiation permits radar targets at other distances than the plasma cloud to be eliminated.

The frequency resolution which results from phase coherence also permits radar targets at any range, but at different apparent velocities than the plasma cloud, to be eliminated. Thus, in addition to permitting high-resolution spectral analysis of motions in the plasma cloud, this coherent-pulse-doppler characteristic allows the many types of potential contaminants to the data to be excluded. The high signal-to-noise ratio which results from this technique is the essential feature which permits plasma cloud data to be given detailed examination.

The data have been analyzed in several ways. Spectral analysis has permitted the apparent velocities, sizes, lifetimes, and growth and decay rates of scattering entities to be measured. Statistical analysis of the radar pulse data has permitted certain prominent characteristics of the scattering entities to be discerned. Comparison of cross-polarized receiving channels also has indicated certain important features of these scatterers. Autocorrelation has, in some cases, revealed notable temporal behavior. Finally, the data from independent experiments have been compared, which permits a number of distinctive characteristics to be associated with plasma cloud development. A phenomenological model has been constructed to describe these characteristics of behavior.

It will be the purpose of this section to present examples of the important characteristics of plasma cloud development and to describe a model which embodies these features. The bulk of the experimental data, much of which simply corroborates with examples to be presented in this section, appears in the Appendix. Some results of these data will be presented in tabular and graphical form.

A total of fifteen successful experiments have been conducted since October 1967. Twelve of these experiments have involved 2-kg payloads of the cesium-plus-high-explosive mixture previously described in the section on chemistry considerations. These packages have been launched to altitudes of 88 to 103 km by a 7-in. HARP* gun, developed and operated by the U.S. Army Ballistic Research Laboratory and located at the NASA Wallops Island Station in Virginia. This location is about 170 km southeast of the radar site. Two 18-kg payloads of the same material have been carried by Nike/Cajun rocket to an altitude of 101 km, also over Wallops Island. In a fifteenth experiment, a 6-kg payload containing barium as the ionizable matter, and no high-explosive, has been launched from Wallops Island by rocket. This latter experiment is included here as an example of plasma cloud behavior similar to the cesium-seeded releases despite its dissimilar material and deflagrative release mechanism. Thus it confirms that the observed behavior is not peculiar to the material or method of deposition.

Table 3 lists the fifteen experiments conducted during this investigation. Three launches occurred in total darkness and covered the altitude interval from 87.5 to 99 km. Three launches occurred at the approximate time of E-layer sunrise and covered the altitude interval from 93 to 103 km. Three launches occurred near the E-region sunset and covered the altitude interval from 93 to 102 km. The other six launches took place between midday and evening and covered the altitude interval from 93 to 103 km. Launches took place in all seasons but only in summer were the launches distributed through the day, from sunrise to sunset. All winter launches were in the midnight-to-dawn interval, and all autumn launches were in late afternoon to late evening. A well-distributed sample of altitudes and times of day was achieved with the ten launches which were conducted between the months of June and September in 1968 and 1969. Nearly all of the important observed characteristics of plasma clouds were detected during these experiments.

*The HARP gun is described in Ref. 1.

Table 3
Digest of Plasma Cloud Experimental Results

| Date | Launch Time (EST) | Payload Size (kg) | Alt (km) | Signature Duration (sec) | Character of Signature | Spectral Dispersion (Hz) | Apparent Size ($m^2$) |
|---|---|---|---|---|---|---|---|
| Oct. 4, 1967* | 1815 | 6 | 102 | 45 | S | 15 | $10^4$ |
| Apr. 12, 1968 | 1323 | 2 | 95.5 | 100 | P | 5.5 | † |
| Apr. 17, 1968 | 1545 | 2 | 94.0 | 65 | S | 5.0 | $10^4$ |
| Sep. 11, 1968-1 | 1615 | 2 | 92.7 | 40 | S | 2.7 | † |
| Sep. 11, 1968-2 | 1815 | 2 | 93.3 | 360 | L, S | 4.0 | $10^4 - 10^5$ |
| Sep. 11, 1968-3 | 2227 | 2 | 87.5 | 45 | S | 3.2 | † |
| Feb. 14, 1969-1 | 0007 | 2 | 99.1 | 230 | P, D | 5.0 | $10^5 - 10^6$ |
| Feb. 14, 1969-2 | 0207 | 2 | 96.8 | 150 | P | 5.5 | $10^5 - 10^6$ |
| Feb. 14, 1969-3 | 0625 | 2 | 103.0 | 3000 | L, E | 10.0 | $10^6 - 10^7$ |
| Jun. 3, 1969 | 1258 | 2 | 102.0 | 1400 | L | $10^{‡}$ | ‡ |
| Jul. 18, 1969 | 1216 | 2 | 95.5 | 1600 | L | 4.0 | $10^5$ |
| Jul. 23, 1969 | 1759 | 2 | 99.1 | 200 | S | 6.0 | $10^6$ |
| Jul. 25, 1969 | 0519 | 2 | 92.4 | 40 | S | 3.4 | † |
| Aug. 28, 1969 | 1303 | 18 | 102.1 | 1500 | L, E | 6.0 | $10^{8‡}$ |
| Aug. 29, 1969 | 0500 | 18 | 103.3 | 1200 | L | 10.0 | $10^7 - 10^8$ |

*Deflagrative barium release, not to be compared quantitatively with the explosive releases.
†Radar clutter in range, doppler partially obscured this signature.
‡Some receiver saturation affected these data.

S—Highly irregular; several intense specular components of a few seconds duration.
L—Long duration; undulatory in amplitude and spectral dispersion with periods of less than 1 min to several minutes.
P—Behaved as single stable reflector for several seconds immediately after blast phase.
D—Displayed sudden disappearance after stable period; returned a few seconds later.
E—Formed sporadic-E-like reflecting layer.

## Some General Features of the Data

Figure 1 is a scatter plot of signature duration vs altitude. The trend of increasing duration with altitude (except for the barium release) and the magnitudes represented in Fig. 1 are consistent with the results of other series. The short duration of the barium plasma cloud may be attributed to the circumstance that ionic barium forms a short-lived ionic oxide much more readily than cesium does. Accompanying each point are the symbols (from Table 3) which indicate its character. Of the seven cases in which a highly irregular spectral behavior was discerned (labeled S in Table 3 and Fig. 1), five occur at altitudes of 94 km and below. Four of the six long-duration signals (labeled L), which display undulation in amplitude and spectral dispersion, occur at altitudes of 102 km and above. This circumstance probably does not indicate that the irregular behavior is absent above 94 km. It is far more likely that it is simply more evident in the radar data from lower altitudes. The plasma cloud is imbedded in a more rigid fluid mechanical system (i.e., the atmospheric density and pressure are greater) toward the lower end

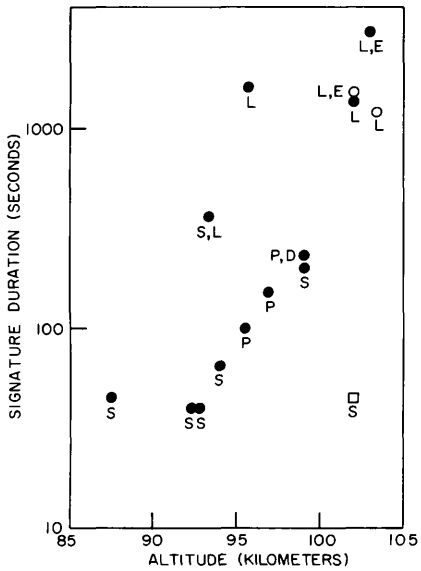


Fig. 1 - Signature duration vs altitude. The 2-kg releases are indicated by filled circles, the 18-kg by open circles, and the 6-kg barium release by an open square.

of the altitude interval, and fewer degrees of freedom or modes of oscillation are likely. Furthermore, the plasma cloud is physically smaller at lower altitude. It is probable that the irregular behavior below 94 km simply indicates that the fewer permitted modes of vibration are more readily distinguished there than at higher altitudes, where many more modes are superimposed.

It is of importance that the barium release is also included among these examples designated as irregular in behavior. The deflagrative release mechanism is less efficient in the creation of ionization than is the explosive mechanism, and this circumstance probably helps explain its short duration and smaller size. The prominence of irregular behavior, interpreted as above to indicate that only a few degrees of freedom exist in the plasma cloud, is probably a result of the smaller less-dense plasma cloud formed in this instance.

There are several releases, most of them above 102 km altitude, designated by L in Table 3 and Fig. 1 which lasted for 5 min or more and displayed a series of periodic undulations in spectral dispersion and amplitude with periods of several tens of seconds to several minutes. These periodic variations may have been evident in all releases, had they lasted long enough. They are worthy of note because they appear in most cases at less than the Vaissala-Brunt period which characterizes the natural frequency of atmospheric oscillations, caused by density disturbances, and represents a short-period cutoff for atmospheric internal gravity waves. This parameter has a magnitude of about 5 min in the lower E layer.

Also indicated in Table 3 and Fig. 1 are two examples, labeled E, in which a sporadic-E-like reflecting layer was formed by the cesium plasma cloud. This result is of interest because it may permit some aspects of the formation of naturally occurring sporadic E to be discerned; it will be discussed in greater detail below.

The designation P in Table 3 and Fig. 1 describes a phase of plasma cloud development which all examples display for at least a few seconds, but which is extended to tens of seconds for the three cases indicated. In this phase, which also will be treated below, the plasma cloud displays a regularity of behavior in signal amplitude and discreteness of spectral dispersion which suggests that it is an effective single scatterer for the radar illumination. It is likely in this phase that the cloud is of a prolate spheroidal shape, with no protuberances or re-entrants which would be discerned by their effect on the radar data.

The single case labeled D in Table 3 and Fig. 1 is a curiosity — the signature disappeared completely after the first 20 sec, was absent for about 20 sec, and then returned with its earlier intensity and remained for several minutes. This behavior is not fully understood. It could not have been a lapse period after the decay of the initial thermal ionization, lasting until the effects of solar ionization were felt, because this release occurred at midnight. It could only have been indicative of a period in which the ionization was so dispersed as to be subcritical for reflection of the radar wavelength until

some reordering process compressed the plasma into a small enough volume for reflection to occur. This likelihood is relevant to the discussion of plasma instabilities to be presented below.

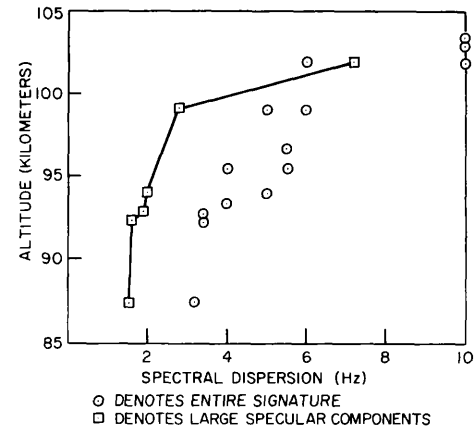


Fig. 2 - Maximum spectral dispersion vs altitude

Also indicated in Table 3 is the maximum spectral dispersion, in Hertz, for each of the fifteen releases. This parameter is plotted in Fig. 2 for the fourteen explosive releases, as indicated by open circles. There is displayed in Fig. 2 an obvious tendency for widened spectral dispersion with increasing altitude. This circumstance is indicative of the likely greater freedom of motion (or greater number of modes of oscillation) allowed for releases at higher altitudes. The open squares in Fig. 2, joined by straight lines for emphasis, indicate the spectral dispersion among the intense spectrally narrow components in six of the seven cases labeled S in Table 3 and Fig. 1. These six cases displayed the most distinctive examples of this behavior, and their tendency for increased spectral dispersion with altitude is pronounced.

The evolution of a plasma cloud deposited in the lower ionosphere has been found in this investigation to display a clearly demarcated sequence of four phases. Phase I is a period of blast-wave expansion which has been described partially in the last section of Part I above, and which will be discussed in greater detail in the first section of Part III to follow. This phase lasts from 4 to 8 sec and involves an ordered, or stable, expansion of the slightly ellipsoidal fireball, oriented along the magnetic field, followed by a few reverberations as a sequence of shocks encounters the contact surface. The behavior in this phase is similar to Brode's hydrodynamic model except there is strong evidence of magnetic field constraint. The decameter radar data indicate that the reverberation time is 1 to 2 sec and that after two or three reverberations the expansion is complete. At that time pressure equilibrium with the ambient is achieved, and the fireball has cooled from its initial temperature of 4000°K to about 700°K and is thus slightly overexpanded. Data indicate that the geomagnetic field, excluded from the expanding bubble until this time, now penetrates it and presumably achieves its unperturbed configuration. Phase II is a period designated *ordered* diffusion in which the ellipsoidal plasma cloud remains a single scatterer to decameter radiation. This phase is exemplified most clearly by the data labeled P in Table 3 and Fig. 1. Phase III is a period of highly irregular motion, often of several minutes duration, in which some manner of collective behavior involving the entire plasma cloud occurs. This phase is most pronounced in the data labeled S in Table 3 and Fig. 1. Phase IV is a stage of development which occurs only in the two cases labeled E in Table 3 and Fig. 1 and corresponds to the formation of a stable sporadic-E-like reflecting layer for the decameter radiation. This phase may last several tens of minutes.

In the next three sections, Phases II-IV will be described with the aid of examples selected from the radar data.

## Phase II: Ordered or Stable Diffusion

At the end of Phase I there begins a period (Phase II) in which the cloud continues to expand, by diffusion, but remains more or less a single scatterer of the decameter radar energy. Hence Phase II is called ordered or stable diffusion, although in all likelihood a turbulent diffusion law must be cited to account for the rapidity with which it proceeds.

It is supposed that a process of anisotropic ambipolar diffusion, including magnetic field effects and neutral-gas turbulence, must be cited in an accounting of motion in Phase II and probably underlies the disordered motion which is apparent in later phases. The data indicate that Phase II lasts from a few seconds to as much as a minute and is characterized by anticorrelation of the two antenna polarizations. Figure 3 illustrates this behavior. The data are plotted as doppler shift vs time, with intensity (or whiteness) indicative of signal amplitude. The two right-hand photographs, in which thresholding has been used to accentuate signal amplitude peaks, illustrate the anticorrelated behavior from 0707:20 to 0708:00 GMT; the upper trace has one dark band (indicating absence of the echo) in the middle, whereas the lower one has a bright spot in the middle with dark bands on either side. Thus in the case shown the ordered diffusion phase lasts for 40 sec. The anticorrelation of the data from cross-polarized receiving channels indicates that the signal-intensity variations arise, not from interference among a number of component scatterers, but from rotation of the plane of polarization due to the Faraday effect in a more or less regularly shaped single-scattering entity.

Figure 4 is a plot of the apparent radar cross section vs time in which the copolarized data are shown as a solid line connecting filled diamonds, and the cross-polarized data are shown by a dashed line connecting filled circles. This illustration does not correspond to the example in Fig. 3 but to a second case in which the regularity of radar cross-section behavior in Phase II is more pronounced. Notice that from 0507:15 to

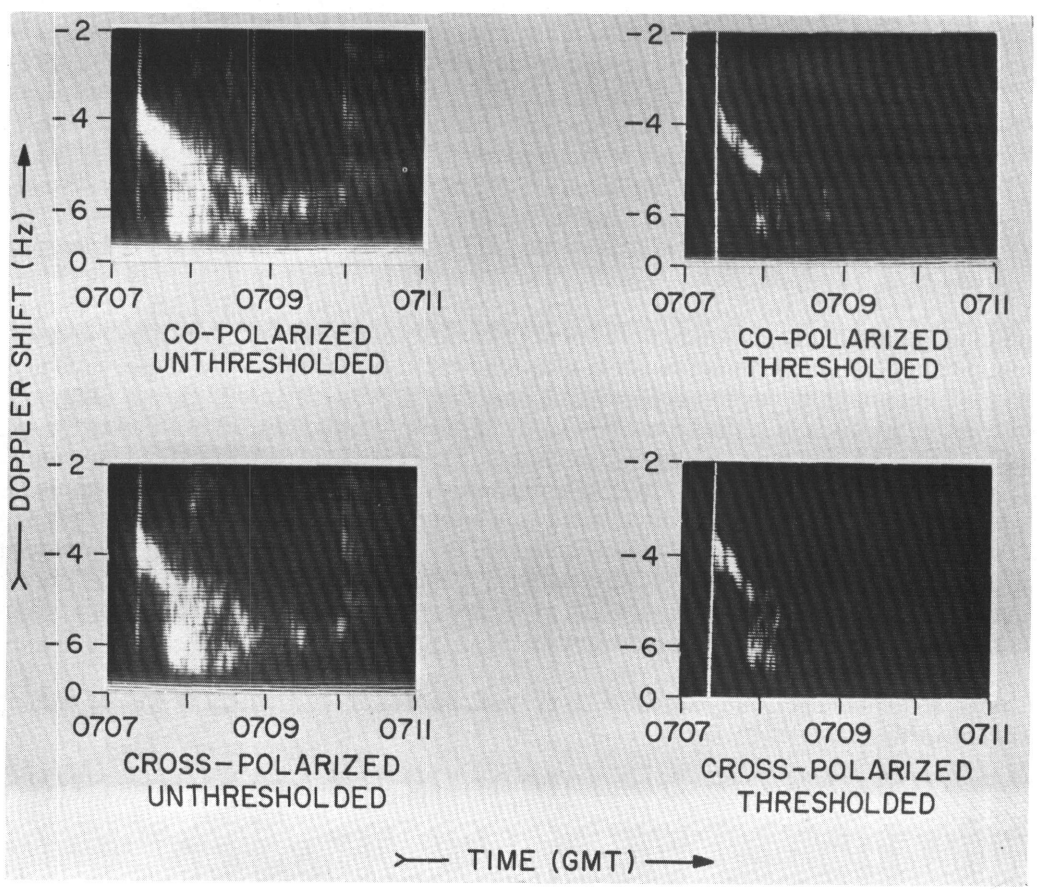


Fig. 3 - Doppler shift vs time for co- and cross-polarized data from cesium release No. 2, Feb. 14, 1969

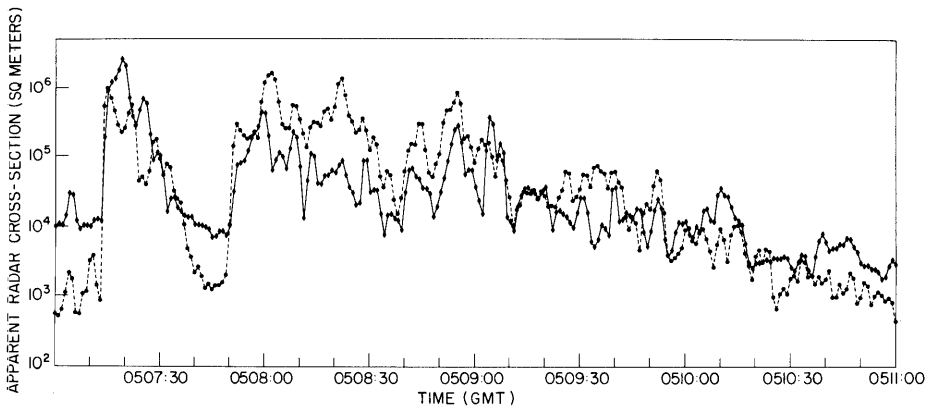


Fig. 4 - Apparent radar cross section vs time for cesium release No. 1, Feb. 14, 1969. Copolarized data are shown by solid line; cross-polarized data are shown by dashed line.

0507:30 GMT the four peaks in one curve correspond very closely to the four nulls in the other. Thus, in this 15-sec period, two cycles of polarization rotation occur in each channel, 90° out of phase with each other, indicating stable or ordered diffusion. At the end of Phase II (0507:30 GMT) the signals in both channels disappear, and then reappear 20 sec later. For the remainder of the cloud's lifetime the two channels show no strong evidence for either correlated or anticorrelated behavior, although several examples of both can be discerned.

In Fig. 4 it is evident that the abrupt disappearance of the signal corresponds to the end of Phase II. Other examples tend to confirm this tendency, although less strikingly. Notice, for example, that in the right-hand pair of photographs in Fig. 3 there occurs an abrupt lessening of intensity at about 0708 GMT, corresponding to the end of Phase II. In this latter case the signals do not disappear completely but only lessen in amplitude.

Phase III: Irregular Motion

During Phase III, in concert with the occurrence of no consistent tendency for correlated or anticorrelated behavior between the two polarizations, the signals both become diffuse in spectral dispersion, with approximately the same overall appearance. As indicated in Fig. 2 above, the total spectral dispersion is typically from 3 to 10 Hz, with the latter extreme confined to altitudes above 102 km. In the 85-100 km region a spectral dispersion of 3 to 6 Hz is prevalent, corresponding to equivalent scatterer velocities of 30 to 60 m/sec.

Phase III may last from as little as 1 min, at the low end of the altitude interval under nighttime conditions, to as much as 1 hr at the upper end of the altitude interval under solar illumination. It is clear that the lifetime of this phase is controlled by environmental conditions and cannot be analyzed in detail. The rather complicated ion chemistry of the ionosphere, as well as a probable turbulent diffusion process, are involved.

Of principal interest in Phase III is the appearance, repeatedly, of short-duration highly specular scatterers. These apparently coherent reflectors display extremely rapid growth, with e-folding time constants sometimes comparable to the widest-bandwidth analysis filter (2.4 $sec^{-1}$), lifetimes typically of 2 to 6 sec, and abrupt

disappearance. They appear to be monochromatic and of an apparent size often as large as the physical cloud's radar cross section itself. Data from a second receiving site, symmetrically located relative to the geomagnetic field, indicate that the scatterers are probably symmetric about the magnetic field direction.

Figures 5 through 7 illustrate the main features of these specular scatterers. In Fig. 5 there appear two photographs of a doppler-shift vs time display. The upper two

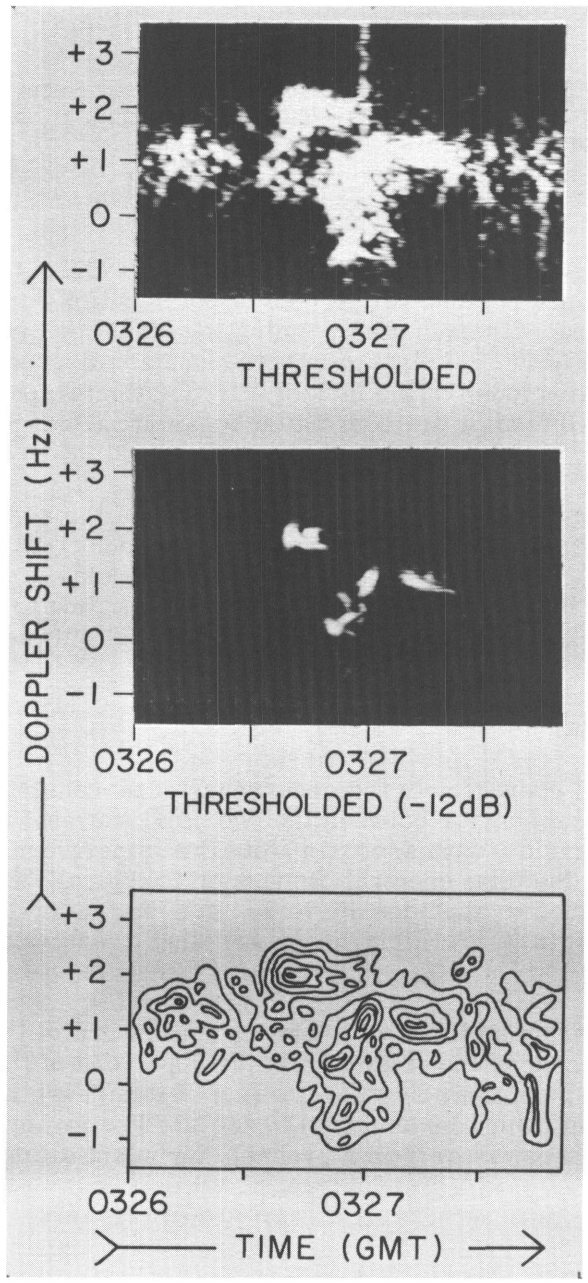


Fig. 5 - Doppler shift vs time for cesium release No. 3, Sept. 11, 1968

photographs show the plasma cloud echo at two levels of signal processor sensitivity, separated by 12 dB. A small degree of thresholding is used in both photographs to suppress low-level noise and clutter. The grainy band which occurs across the top photograph is a residue of the radar clutter echo and can be ignored. The drawing at the bottom is a contour plot drawn to the same scale as the photographs, with contours 6 dB apart. The predominance of three or four principal spectral components is evident, with the largest at about +2 Hz and occurring at 0326:40 GMT.

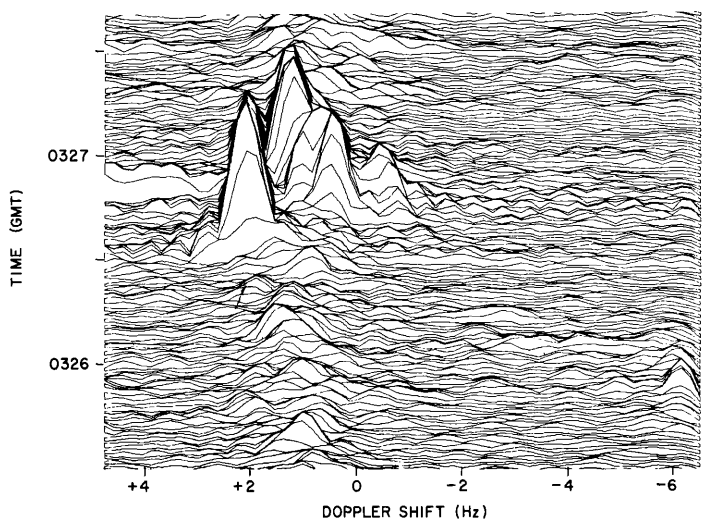


Fig. 6 - Time plot of computer-analyzer signal intensity vs doppler shift for cesium release No. 3, Sept. 11, 1968

Figure 6 contains the same information spectrum analyzed with a Fast Fourier Transform technique on a large-scale digital computer. (Figure 5 was produced by the special-purpose hybrid computer associated with the decameter radar.) Notice that the time and doppler shift axes in Fig. 6 are rotated counter clockwise by 90° relative to those in Fig. 5. The virtual third axis in Fig. 6, which appears to extend out of the page, indicates signal amplitude. The three or four large spectral components are apparent in Fig. 6 and clearly dominate the signature.

Figure 7 is a collection of spectral displays acquired by placing a 0.3-Hz resolution analysis filter at a succession of points in time, separated by 3 sec each, during the lifetime of the plasma cloud. (This spacing is consistent with the 3.3-sec time resolution afforded by the 0.3-Hz filter resolution bandwidth.) Figure 7 may be considered to be a series of horizontal cuts across the portion of Fig. 6 from -2.4 to +3.8 Hz which permits a more detailed inspection of the rapid growth and spectral discreteness of the dominant signal components. The first photograph, at 0326:30 GMT, shows the prerelease condition, with a small radar clutter echo just above an apparent doppler shift of zero. The time of burst is 0326:36 GMT, which occurs just at the end of the period included in the second photograph. The blast-wave echo, and possibly a beginning portion of the first, large, spectrally narrow component, are visible in this photograph. The photographs from 0326:36 to 0326:42 GMT show this first, and largest, specular echo at about +2 Hz, which then decays rapidly by 0326:45 GMT. The second large spectral component begins to build up at 0326:42 GMT with an apparent doppler shift of +1.5 Hz. It persists until

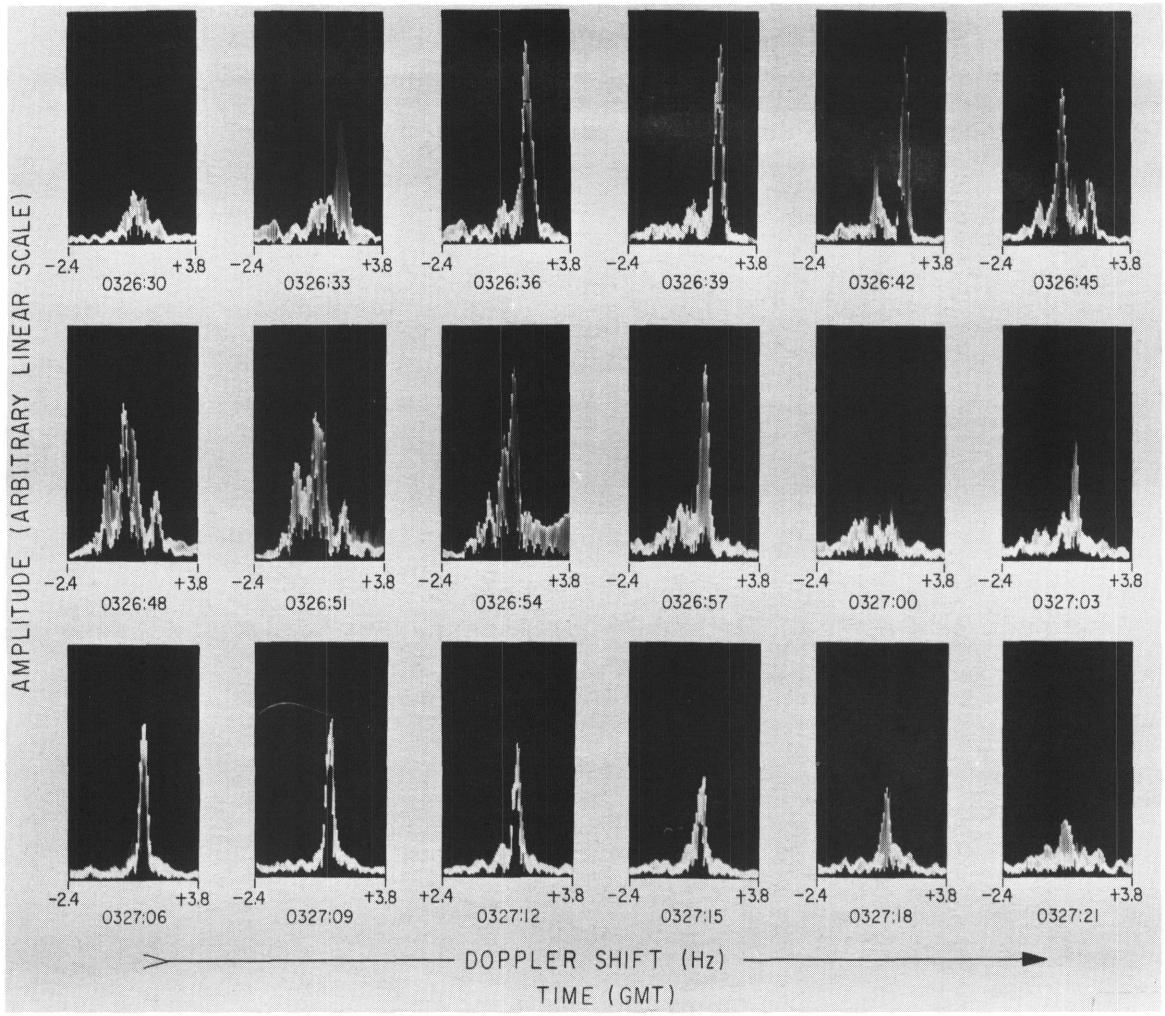


Fig. 7 - Amplitude spectra for cesium release No. 3, Sept. 11, 1968

0326:57 GMT, after which it decays quite abruptly. A third component, but lower in amplitude, also appears at -0.6 Hz in the photographs from 0326:45 until 0326:54 GMT. There occurs a period of quiescence at 0327:00 GMT in which only the clutter echo is evident. Finally, at 0327:03 a fourth spectrally narrow component appears suddenly, grows to a peak at 0327:06, begins to decay at 0327:09, and disappears by 0327:21 GMT when only the clutter echo remains. It should be emphasized that the 0.3-Hz resolution bandwidth used for this illustration forces even a truly monochromatic signal to display a bandwidth of 0.3 Hz. The four components described above all have, in Fig. 7, an appearance which closely approximates the filter characteristic, and hence must be narrower than 0.3 Hz in their actual bandwidth. Similarly, the 3.3-sec time resolution afforded by this filter bandwidth is inadequate to actually discern the growth rates of these signals,* which are actually on the order of several tenths of seconds. The fortuitous temporal relation among the photographs from 0326:57 to 0327:03 GMT, in which the

*Wider-bandwidth filters have been used for such measurements but do not permit so concise and illustrative a display as Fig. 7.

0.3-sec overlap coincides with the rapid decay of one component and the beginning growth of another, gives some indication of the rapidity with which growth and decay actually occur. The four dominant spectral components display lifetimes of 6 to 10 sec, which are somewhat longer than typical lifetimes.

It should be noted that although the first three spectral components are seen to decay within the space of two photographs (less than the 3.3-sec temporal resolution), the fourth one decays over a period of about 9 sec. Thus the decay process displays less consistent behavior than the growth process.

The discrete spectral components in Figs. 5-7 are representative of the type of behavior which is discerned in nearly all of the plasma cloud releases, particularly those labeled S in Table 3 and Fig. 1. Their apparent sizes, as indicated by signal amplitudes, are typically at least as great as the apparent radar cross section of the entire plasma cloud echo measured in its quiescent periods. (In this example, of course, they are much greater.) This fact, together with their spectral discreteness, indicates that each of them arises from a coherent scattering entity which (a) occupies a large fraction of the plasma cloud's spatial volume, (b) is formed within tenths of seconds, (c) exists as an ordered structure for a few seconds, and (d) decays within a period of a few tenths of seconds to a few seconds. The explanation for this behavior can only lie in a collective process involving nominally the entire plasma cloud.

### Phase IV: Sporadic-E Formation

In releases which form plasma clouds that remain for more than about 5 min, most commonly those above 100 km altitude, there is evident a long-period modulation in both spectral dispersion and signal amplitude. Figure 8 contains data from a release of long duration which displays this behavior. Once again, the data appear in an intensity-modulated doppler shift vs time format with both receiver channels (the cross-polarized one in the top half of each photograph, and the copolarized one below). The periodic modulation in spectral dispersion is evident in both channels, which are readily seen to be in phase. Thus this modulation is not indicative of magnetoionic polarization rotation and is, indeed, a manifestation of true motion in the reflecting surface. The predominant period of this fluctuation in spectral extent is about 50 sec. It persists from very shortly after the burst (at 1125:20) until about 1150 GMT. There is also modulation in intensity of a much longer period, which manifests itself in Fig. 8 as a lessening in intensity of the signature at 1138, 1148, and 1153 GMT. The blank period between 1203 and 1206 GMT represents an absence of data due to a radar malfunction. After this malfunction was corrected at 1206 GMT, the receiver sensitivity was raised by 12 dB to accommodate a weakening signal, and several local aircraft targets (indicated by intense wavy lines) appear. They are more intense in the copolarized channel, of course. Vertical bars which occur on the photographs are caused by random errors in the digital data storage apparatus and can be ignored. The important features of Fig. 8 are (a) the pronounced 50-sec modulation in spectral dispersion, (b) the phase coincidence of this modulation in both receiver channels, and (c) the sudden change in character of the signal at about 1150 GMT, when this modulation ceases and the signature becomes quite diffuse.

Figure 9 is a computer-processed version of most of the same data as Fig. 8, with an axis rotation of 90° as before. The virtual third axis, which appears to extend out of the page, represents intensity. The modulation in spectral extent is less evident than in Fig. 8, but a strong modulation in intensity is obvious. This behavior is most striking in the period from 1140 to 1146 GMT when sharp narrow spectral peaks appear in a manner reminiscent of those in Fig. 6. In this higher altitude release (103 km vs 87.5 km in the former example) the discrete spectral components are less apparent, but are present nevertheless. The striking feature of Fig. 9 is their cyclically recurrent behavior.

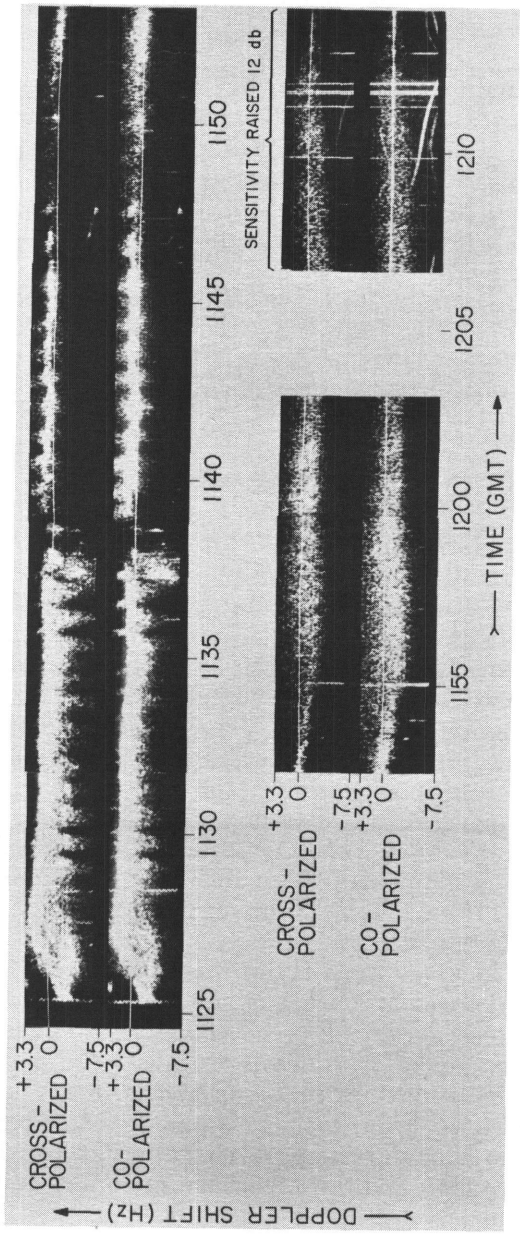


Fig. 8 - Doppler shift vs time for cesium release No. 3, Feb. 14, 1969

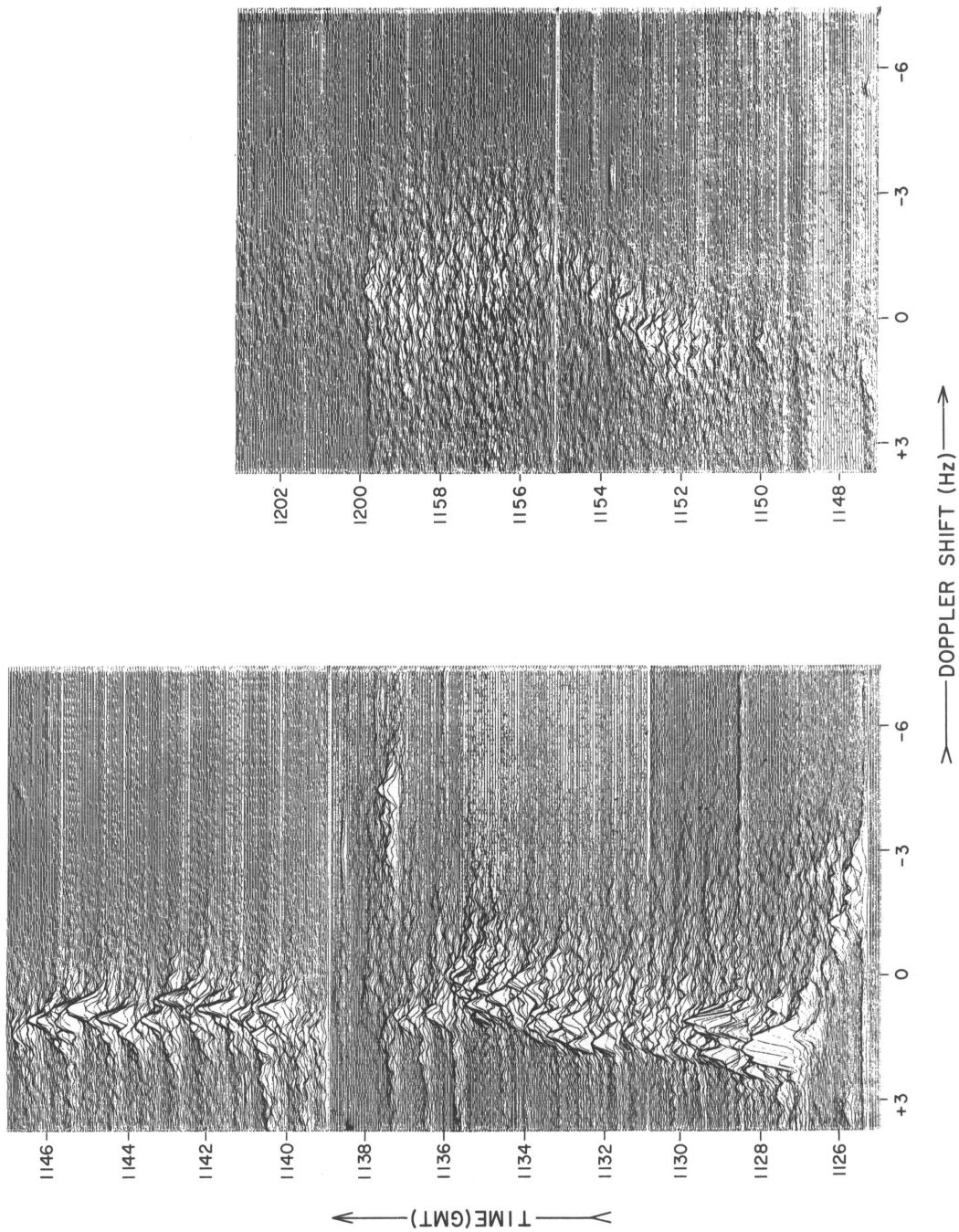


Fig. 9 - Time plot of computer-analyzed signal intensity vs doppler shift for cesium release No. 3, Feb. 14, 1969

There are several specular components in the 1126-1130 GMT period also, where they display a longer duration ridge-like appearance. The intensity dropouts at 1138, 1148, and 1155 GMT are also apparent in Fig. 9, as is the broadened and diffused spectral character which begins to develop after about 1150 GMT. The sudden change in amplitude at about 1200 GMT is an artifact of the data (which was compensated in Fig. 8) and can be ignored.

Figure 10, which is a plot of the apparent radar cross section vs time for the same release described in Figs. 8 and 9, permits the intensity variations to be displayed more quantitatively. The 50-sec modulation is most pronounced in the 1136-1150 GMT period, in which peak-to-null ratios as great as 20-dB may be discerned. The longer term modulation also is evident. These data were subjected to an autocorrelation calculation, and its result is shown in Fig. 11. The correlation never drops to zero, due to the overall irregularity of the signal, but the modulation-associated peak at 50 sec is apparent.

The characteristic of long-duration releases which makes them of such interest is that on some occasions they can be seen to form themselves into sporadic-E-like reflecting layers. That is, they evolve in such a manner that decameter-wavelength radio waves are reflected obliquely back to earth from them over a relatively broad area, and hence illuminate the earth much as a short-wave broadcast station's signals are propagated beyond the horizon. This condition has been effected in two of the fifteen releases in this investigation with such efficiency of illumination that return signals from the

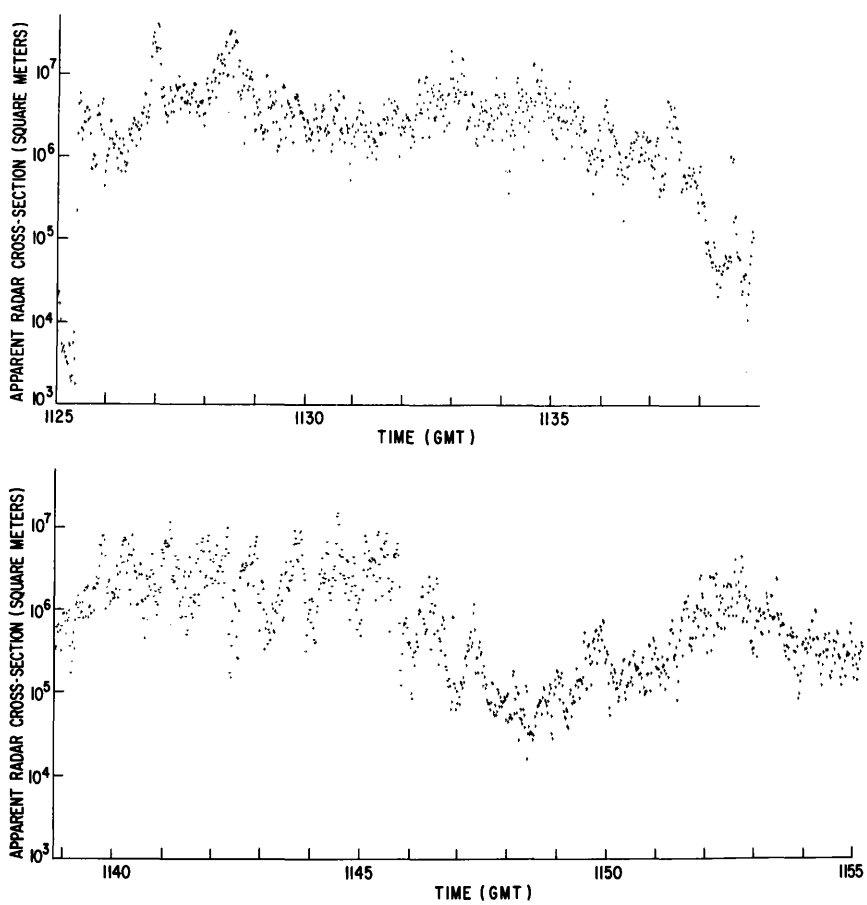


Fig. 10 - Apparent radar cross section vs time for cesium release No. 3, Feb. 14, 1969

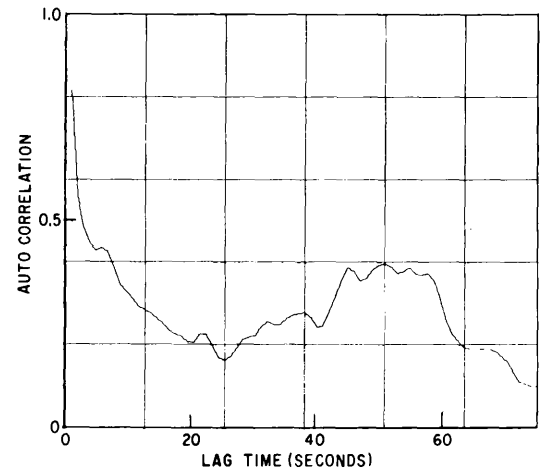


Fig. 11 - Autocorrelation function from apparent radar cross section for cesium release No. 3, Feb. 14, 1969

earth have been received at the radar site via a second plasma cloud reflection. On these occasions the earth-backscattered signals have displayed behavior similar to that which is observed with sporadic-E illumination, and it is believed that these plasma clouds have in fact formed themselves into artificial sporadic-E patches.

Figure 12 is an intensity-modulated doppler shift vs time display of the earth-backscattered signal which was acquired for nearly a half-hour via the plasma cloud described in Figs. 8-11. The time and frequency scales are the same as those in Fig. 8. The earth-backscattered signal begins to appear in Fig. 12 at about 1132 GMT, but it is partially obscured by a spurious spectral component at 0 Hz until about 1136 GMT. It continues to build up in intensity, with gradual slight deviations in doppler shift, until 1159 GMT and then begins to disappear. By 1207 GMT it is once more obscured by the spurious component at 0 Hz.

In contrast to the directly reflected plasma cloud echo in Fig. 8, there is no evidence of periodic modulations in spectral dispersion. Secondly, the total spectral bandwidth is at no time greater than about 2 Hz, whereas in the direct echo it often approaches 10 Hz.

Figure 13 is a computer-processed version of the earth-backscattered signal, similar to Fig. 9. (Notice, however, that only about 7 Hz of the spectral extent are shown in Fig. 13, while 11 Hz are shown in Fig. 9.) The broad spectrum bands shown (those at 1138, 1145 and 1155 GMT are the most apparent) are meteor echoes and can be ignored. The earth-backscattered data show no evidence of the 50-sec modulation in intensity; they also show very little evidence of the longer period variations displayed by the direct echo. The intensity builds up continuously until about 1159 GMT and has a single predominant spectral component at nearly all times. The signal reaches a peak at 1159 GMT (once again, the sudden decrease at about 1200 GMT is an artifact, which has been corrected in Fig. 12) and then begins to decay. Figure 14 is a radar cross-section plot which shows this gradual buildup, and also shows scant evidence of the cyclic amplitude variations which are so apparent in Fig. 10 between 1136 and 1150 GMT. The abrupt dropouts at 1138, 1148, and 1155 GMT in Fig. 10 also are absent from Fig. 14.

It may be concluded that, in the circumstances which lead to formation of a plasma cloud into a sporadic-E-like reflector, the motions which lead to periodic modulation in amplitude and spectral extent take place chiefly in the horizontal direction. (A two-way oblique path from radar to cloud to earth and back again is sensitive only to vertical motions.) Thus the mechanism by which the plasma cloud is formed into such a layer must act so as to spread it pancake-like, rather than isotropically, with a preferred

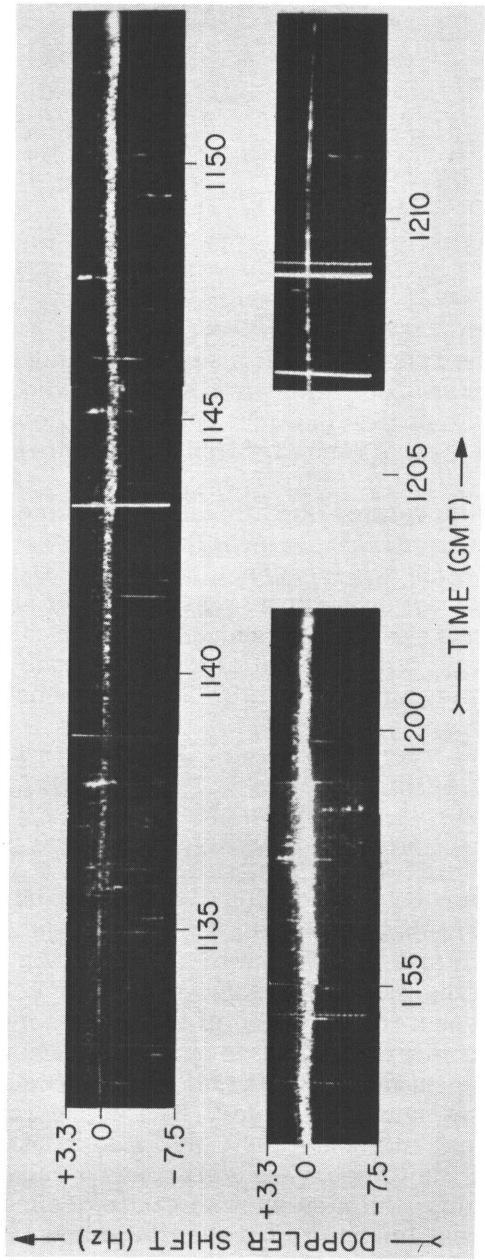


Fig. 12 - Doppler shift vs time for earth-backscattered signal from cesium release No. 3, Feb. 14, 1969

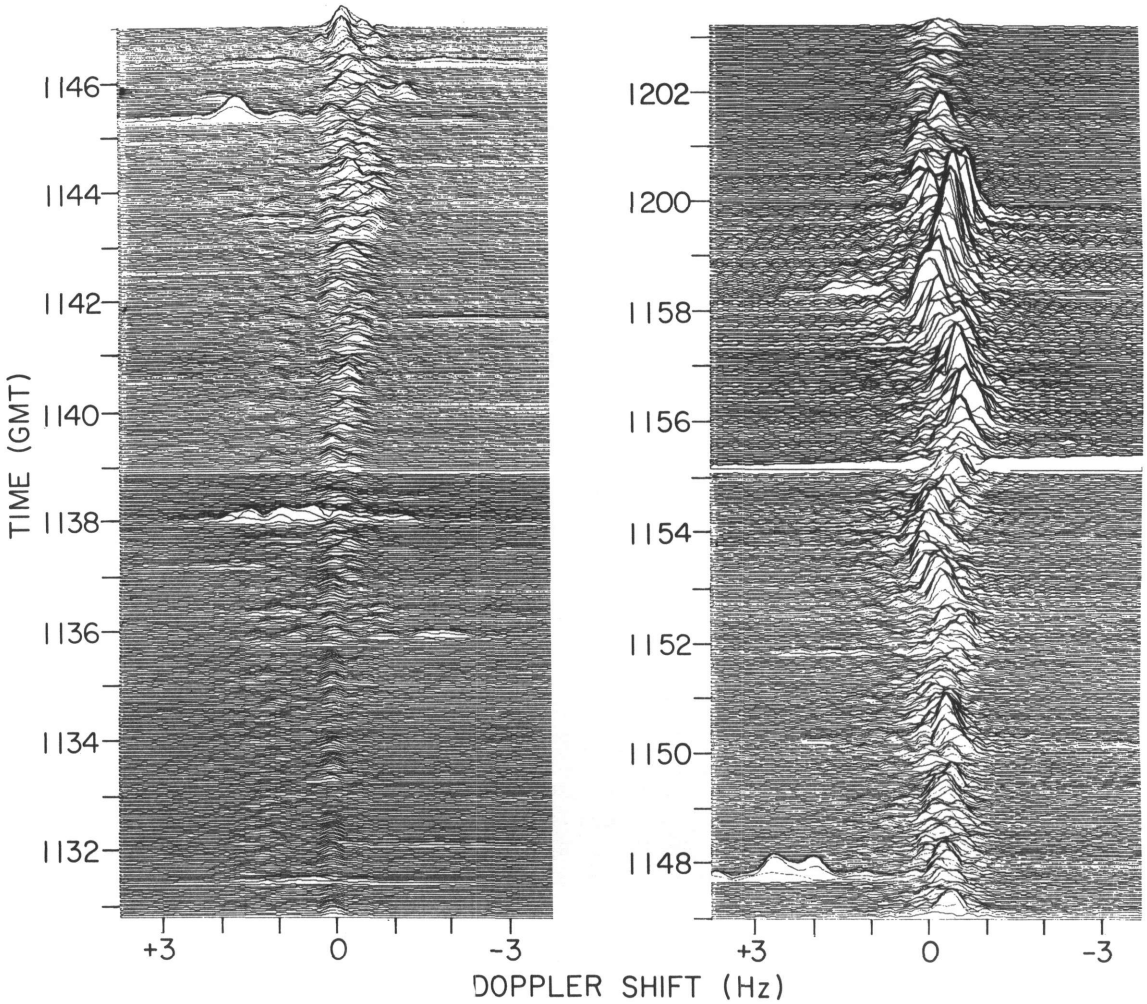


Fig. 13 - Time plot of computer-analyzed signal intensity vs doppler shift for earth-backscattered signal from cesium release No. 3, Feb. 14, 1969

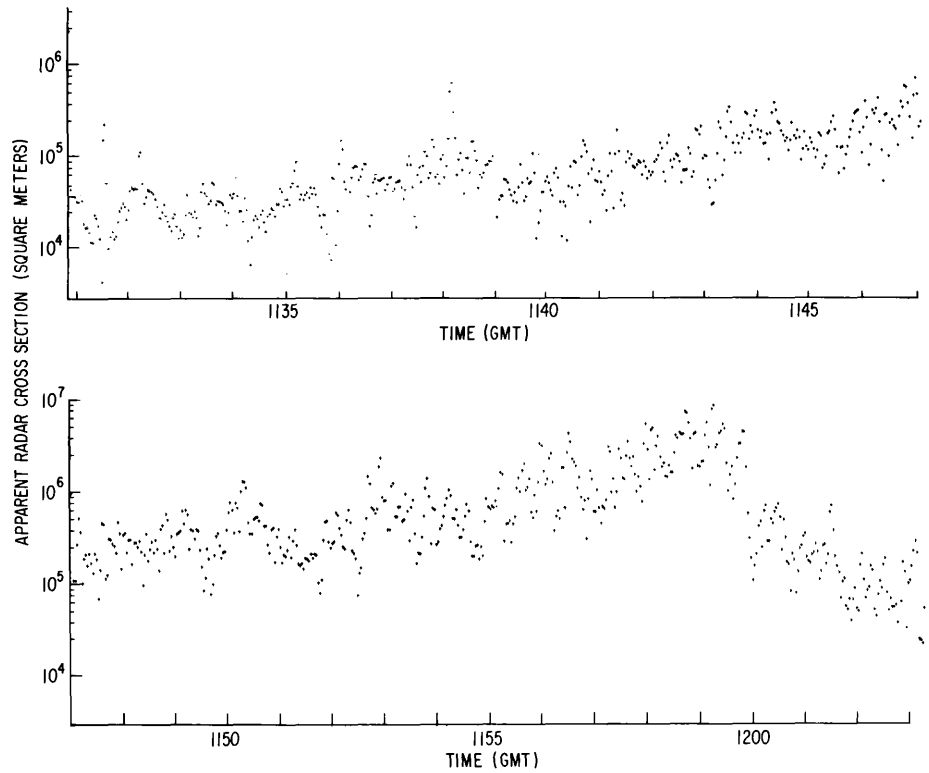


Fig. 14 - Apparent radar cross section vs time for earth-backscattered signal from cesium release No. 3, Feb. 14, 1969

horizontal motion (which is difficult to distinguish, at the 50° northern geomagnetic latitude of Wallops Island, from motions perpendicular to the geomagnetic field). This indication is consistent with the characteristics of naturally occurring sporadic E, which is believed to have a thin pancake-shaped configuration.

## PLASMA CLOUD RADAR ECHO STATISTICS

### Scattering Entity

The cesium cloud is a multiple scatterer. Its doppler spectrum is generally diffuse, indicating that a distribution of velocities (or rates of motion of the effective reflecting surfaces) exists. At times, its doppler spectrum becomes quite discrete, indicating that either the motion has become temporarily ordered (i.e., that the multiple scatterers have a coordinated rate of evolution or motion) or a dominant single scatterer has been formed. The fact that the large, discrete, spectral components rise from the diffuse spectral background extremely rapidly, live for a few seconds, and descend back into a background which appears unchanged, and have an apparent size which often exceeds the observed physical size of the cloud itself, argues decisively against the possibility of such a large dominant single scatterer. It is likely, instead, that these short-lived, discrete, spectral components are indicative of collective behavior in the plasma cloud which temporarily forms nominally the entire cloud into an ordered distribution of scattering centers with phase reinforcement of radar energy backscattered in the direction of the radar. This formation is termed the scattering entity.

A statistical feature of the radar data also bears upon this conclusion and suggests that the plasma cloud motion is ordered to some extent throughout its lifetime. The effective scatterer for decameter radar energy displays certain characteristics which may be ascribed to a collective entity, as indicated by the lognormal character of the radar data.

Figure 15 is a cumulative distribution function determined from radar data. Matched to the data (shown by small symbols) is a straight line which corresponds to lognormal statistics. Over the 60-dB linear dynamic range of the radar receiver (three decades on the abscissa, centered on about 2), the lognormal curve is seen to fit the data extremely well. Attempts to fit Rayleigh and higher order Rice distributions have failed, and it is concluded that the data are indeed lognormal. This circumstance confirms that the effective radar scattering elements are not completely independent (as would be indicated by Rayleigh statistics), and that they do not consist of independent scatterers with certain of them dominant (as would be indicated by higher order Rice distributions).

## Effects of Atmospheric Fluid Properties

It is postulated that the lognormal character of all plasma cloud radar echoes, including even those corresponding to periods when no large discrete components appear above the diffuse spectral background, indicates that the cloud displays some evidence of collective behavior throughout its lifetime. Before this postulate can be justified, a brief description of atmospheric fluid dynamics in the lower E layer must be made, due to the influence of the highly irregular fluid motion in the lower E layer upon plasma cloud behavior. It has been mentioned in the earlier section on "Sporadic E..." that turbulent theories of sporadic E are, at least to some degree, competitive with the wind-shear and

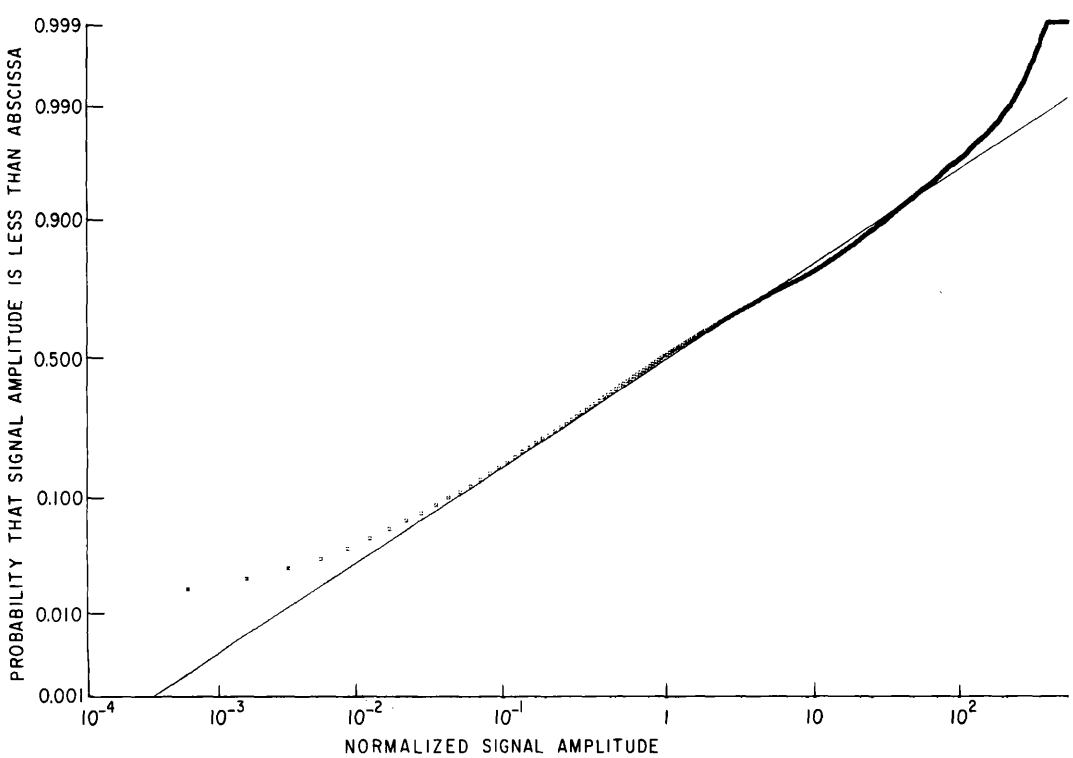


Fig. 15 - Cumulative amplitude distribution of signal components for cesium release No. 2, Sept. 11, 1968

plasma instability theories, and may even be compatible with the latter. It has been considered by many workers (83-86) that neutral turbulence (or, more intuitively, eddy dimensions) of decameter scale size in the lower E layer fall at the short-wavelength extreme of an inertial turbulent subrange as described originally by Kolmogorov (87,88). This type of turbulence is characterized by a cascade of energy transfer in which the largest eddies (i.e., those of a scale at which vorticity is created) continuously feed energy to smaller ones, which in turn pass it on to even smaller eddies, ultimately releasing the energy into viscous dissipation at the small-scale (or short-wavelength) extreme. The limited data available indicate that turbulence in the decameter-wavelength region displays a decorrelation time of a few seconds at most. Blamont and Barat (86) give examples in which maximum possible values of from 2.7 to 5 sec for this decorrelation time were measured. However, the true values could well have been smaller, since these times were measured at minimum resolution. It may be concluded that the effect of neutral turbulence on scattering entities of decameter scale size is random over a period of 2-5 sec, and possibly shorter. The predominant 2- to 6-sec lifetimes of the large-amplitude spectral components (illustrated in Fig. 2) tend to confirm this decorrelation time.

The time separation of radar data samples from which the cumulative probability distributions were constructed, and of which Fig. 15 is typical, is about 2 sec; hence data from one or two sample separations should be independent from the standpoint of neutral turbulence. Furthermore, a typical cloud dimension is between 150 and 500 m, as compared with the typical decameter radar wavelength of 20 m. Thus, spatial resolution is adequate to insure that received data include independent samples from several points on the irregularly shaped cloud.

## Lognormal Statistics and an Analogy

The cumulative probability distributions were constructed from Fourier amplitudes of the radar pulse data, and hence achieved resolution of the spectral components (and, presumably, of spatial structure) as well as of time. The statistical variate then is the size of a scatterer, at a particular time in the cloud's evolution, and moving at a particular velocity.

The lognormal probability distribution pertains to a variate whose logarithm obeys the normal law of probability. Inasmuch as normal statistics arise from a theory of elementary errors combined by addition, then lognormal statistics arise from a theory of elementary errors combined by a multiplicative process. An illustrative development is presented by Aitchison and Brown (89), who refer to Cramer's (90) example of biological organ growth. If the variate is the size of an organ, which can be considered to depend on a large number of mutually independent stimuli acting in sequence, and if the response of the organ to each stimulus is proportional to its current size, then the variate will obey lognormal statistics.

In the case of the cesium plasma cloud data, the variate of spectral amplitude is sampled both in time and in velocity, and hence a somewhat more sophisticated analogy must be drawn. The cesium cloud acts as a diffraction grating in that its scattering pattern is the result of a multiplicative effect of the scattering patterns of all the scattering elements, just as the interference pattern created by a diffraction grating is a multiplicative effect of all its slits. If, in addition, the diffraction grating is composed of randomly distributed slits, then the analogy with the cesium plasma cloud at any one time is made even more complete. For either the plasma cloud or diffraction grating, if samples are taken at random points in space, then their statistics are lognormal. Furthermore, in view of the fact that the scattering elements (or analogous diffraction slits) are distributed randomly, the statistics will still be lognormal if samples are taken at regular

intervals in space, or even if taken at regular intervals of time as the scatterer moves by a single observing position.

Thus far the analogy is a simple one. Now, however, it is noted that the Fourier amplitudes represent amplitudes sampled in a second dimension as well as space (or time); they represent sampling in velocity as well. For lognormal statistics to be expected, then, the velocity of any one scattering element should be multiplicatively related to the velocities of other scattering elements. The circumstances under which such behavior might be expected are simple to visualize in the diffraction grating analogy. Suppose the grating is rotated in time about some axis, rather than simply moved past the sampling point. Then the rate of motion of any slit is related to that of any other slit in proportion to their radial distances from that axis; they will display multiplicatively related velocities. The grating need be considered neither planar nor rigid for this behavior to be maintained, since a proportionate relation of velocities could result from flexion, stretching, twisting, or other such deformations. The lognormal character of the statistics simply requires an ordered deformation. And hence, extending this intuitive picture to the cesium plasma cloud, the lognormal probability distribution of Fourier amplitudes suggests that the evolution of the scattering elements is ordered, with motion in any part of the cloud related to motion in all other parts of the cloud.

It should be emphasized that this interpretation is but one possible analysis of the lognormal character displayed by both the amplitudes and apparent velocities of the radar data. This analysis permits an intuitive picture of the plasma cloud to be visualized, and hence has some merit.

It would be naive to attempt to interpret the lognormal character of the radar data as indicating the actual type of motion or evolution, since changes in scatterer size and shape cannot be visualized in terms of this simple analogy.

# PART III. PLASMA DIAGNOSTICS AND INTERPRETATION OF THE RESULTS

## DYNAMICS OF THE MOTION AND A SURVEY OF POSSIBLE INSTABILITY MECHANISMS

### Fluid Environment

Figure 16 contains profiles of atmospheric number density and pressure for the 70-130 km altitude region, extracted from the "U.S. Standard Atmosphere, 1962." The two curves at first draw closer together with altitude between 70 and 80 km, remain nearly parallel up to about 95 km as the temperature remains nearly constant in this region, and then at higher altitudes diverge at an increasing rate as temperature rises rapidly. In the 90 to 110 km region of concern for this investigation, these quantities decrease by more than an order of magnitude.

Figure 17 illustrates the unique characteristics which result from this variation in pressure, temperature, and density in the lower E layer, and which are responsible for the chaotic behavior which takes place there. The solid curves are collision profiles for particles of molecular mass 29 (the approximate mean molecular mass of particles in this altitude interval, labeled $\nu_{nn}$), and for electrons (labeled $\nu_{en}$) with neutral particles. The ion-neutral collision frequency for the dominant molecular ion (of mass 30) is very nearly the same as that for particles of mass 29 and is in general consistent with the model proposed by Chapman (91) in which the ion-neutral collision frequency $\nu_{in}$ obeys the relation

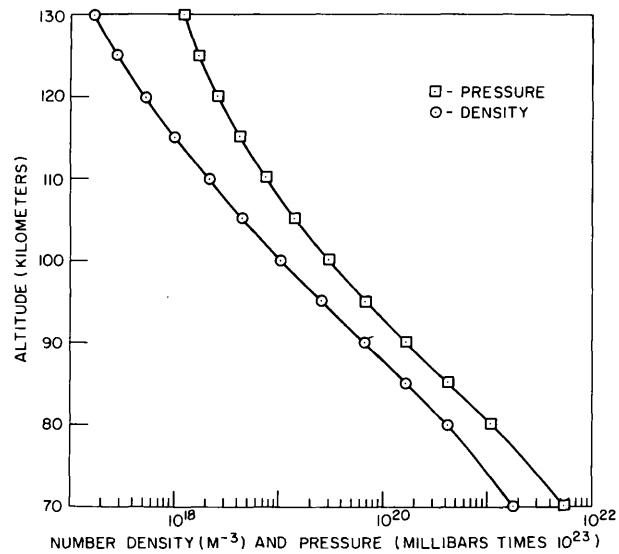


Fig. 16 - Atmospheric number density and pressure vs altitude from "U.S. Standard Atmosphere, 1962"

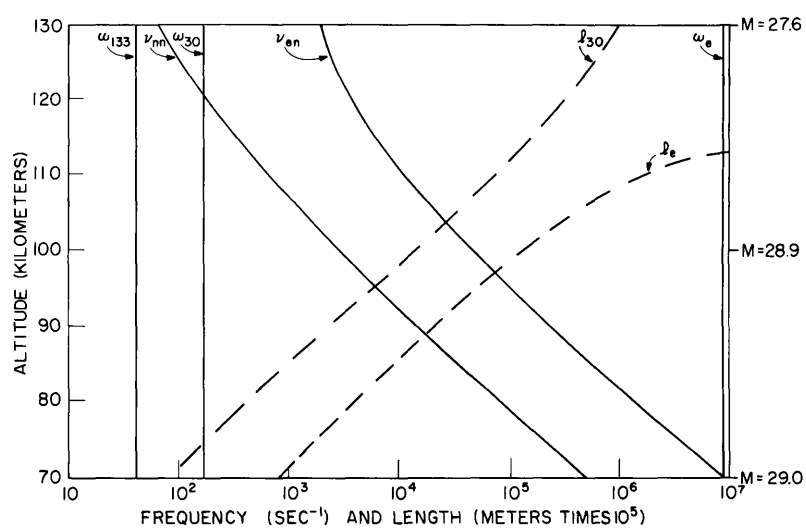


Fig. 17 - Profiles of collision frequency and mean free path for electrons and for ions of molecular masses 30 and 133

$$\nu_{in} = 2.6 \times 10^{-15} \rho_n W^{-1/2}$$

where $\rho_n$ is the neutral particle density in $m^{-3}$, and W is the molecular mass in atomic mass units. Cesium ions of mass 133 would collide with neutrals at about 47% of the rate shown as $\nu_{nn}$ in Fig. 17. The electron-neutral collision frequency is determined from Chapman's model (91) by

$$\nu_{en} = 5.4 \times 10^{-16} \rho_n T^{1/2}$$

where T is the temperature in degrees Kelvin. Thrane and Piggott (92) indicate that measured values of this quantity are in general agreement with the model at altitudes below 90 km. They state that measured electron-neutral collision frequencies frequently exceed the model values at higher altitudes, however, and suggest that this behavior may be explained by electron temperatures in excess of the neutral-gas temperature. For such a circumstance to exist, the electrons could not be in thermal equilibrium with their environment, although observed and predicted mean electron lifetimes would seem to allow them to reach thermal equilibrium. This apparent contradiction must be considered as yet unresolved. For the purposes of this investigation, the model values will be used, and it will be understood that they may be underestimates by a factor of as much as two.

Also included in Fig. 17 are vertical bars which indicate the gyrofrequencies of monovalent ions of masses 30 (labeled $\omega_{30}$) and 133 (labeled $\omega_{133}$) and of electrons (labeled $\omega_e$) in the geomagnetic induction field of $6\times10^{-5}$ webers/m$^2$. The $\nu_{nn}$ curve has values well above $\omega_{133}$ and $\omega_{30}$ for nearly the entire altitude region shown, while the $\nu_{en}$ curve falls below $\omega_e$ everywhere. Thus, electron motions are predominantly governed by the geomagnetic field, while at altitudes up to 120 km the ion motions are governed by collisions with neutrals.

The dashed curves are profiles of mean free path for ions and electrons, labeled $\ell_{30}$ and $\ell_e$, respectively. These profiles were calculated simply by dividing the thermal velocity of each constituent by its collision frequency with neutral particles. Due to the fact that both of these quantities display a $W^{-1/2}$ dependence, the mean free path for cesium ions is the same as that for ions of mass 30 at the same temperature.

Along the right-hand edge of Fig. 17 is an indication of the mean molecular mass with altitude. The predominant neutral constituents are $N_2$, $O_2$, NO, and O, with an increasing proportion of O with altitude. The predominant ionic species are $O_2^+$ and $NO^+$.

The region between 90 and 110 km is of principal concern for this investigation. It is in this interval, known as the dynamo region because of the strong electric currents which flow in it, that the principally hydrodynamic motions of the lower atmosphere gradually give way to the principally magnetohydrodynamic (MHD) motions which predominate in higher regions. Evidence indicates that the mixed hydrodynamic-MHD motions which characterize this region display a highly irregular behavior, as has been stated above. Phenomena which occur in this altitude region include (a) the flow of the equatorial electrojet, (b) the formation of sporadic-E layers, and (c) the appearance of aurorae.

## Equations of Motion

The purpose of this survey is to select a likely mechanism for instability in the cesium plasma cloud. Identification of a probable instability mechanism must rest upon the growth rate, apparent characteristic size or wavelength, and apparent rate of motion as discerned from radar measurements. For this reason, the survey has been based upon a perturbation treatment which has utilized harmonic analysis of the linearized equations of motion. Characteristic lengths, growth rates, and phase velocities have been estimated from the resultant dispersion relations.

Beginning with the Boltzmann equation, there are two possible approaches. Farley (93), in an analysis of plasma instabilities in the equatorial electrojet, allows small perturbations in the distribution function, magnetic induction, and electric field, and conducts his analysis in those quantities. Farley's analysis concerns a two-stream plasma instability, and hence he perturbs the velocity distribution of the constituent particles.

Nearly all other workers precede their perturbation analysis with extraction of the first two moments of the Boltzmann equation; this latter approach will be followed in this investigation.

The equation of continuity from the first moment is

$$\frac{\partial N^s}{\partial t} + \nabla \cdot (N^s \mathbf{v}^s) = S^s_{coll} \tag{1}$$

where $S^s_{coll}$ is the rate at which particles of species $s$ are created due to collisions, and $N^s$ is the number density of particles of species $s$. The rate $S^s_{coll}$ includes all ionization, attachment, and recombination processes; as indicated by the discussion of chemistry above, this term is so small as to be negligible. The momentum equation results from the second moment, and is best written in component notation as

$$N^s m^s \left( \frac{\partial}{\partial t} v_i^s + v_j^s \frac{\partial v_i^s}{\partial x_j} \right) + \frac{\partial \psi^s_{ij}}{\partial x_j} - N^s q^s (E_i + \epsilon_{ijk} v_j^s B_k) = (A_i^s)_{coll}$$

where repeated indices indicate summation, $(A_i^s)_{coll}$ represents the rate of change of momentum due to collisions, and $\psi^s_{ij}$ is the pressure tensor. $(A_i^s)_{coll}$ is written in terms of a collision frequency $\nu_{sN}$ of particles of species $s$ with neutral particles as

$$(A_i^s)_{coll} = m^s N^s \nu_{sN} (v_i^N - v_i^s) .$$

The quantity $v_i^N$, representing the velocity of the neutral gas, is neglected in analyses which are directed toward investigating the effect of electromagnetic processes, but preserved in those whose object is an analysis of neutral-wind effects. The pressure tensor $\psi^s_{ij}$ is defined to be a scalar quantity and to represent the rate at which momentum is transferred across a surface moving at velocity $v_i^s$. If it is assumed in addition that particles of species $s$ are in collisional equilibrium with themselves (have a Maxwellian velocity distribution), and hence may be assigned a temperature $T^s$, then the remaining constitutive relation necessary for solution is the perfect gas law

$$P^s = N^s k T^s$$

where $P^s \delta_{ij} = \psi^s_{ij}$ is the hydrostatic pressure, and $k$ is Boltzmann's constant.

With these definitions and simplifications, the momentum equation may be written in vector form as

$$N^s m^s \left( \frac{\partial \mathbf{v}^s}{\partial t} + (\mathbf{v}^s \cdot \nabla) \mathbf{v}^s \right) + \nabla P^s + N^s q^s (\mathbf{E} + \mathbf{v}^s \times \mathbf{B}) = -N^s m^s \nu_{sN} (\mathbf{v}^N - \mathbf{v}^s) . \tag{2}$$

The instabilities of interest for this investigation have frequencies $\omega$ much less than $\nu_{eN}$ or $\nu_{iN}$, and hence the inertia term in Eq. (2) may be neglected. Further, the Debye length

$$k_D^{-1} = \left( \frac{\epsilon_0 k T}{N^e e^2} \right)^{1/2}$$

is typically a fraction of a centimeter in the altitude region of interest, while the instabilities are of many meters in wavelength; hence the assumption of quasi-neutrality

$$N^e \approx N^i \approx N ,$$

and the quasi-static assumption

$$\mathbf{E} = -\nabla\phi ,$$

may be made. In most cases, it is assumed in addition that the collision frequencies and the temperature do not vary spatially; hence

$$\nabla P^s = kT^s \nabla N .$$

Defining a particle flux $\Gamma^s = N^s \mathbf{v}^s$, the equation of motion may be written

$$\frac{kT^s}{m^s} \nabla N - \frac{Nq^s}{m^s} (\mathbf{E} + \mathbf{v}^s \times \mathbf{B}) = -\nu_{sN} \mathbf{\Gamma}^s . \tag{3}$$

Defining the coefficient of free diffusion by

$$D^s = \frac{kT^s}{m^s \nu_{sN}} ,$$

the (longitudinal) mobility by

$$\mu^s = \frac{q^s}{m^s \nu_{sN}} ,$$

and the gyromagnetic frequency by

$$\omega_s = \frac{q^s B}{m^s} ,$$

the equation for particle flux may be written

$$\mathbf{\Gamma}^s = -D^s \nabla N + N\mu^s \mathbf{E} - \frac{\omega_s}{\nu_{sN}} \hat{e}_B \times \mathbf{\Gamma}^s \tag{4}$$

where $\hat{e}_B$ is a unit vector in the direction of the magnetic field $\mathbf{B}$. The continuity equation may be written

$$\frac{\partial N}{\partial t} + \nabla \cdot \mathbf{\Gamma}^s = 0 . \tag{5}$$

### Instability Mechanisms Related to the Thermodynamics of the Blast Wave

The explosive release mechanism of the cesium plasma cloud results in the formation of a rapidly expanding high-temperature gas bubble. This bubble, as described by Davis and Moore (94) grows within 4 to 8 sec to a radius of some hundreds of meters.

Initial electron densities of greater than $10^{14}$ $m^{-3}$ are encountered. Decameter- and meter-wavelength radar data acquired during this 4- to 8-sec period indicate that the blast-wave phase is most properly described by Brode's model of spherical high-explosive detonations (80). Some results of the earlier investigation (94) are of interest because they imply a set of initial conditions for later phases of motion.

Figure 18 contains plots of relative radar cross section vs time for four cesium-seeded high-explosive detonations. Each partially connected row of dots contains an indication of the peaks and nulls of apparent radar cross section for the first 10 sec following each release. About 10 dB of dynamic range are represented on each curve, although the data are not intended as an indication of absolute radar target size. The curves are arranged on a vertical altitude scale to indicate the rate at which features on the various curves appear to depend on altitude. It is evident that peaks and nulls occur less rapidly with increasing altitude. The solid lines labeled $P_1$, $P_2$, and $P_3$ indicate the altitude variation in the times of peak radar cross section expected from a sequence of shock-induced undulations in the contact surface as predicted by Brode's model. The dashed lines labeled $N_1$, $N_2$, and $N_3$ indicate the expected altitude-dependence in times of minimum radar cross section (or nulls). This altitude dependence is simply a consequence of the pressure/density variation with altitude illustrated in Fig. 16. It is apparent that the four curves show striking confirmation of the expected altitude dependence, at least in the positions of the first two peaks and nulls. The important consequence of this circumstance is that the value of pressure necessary at each altitude to match the expected behavior to the observations is one-half the value (see Fig. 1) which has been determined by most measurements at that altitude.

It has been suggested that the above disparity is an indication of anisotropy of expansion in the blast wave, and that the effect of the geomagnetic field upon the ionized detonation products is responsible for this anisotropy (94). Because the radar energy impinges upon the expanding plasma bubble from a direction more nearly along the geomagnetic field than perpendicular to it, the effect of magnetic pressure acting on the bubble would tend to elongate it toward the observer, and hence to delay encounters of the sequence of shock waves with the contact surface relative to an isotropically expanding case. Such a delay in the sequence of radar cross-section fluctuations would explain the disparity between directly measured pressures and the cesium-seeded blast-wave data. In view of this possible explanation of the radar data, it has been suggested that the expanding plasma bubble at least partially excludes the geomagnetic field in the blast-wave phase.

One further result is of interest. Figure 19 contains radar cross-section measurements from a cesium-seeded detonation in which data acquired by decameter-wave radar on an antenna polarized parallel to the transmitting antenna (shown as connected squares) are compared with those acquired on a cross-polarized antenna (shown as connected circles). Also shown as a dashed line on Fig. 19 is a tracing of meter-wave data which, unfortunately, were subject to receiver saturation at a radar cross section of $5 \times 10^4$ $m^2$ until nearly 8 sec after the detonation. It should be noticed that the positions of peaks and nulls in the decameter-wave data are highly correlated until about

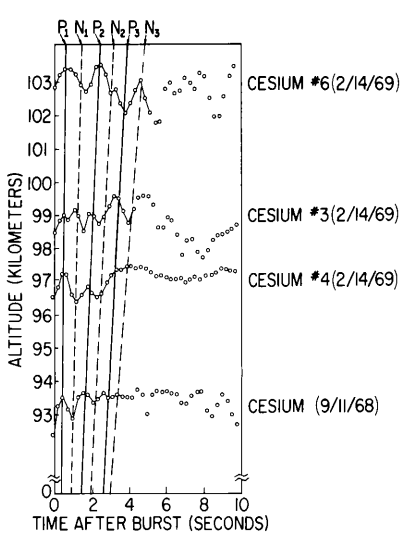


Fig. 18 - Plots of relative radar cross section vs time for four cesium releases during Phase I, distributed on vertical scale in relation to release heights

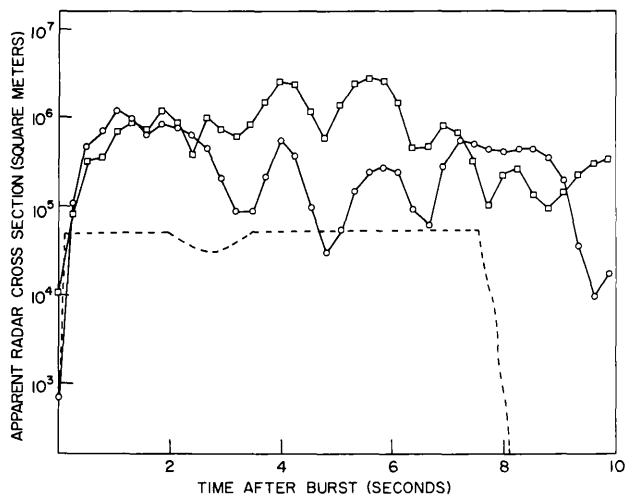


Fig. 19 - Apparent radar cross-section vs time for co- and cross-polarized decameter-wave radar data (shown as solid lines connecting squares and circles, respectively) and meter wave data (shown as dashed line) for Phase I of cesium release No. 1, Feb. 14, 1969

7 sec after the detonation, when they become decorrelated. At the same time, the previously saturated meter-wave data drop by several orders of magnitude, presumably from a level approximately the same as the decameter-wave data, in less than 1 sec.

The high degree of correlation between the cross- and co-polarized decameter-wave data during the first 7 sec indicates that no rotation of the plane of polarization due to the Faraday effect occurs during this period. Hence, either no penetration of the magnetic field into the ionized region from which the radar energy is reflected occurs, or this energy is reflected in such a thin shell that no significant polarization rotation takes place. It is probable that the meter-wave data result from the latter circumstance. The extremely rapid decrease in meter-wave radar cross section at the presumed end of the blast-wave phase is too fast to be reasonably explained by diffusion of a previously overdense concentration, and is more credibly interpreted as resulting from sudden disappearance of a sharp electron density gradient as the detonation wave dissipates. Thus the meter-wave data are probably explained by partial reflections from an electron density gradient. The decameter-wave data show no such sudden decrease, however; it is therefore suggested that their behavior is best explained by some combination of partial and total reflection, in which at least some contribution may be made by a thin overdense shell of electrons until 7 sec after the detonation. At this time the partially excluded magnetic field begins to penetrate the reflecting shell, which also begins to diffuse.

With this description of the blast-wave phase, it is necessary to investigate possible instability mechanisms which can occur during the expansion of the plasma bubble, and also during the period immediately thereafter, before it reaches thermal equilibrium with its environment. It should be added that such an investigation is also necessary to ascertain whether some other explanation is possible for the radar data which were interpreted in terms of Brode's model; that is, if an instability mechanism is found to be possible during the expansion phase, and would lead to the magnitudes and periodicities of the radar cross-section fluctuations observed, then their interpretation as manifestations of shock-wave perturbations of the contact surface would be suspect.

The plasma bubble, at its instant of formation, is comprised of high-density gases at a temperature of several thousand degrees Kelvin and several hundred times ambient pressure. By the time the contact surface has expanded to its maximum radius, and slightly before it is first buffeted by a shock wave (actually the second shock, since the first one precedes the contact surface), its mean temperature is about three times that of the ambient temperature of 200° to 250°K (13). By this time (less than 1 sec for most of the cesium-seeded detonations discussed here), pressure equilibrium has been reached between the detonation-produced gas bubble and the ambient atmosphere. Due to the difference in temperature, however, the mean density of the fully expanded bubble is about one-third that of the environment.

An obvious candidate instability mechanism during this initial period is the purely hydrodynamic Taylor instability (95). At the upper surface of the bubble, where a dense gas lies above a less dense one in the earth's gravitational field, Taylor's analysis indicates that a growth rate $\alpha$ for instabilities of wave number $K$ is given by

$$\alpha = \left[ Kg \frac{\rho_2 - \rho_1}{\rho_2 + \rho_1} \right]^{1/2}$$

where $g$ is the acceleration of gravity, $\rho_2$ is the density of the dense fluid, and $\rho_1$ is the density of the less-dense fluid. Assuming that instabilities generated on the top of the plasma bubble can be detected by radar either through the bubble or after propagating along the interface to its lower surface, it may be hypothesized that irregularities of the order of 20 m would be the dominant contributors to the decameter-wavelength radar data. Letting $\rho_2 \approx 3\rho_1$, there results a growth rate of 1.16 $sec^{-1}$ for instabilities of this size. While this figure is enticingly close to the fluctuation rates of up to 1 $sec^{-1}$ in Fig. 18, it does not allow the altitude dependence which is so evident in those data. It should also be noted that the meter-wave radar data, which should display a characteristic fluctuation rate, due to Taylor instability, of about three times that of the decameter-wave data, give no indication of such behavior.

The plasma equivalent of the Taylor instability has been analyzed by Kruskal and Schwarzchild (96) for a perfectly conducting completely ionized plasma, and by Furth, et al. (97) for a plasma of finite conductivity. This type of instability requires a jump in magnetic induction, at the boundary between two plasmas, of great enough magnitude to support the denser fluid above the less-dense one against gravity. Thus evaluation of its likelihood depends upon the partial exclusion of the geomagnetic field from the cesium plasma bubble.

Based upon the decameter-wave radar data described above and reported by Davis and Moore (94), it may be assumed that magnetic pressure acting transverse to the geomagnetic field is responsible for the anisotropic bubble expansion. If it is assumed that all particles of the detonation-produced gases have the same initial energy, then it may be estimated that they do the same amount of work in the expansion phase. If the equivalent pressure indicated by the radar data for isotropic expansion at a point on the bubble obliquely along the magnetic field from the detonation point is one-half of the estimated ambient pressure, then the pressure at a point directly across the magnetic field may be assumed to be about twice the ambient value. Thus, as a crude estimate, the magnetic pressure required at 100 km altitude to explain the radar observations is approximately $10^{-4}$ mbar, or 0.01 $N/m^2$. The difference in magnetic induction necessary to provide this pressure is determined from

$$P_B = B^2/2\mu_0 = 0.01 \ N/m^2 \ ,$$

which yields $B = 1.5\times10^{-4}$ w/m$^2$. Thus, in order for the radar data to be accounted for by magnetic field-associated anisotropy of expansion, there must be created in the detonation a magnetic induction field of nearly three times the ambient field around the plasma bubble.

To determine whether the cesium plasma bubble is capable of conducting a high enough boundary current to permit such a magnetic induction jump, it may be assumed that current flows about the ellipsoidal bubble in a ring of perhaps five-electron-mean-free-paths thickness (about 5 m at 100 km altitude). Approximating the differential form of Ampere's law

$$\nabla\times\mathbf{B} = \mu_0\mathbf{J}$$

by the relation

$$\Delta B_z/\Delta r = \mu_0 J_\phi \ ,$$

with

$$\Delta B_z = 1.5\times10^{-4}\ \omega/\mathrm{m}^2 \quad \text{and} \quad \Delta r = 5\ \mathrm{m}\ ,$$

gives a current density of $J_\phi \approx 24$ A/m$^2$. The electron velocity at a charge density of $2\times10^{14}$ electrons/m$^3$ necessary to yield this current is about $7.5\times10^5$ m/sec. This value is greater than the thermal velocity of electrons at the expected mean bubble temperature of 700°K. However, the repeated shocking of the electrons in the outer region raises their temperature to greater than 1000°K (13) and probably results in a much greater degree of ionization than in the rest of the bubble. Further, the assumption that this ring current flows in a belt only five-electron-mean-free-paths thick is only conjecture. If a greater belt thickness is allowed, the current density and associated charge velocities could be a good deal less.

Based upon these crude estimates, it can be concluded that the apparent anisotropy of bubble expansion might be due to interaction with the geomagnetic field. As one final exercise, a calculation may be made of the magnetic induction field which exists in the expanded plasma bubble when enough magnetic flux is swept into a thin shell on the boundary of the bubble to yield the required magnitude of magnetic induction. The fully expanded bubble at 100 km altitude has an apparent radar cross section of about $4\pi\times10^4$ m$^2$. If the axial ratio is taken to be consistent with a two-to-one effective pressure anisotropy, then the minor axis will be about 356 m. Taking a current ring radius of 178 m for $J_\phi$ and assuming the magnetic induction within the bubble to be constant, the magnetic induction in the bubble is about $0.25\times10^{-5}$ W/m$^2$ in the opposite direction to the undisturbed induction field of about $6.0\times10^{-5}$ W/m$^2$.

Thus, if these estimates are valid, a conceptual model may be constructed in which the hot plasma bubble is bounded by an intense diamagnetic ring current which results in near removal of the interior magnetic field, and in a highly concentrated shell of magnetic induction at its boundary.

The analysis by Furth et al. (97) is, at least outwardly, appropriate to this survey, because the nonzero resistivity which distinguishes their treatment from Kruskal and Schwarzchild's (96) is a prominent feature of charged-particle motion in the 90-110 km altitude region. The mode which they term a "gravitational interchange" mode (because it owes its existence to the interchange of gravitational potential energy and fluid kinetic energy, as does Taylor's instability) is of concern here. The high-gravity extreme in Furth's treatment, however, is appropriate for the environmental conditions and instability wavelength appropriate to this investigation, and in this extreme the Kruskal and Schwarzchild approach is probably equally valid. Accordingly, the latter's instability criterion is

$$2\left(1 + \frac{P_{amb}}{P_B}\right) K_{\parallel}^2 < h\,|K_{\perp}|$$

where $P_{amb}$ and $P_B$ are the pressure in the ambient atmosphere and that due to the magnetic field, respectively, $K_{\parallel}$ and $K_{\perp}$ are the instability wave number components parallel and perpendicular to the magnetic field, and $h$ is an inverse scale parameter for mass density variation in the plasma. Selecting $P_{amb} = P_B$, $K_{\parallel}$ appropriate to a plasma bubble of 455 m length, and $K_{\perp}$ appropriate to the 20-m decameter radar illumination, there results the requirement that

$$h > 2.44 \times 10^{-3} m^{-1}$$

or the atmospheric scale height $h^{-1}$ must be less than 400 m. This parameter is given as

$$h^{-1} = \frac{P_0}{g\rho_0}$$

Since the plasma bubble is at about three times ambient temperature (and hence the quantity $P_0/\rho_0$ is about three times that of the ambient), the quantity $h^{-1}$ must be larger than the normal value of about 6 km for 100 km altitude. Thus the Kruskal-Schwarzchild instability is probably not possible.

## Instability Mechanisms which Require Anisotropy in the Velocity Distribution

Most instabilities which rely upon anisotropy in velocity distribution are of only academic interest here because their phase velocities are typically near the acoustic velocity of the medium. This quantity is several hundred meters per second at 100 km altitude, and would yield radar doppler shifts many times the observed values of less than 10 Hz. However, the success which the two-stream instability described by Farley (93) has met in explaining sporadic-E irregularities in the equatorial electrojet demands that the distinction between that case and the present investigation be made clear.

Farley's analysis is based, in part, upon the same circumstance that is assumed to prevail in the region studied in this investigation — the narrow interval of altitude in which conductivity is adequate to support the flow of substantial electric current. In the equatorial region, where the magnetic field is nearly horizontal, current flow (also horizontal, but across the field) gives rise to a vertical Hall current. However, the rapid decrease in conductivity with altitude just a few kilometers above and below the 100-km level prohibits this current from flowing freely and creates a vertical electric polarization field. This field, in turn, interacts with the horizontal magnetic field to enhance current flow horizontally across the magnetic field. The equatorial electrojet current which results is estimated to flow at velocities as great as 500 m/sec according to Farley, and exists only within 2° or 3° of latitude of the geomagnetic equator. The two-stream instability arises from the circumstance that this current flows faster than the ion thermal velocity. The instability which results has a phase velocity of approximately the same magnitude and direction.

At temperate latitudes, the tilted character of the geomagnetic field prevents the self-enhancing feature of the equatorial electrojet from operating, and the two-stream instability cannot be triggered by normal ionospheric currents. It might be argued that the rapid expansion of the cesium plasma bubble, which takes place within the first second or so after detonation, and the intense ring current, which has been postulated as

encircling the bubble until it achieves pressure equilibrium after 4 to 8 sec, could constitute the proper streaming current for this instability. However, the fact that the radar data display no doppler-shifted spectral components sufficiently displaced from that of the stably expanding plasma bubble confirms that no such instability takes place.

The remaining possibility is that, at any time in the plasma cloud's lifetime, a stream of energetic electrons could impinge upon it from, say, the direction of the sun and trigger an instability. However, because any such particle flux would be constrained to flow along the geomagnetic field, it would not provide the proper geometric conditions for the two-stream instabilities.

Kadomtsev and Nedospasov (98) and Hoh (99) have analyzed instabilities in a cylindrical plasma column aligned along a magnetic field when a longitudinal current flows through it. This case would correspond to the cesium plasma cloud being struck by a stream of solar particles. In Hoh's treatment it is demonstrated that a helical perturbation of plasma density would, due to the difference between the electron and ion Hall mobilities, create an azimuthal space-charge field whose effect on radial electron drift would tend to increase the perturbation. This instability relies on an axial electric field to "lift" the electron component of the helical perturbation, and hence combat the stabilizing effect of diffusion by accentuating the azimuthal electric field. The axial electric field is, of course, created by the axial flow of current. However, this instability can exist only for wavelengths much larger than the radius of the container (in the present investigation, this radius would be the hundreds of meters radius of the plasma cloud), and hence cannot correspond to the decameter-wavelength radar data. The instability criterion postulated both by Hoh and by Kadomtsev and Nedospasov may be expressed as

$$K_1 x^4 + F_1 x^2 + G_{d1} + G_{r1} \leq 0.163\, m \left[ \frac{v_{ez} R \mu_e x}{\alpha_0 D_e \mu_i} \right]$$

where

$$K_1 = 0.87/y\,, \quad F_1 = (0.9 + 0.56y)/y(1+y)\,, \quad y = \mu_i \omega_e^2 / \mu_e \nu_{eN}^2$$

$$G_{d1} = \frac{0.21}{y} \left( \frac{1 - 0.16y}{1 + y} \right), \quad G_{r1} = 0.082 \frac{\mu_e}{\mu_i} \left( \frac{1}{1 + y} \right),$$

and

$$x = \frac{KR\omega_e}{\alpha_1 \nu_{eN}}$$

where $\mu_i$ and $\mu_e$ are the longitudinal ion and electron mobilities, respectively, $\omega_e$ and $\nu_{eN}$ are the electron gyromagnetic and collision frequencies (the latter with neutrals) respectively, $D_e$ is the coefficient of free diffusion for electrons, $\alpha_0$ and $\alpha_1$ are, respectively, the first roots of the zero- and first-order Bessel functions

$$J_m \left( \alpha_m \frac{r}{R} \right),$$

$R$ is the radius of the container, $K$ is the instability wavenumber, and $v_{ez}$ is the electron streaming velocity along the earth's magnetic field.

For the cesium plasma cloud at 100 km altitude, the values of the parameters are

$$\omega_e = 10^7 \text{ sec}^{-1} ,$$

$$\nu_{eN} = 4 \times 10^4 \text{ sec}^{-1} ,$$

$$\mu_e/\mu_i = \frac{1}{3} \times 10^4 ,$$

and

$$D_e = 7.5 \times 10^4 \text{ m}^2/\text{sec (after temperature equilibrium)} .$$

Letting $R = 200$ m, and selecting $K = 1/R$ as the largest wavenumber for which the instability is likely to be possible, the required electron streaming velocity is $9.5 \times 10^3$ m/sec for the $m = 1$ mode. The necessary longitudinal electric field is only 2.14 V/km. The rotational velocity of the electron helix is 0.157 $\text{sec}^{-1}$. Hence the helical instability would be expected to require only moderate electric field strengths and to be characterized by long wavelengths (hundreds of meters) and slow rotation rates (tenths of Hertz).

While this type of instability is unlikely to be responsible for the decameter-wave radar data (which correspond to instability wavelengths of a few tens of meters, and whose spectral behavior suggests growth and rotation rates of a few Hertz), it could certainly be important in the larger-scale motions of the plasma cloud and might be discernible in photographs of resonance-scattered light from the ions in the cloud. Cesium has no intense resonance lines in the visible spectrum (the brightest one is at 8521 Å), and no cloud photographs are available for the releases conducted in this investigation.

Figure 20 is a photograph taken during the 6-kg barium release previously discussed in the first section of Part II. The barium cloud was released at dusk and at an altitude of 102 km. Decameter-wavelength radar data displayed similar evidence of plasma instabilities in this cloud as in the cesium clouds, and it is believed that the two different materials and release mechanisms (the barium was not mixed with high explosive, but was burned in a thermite mixture with cupric oxide, which resulted in a slightly slower reaction rate and slightly lower temperature) did not materially affect the plasma cloud composition at the time this photograph was made (about 50 sec after the release). The cloud shown in Fig. 20 was photographed in a resonance line of the barium ion and is presumed to represent the configuration of the ion/electron pairs in the cloud. It is oriented roughly along the magnetic field (indicated by the six parallel lines) and has a length of about 5 km. This multiple-spiral character was seen to grow out of an initially ellipsoidal bubble, somewhat smaller than the knoblike ring at the top of the picture, in a period of a few tens of seconds. During this same period, but not obviously associated with its development, decameter-wavelength radar data showed pronounced evidence of the plasma instabilities which are the subject of this investigation. Figure 20 is presented to suggest that a larger-scale process, such as the helical instability discussed here, may be operative simultaneously.

## Instability Mechanisms Dependent Upon Plasma Inhomogeneity

There exist possible instabilities which depend on interactions between a plasma density gradient and a magnetic or electric field (or both). Due to the importance of collisions in the altitude region of concern for this investigation, only the dissipative type need be considered. Timofeev (100) has analyzed what he terms a "dissipative-drift" instability, in which a plasma density gradient exists perpendicular to the direction

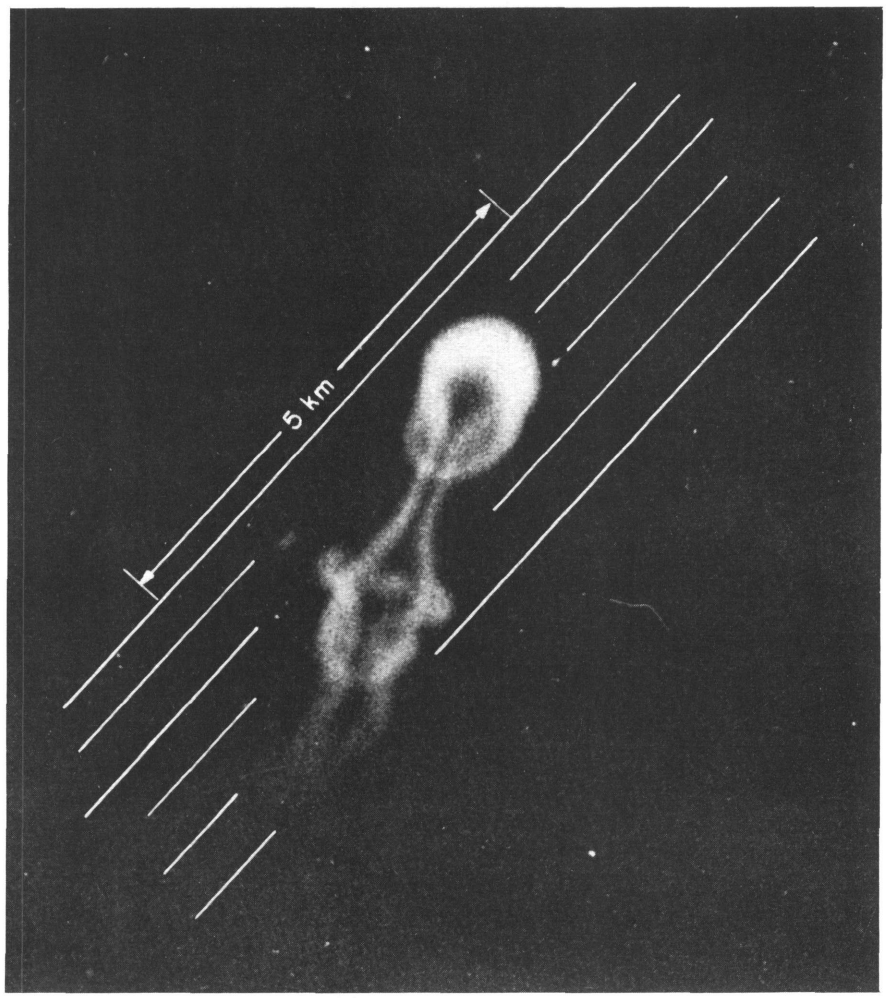


Fig. 20 - Photograph of barium cloud, Oct. 4, 1967, about 50 sec after release, showing direction of geomagnetic field

of the magnetic field. As has been pointed out by Self (101), the energy for this instability arises from the potential energy of the inhomogeneous plasma and not from kinetic energy of the drifting particles due to the electric and magnetic fields. The analysis of this instability differs slightly from that begun above, in the subsection on "Equations of Motion," in that the inertia term is not neglected in the equation for ion motion. Once again, this mechanism may be of only academic interest because it is found that the phase velocity of the instability is greater than the ion thermal velocity. The conditions under which it can occur are critically dependent upon the relation of the characteristic dimension of the instability to the ion mean free path and the ion Larmor radius. Timofeev defines the parameters

$$\xi = \ell_i (1/N)(\partial N/\partial r)$$

and

$$\eta = \omega_i/\nu_{in}$$

where $(1/N)(\partial N/\partial r)$ is a characteristic length of the plasma inhomogeneity, and the other parameters have their usual meaning. Figure 21 is a sketch of Timofeev's instability

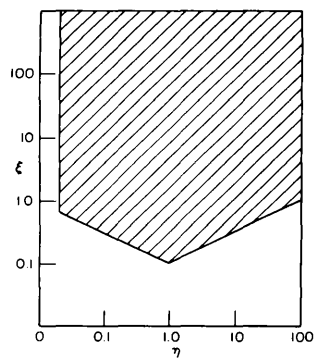


Fig. 21 - Sketch of Timofeev's diagram for dissipative-drift instability

diagram in which the cross-hatched region indicates instability. For the cesium plasma cloud at 100 km altitude, the pertinent values are

$$\frac{1}{N}\frac{\partial N}{\partial r} \approx \frac{1}{200}\ \mathrm{m}^{-1} ,$$

$$\nu_{in} \approx 1.3 \times 10^{3}\ \mathrm{sec}^{-1} ,$$

$$\omega_i \approx 45\ \mathrm{sec}^{-1} ,$$

and

$$\ell_i \approx 0.15\ \mathrm{m} ,$$

from which

$$\xi = 7.5 \times 10^{-4}$$

and

$$\eta = 46$$

The plasma is well out of the instability region and could only be brought into instability if the plasma density gradient were made three orders of magnitude smaller. This circumstance would require the density gradient to be of the same magnitude as the ion mean free path, which is clearly unreasonable.

The prominent remaining candidate is an instability in which crossed electric and magnetic fields interact with a plasma inhomogeneity, leading to unlimited growth of a density perturbation. This mechanism has been treated for laboratory plasmas by Simon (102) and Hoh (103), and for conditions appropriate to the normal E layer by several others (104-113). It results from Hall or Pedersen drift of the plasma in the presence of a plasma density gradient. Because the ions and electrons drift at different speeds (and, for Pedersen drift, in opposite directions), the drift motion gives rise to a space-charge electric field which then interacts with the unperturbed magnetic field to cause what may be termed a first-order drift. If the unperturbed electric and magnetic fields bear the proper geometrical relation to each other and to the unperturbed plasma density gradient, then small perturbations in plasma density will be accentuated. In the lower E layer the Hall mobility is much higher than the Pedersen mobility for electrons and is about three thousand times the Hall mobility for ions. Thus only the Hall drift of electrons need be considered. Under these circumstances the correct configuration for the drift instability, which shall be called the $\mathbf{E} \times \mathbf{B}$ instability for brevity, requires the unperturbed electron density gradient to be parallel to the unperturbed electric field, and requires these two vectors to be perpendicular to the unperturbed magnetic field. Small perturbations in electron density in a direction perpendicular to the magnetic field (i.e., in the direction of the electron density gradient and the electric field) will be unstable, and the irregularities which result will be aligned with the magnetic field.

In all analyses cited above it has been found necessary to postulate a specific shape for the perturbation, and in some cases to impose a specific spatial dependence for other parameters (such as electron production and loss rates) as well. Simon (102), and many who have attempted to apply the treatment to the ionospheric E layer (104,108-110,112), have used cartesian coordinates and have treated a plasma slab which has been perturbed by a sinusoidal density perturbation. Hoh (103) has performed a dimensional analysis in cylindrical geometry which has involved an unspecified functional dependence of density upon radius (the stipulation was that $\partial/\partial r \rightarrow \pm\alpha_1/R$, where $\alpha_1$ is defined as above).

Whitehead (106,107), Reid (111), and Chimonas (113) have all used a horizontal slab geometry and have required the density perturbation to have an exponential height dependence. In addition, Whitehead (106,107) has imposed an artificial height-dependence on the production and loss rates of electrons. (Other workers have ignored these latter two quantities.)

In most cases in which specific application to the lower E layer has been made, instabilities of tens-of-meters wavelength have been predicted and have displayed growth times of a few tenths of seconds to a few tens of seconds. Phase velocities have been a few meters per second to a few tens of meters per second. These predicted values are compatible with the decameter wavelength radar measurements, and it is thus concluded that the $\mathbf{E} \times \mathbf{B}$ instability is the strongest likely candidate instability for the observations. The next section below will include a specific application of this instability mechanism to the geometry and initial conditions of the cesium plasma clouds which are the subject of this investigation. Detailed quantitative analysis will be deferred to that section.

It should be noted that the $\mathbf{E} \times \mathbf{B}$ instability has been postulated as a cause for temperate-latitude sporadic E (104,108,110,112). Whitehead (106,107) claims that it is ineffective for providing the principal impetus for sporadic-E formation, but finds that it can accentuate an existing sporadic-E layer. His conclusions may be questioned, however, due to the artificialities inherent in his analysis.

The effect of all this work has been to introduce a plasma-instability theory of sporadic E in competition with the wind-shear theory which has been found to fail in several experimental tests (as indicated above in the section on "Sporadic E..."). The difficulty of making a definitive experimental test of the plasma-instability theory has made it a rather weak contender. This situation is perhaps a consequence of the researcher's proclivity to concentrate on areas of investigation which he believes are readily amenable to experimental investigation, and may not represent a true evaluation of the two theories' relative potential. The results of this investigation may permit a more realistic appraisal to be made.

## APPLICATION OF THE $\mathbf{E} \times \mathbf{B}$ INSTABILITY

### $\mathbf{E} \times \mathbf{B}$ Instability Applied to Phase III in Plasma Cloud Evolution

It was previously indicated in the first section of Part III that several workers have attempted, with some success, to apply the $\mathbf{E} \times \mathbf{B}$ instability theory to E-layer irregularities and sporadic E. It is the purpose of this chapter to describe an application of the $\mathbf{E} \times \mathbf{B}$ instability theory to the cesium plasma clouds which are the object of this investigation.

While the previous E-layer-directed studies have made use of a slab geometry, the plasma clouds investigated here are more properly described in cylindrical coordinates. Rao and Russell (114) have performed a perturbation analysis in this geometry specifically for application to high-altitude chemical releases. Although their analysis is intended for use with barium releases at much higher altitude than the lower E layer, it can be used, with some slight modifications, for cesium plasma clouds in the 80-120 km altitude region. Their development will be described in moderate detail here (as it is unpublished), but mathematical minutiae will be excluded.

The equation for the flux of particles of species $s$, as written in Eq. (4), is

$$\Gamma_s = -D^s \nabla N + N\mu^s \mathbf{E} + \frac{\omega_s}{\nu_{sN}} \hat{e}_B \times \Gamma_s \tag{6}$$

In cylindrical coordinates the components may be written as

$$\Gamma_r{}^s = -D^s \frac{\partial N}{\partial r} + N\mu^s E_r + \frac{\omega_s}{\nu_{sN}} \Gamma_\phi{}^s \tag{7a}$$

$$\Gamma_\phi{}^s = -\frac{D^s}{r}\frac{\partial N}{\partial \phi} + N\mu^s E_\phi - \frac{\omega_s}{\nu_{sN}} \Gamma_r{}^s \tag{7b}$$

$$\Gamma_z{}^s = -D^s \frac{\partial N}{\partial z} + N\mu^s E_z \tag{7c}$$

Equations (7a) and (7b) may be solved simultaneously for $\Gamma_\phi{}^s$ and $\Gamma_r{}^s$ to give

$$\Gamma_r = \frac{1}{\left(1 + \frac{\omega_s{}^2}{\nu_{sN}^2}\right)} \left[-D^s \left(\frac{\partial N}{\partial r} + \frac{\omega_s}{r\nu_{sN}} \frac{\partial N}{\partial \phi}\right) + N\mu^s \left(E_r + \frac{\omega_s}{\nu_{sN}} E_\phi\right)\right] \tag{8a}$$

and

$$\Gamma_\phi = \frac{1}{\left(1 + \frac{\omega_s{}^2}{\nu_{sN}^2}\right)} \left[-D^s \left(\frac{1}{r}\frac{\partial N}{\partial \phi} - \frac{\omega_s}{\nu_{sN}} \frac{\partial N}{\partial r}\right) + N\mu^s \left(E_\phi - \frac{\omega_s}{\nu_{sN}} E_r\right)\right] \tag{8b}$$

Defining

$$D_p{}^s = \frac{D^s}{1 + \frac{\omega_s{}^2}{\nu_{sN}^2}}, \quad \mu_p{}^s = \frac{\mu^s}{1 + \frac{\omega_s{}^2}{\nu_{sN}^2}},$$

$$D_H^s = \frac{\frac{\omega_s}{\nu_{sN}} D^s}{1 + \frac{\omega_s{}^2}{\nu_{sN}^2}}, \quad \text{and} \quad \mu_H^s = \frac{\frac{\omega_s}{\nu_{sN}} \mu^s}{1 + \frac{\omega_s{}^2}{\nu_{sN}^2}},$$

Eqs. (8) may be written

$$\Gamma_r{}^s = -D_p{}^s \frac{\partial N}{\partial r} + \mu_p{}^s N E_r - \frac{D_H^s}{r}\frac{\partial N}{\partial \phi} + \mu_H{}^s N E_\phi \tag{9a}$$

$$\Gamma_\phi{}^s = -\frac{D_p{}^s}{r}\frac{\partial N}{\partial \phi} + \mu_p{}^s N E_\phi + D_H^s \frac{\partial N}{\partial r} - \mu_H{}^s N E_r \,. \tag{9b}$$

The next step is to use Eqs. (7c), (9a), and (9b), together with the equation of continuity, in a perturbation analysis. Small perturbations in $N_0$, $\mathbf{E}$, and $\Gamma^s$ of the form

$$N = N_0(r) + N_1(r,t)$$

$$\mathbf{E} = \mathbf{E}_0(r) + \mathbf{E}_1(r,t)$$

$$\Gamma^s = \Gamma_0^s(r) + \Gamma_1^s(r,t) \ ,$$

are introduced.

Due to the high value of longitudinal conductivity, $E_z$ is assumed to be zero, and $N$ is assumed to be independent of $z$. $\mathbf{E}_0$ is taken to be a constant vector. The quantity $N_0$ is taken, for convenience, to be of the form

$$N_0(r) = N_c e^{-(r/r_0)^2}$$

This gaussian radial dependence may not conform to the plasma cloud's configuration immediately after the end of the blast phase, but it is probably adequate after a few seconds (perhaps 10 sec) when diffusion has operated to smear the initial plasma distribution. The perturbation in $N$ is taken to be of the same form as $N_0$, i.e.,

$$N_1 = N_c \, e^{-(r/r_0)^2} \, e^{-i(\omega t - k_\phi \phi)} \ ,$$

and is decomposed into a harmonic series of frequency $\omega$ and wave number $k_\phi$ appropriate to waves traveling in an azimuthal direction. The irregularities, then, are aligned with the magnetic field, which is taken to be in the $z$ direction, and appear as flutes on the cylindrical plasma cloud which rotate about the cloud's axis. The perturbed electric field is assumed to be curl free and of the same form as the perturbed plasma density, i.e.,

$$\mathbf{E}_1 = -\nabla V_1 = -\nabla \left[ V_0 \, e^{-(r/r_0)^2} \, e^{-i(\omega t - k_\phi \phi)} \right] .$$

The equation of continuity

$$\frac{\partial N_1}{\partial t} + \nabla \cdot (\Gamma_1^s) = 0 \tag{10}$$

is written for each species (ions and electrons), with the appropriate forms of Eqs. (7c), (9a), and (9b) inserted, and yields a pair of coupled algebraic equations whose determinant is a dispersion relation.

This pair of equations may be written as

$$N_0(-i\omega + A^s + iB^s) + V_0(C^s + D^s) = 0 \tag{11}$$

where

$$A^s = D_p^s \left( \frac{4}{r_0^2} - \frac{4r^2}{r_0^4} + \frac{k_\phi^2}{r^2} \right) + \frac{2r}{r_0^2} \mu_H^s E_0 \sin\phi - \frac{2r}{r_0^2} \mu_p^s E_0 \cos\phi$$

$$B^s = -\frac{\mu_p^s}{r} k_\phi E_0 \sin\phi - \frac{\mu_H^s}{r} k_\phi E_0 \cos\phi$$

$$C^s = \mu_p^s \left(\frac{4}{r_0^2} - \frac{8r^2}{r_0^4} + \frac{k_\phi^2}{r^2}\right)$$

and

$$D^s = \mu_H^s \frac{2k_\phi}{r_0^2}$$

The condition for instability is

$$(C^- - C^+)(A^-C^+ - B^-D^+ - A^+C^- + B^+D^-) + (D^- - D^+)(B^-C^+ + A^-D^+ - A^+D^- - B^+C^-) > 0 , \qquad (12)$$

which reduces to a cubic equation in $k_\phi^2$. A numerical method is used to solve for the regions of instability in $\omega - k_\phi$ space, in which $k_\phi$ is positive and real. This process, as described in greater detail by Rao, yields the maximum and minimum values of $k_\phi$, the e-folding time constant $[\mathrm{Im}\,(\omega)]^{-1}$ for instability growth which is appropriate to these values of $k_\phi$, the e-folding time constant of the instability for a selected wave number within the range of $k_\phi$, and the instability wavelength (defined by $\lambda = 2\pi r/k_\phi$) at any radius.*

The parameters $E_0$, $\nu_{sN}$, and $r_0$ are specified independently. The $\nu_{sN}$ are determined by atmospheric conditions, and hence vary with altitude. They are selected, as indicated in the first section of Part III above, from model values. The parameter $r_0$ is taken to be the radius predicted by the blast-wave model consistent with the blast-wave measurements reported in the same section and in Davis and Moore (94). Thus this parameter also varies with altitude. The wavelength $\lambda$ is selected as that wavelength corresponding to an irregularity propagating around the plasma cloud at a radius $r$. For the gaussian radial dependence of electron density chosen, the instability growth rates reach their maximum values in a broad range of $r$ near $r_0$. Hence a value $r = r_0$ is selected as a basis for calculating wavelength. For calculations of e-folding growth times for irregularities of particular characteristic sizes (wavelengths), it is assumed that the decameter-wavelength radar data are most representative of scattering structure in the 5- to 40-m scale range. Calculations are made for 5, 10, 20, 30, and 40 m. The undisturbed electric field $E_0$ is perhaps the least well known of all input parameters. Electric fields as large as 0.1 V/m have been measured in highly disturbed regions of the E layer, and field strengths of 0.01 V/m are not uncommon. There is no way of knowing the exact magnitude of the electrostatic field appropriate to the cesium plasma cloud case, especially in view of the likelihood that local electric fields due to decameter-scale turbulence in the lower E layer certainly must exist.

If it is assumed (consistent with wind measurements) that a random component of neutral wind velocity of 50 to 100 m/sec characterizes the lower E layer, and that the irregular behavior which is discerned in this region is related to $\mathbf{j} \times \mathbf{B}$ forces generated by charged particles moving with these winds, then fields of the order of $5 \times 10^{-3}$ V/m are possible even in the undisturbed atmosphere. If such fields exist, they would be expected to result in an increase of electron temperature above that of the neutral gas.

*This entire paragraph is abstracted from Rao and Russell (114) which should be consulted for greater detail.

Indeed, as indicated in the earlier section on "Sporadic E," electron temperatures are often measured at levels several hundred degrees above neutral gas temperatures (58, 59,115). They would also give rise to the disparity between theoretically expected and observed values of electron-neutral collision frequency above about 90 km, as mentioned in the first section of Part III (92). Electric fields of this order are much larger than would be expected from ambipolar diffusion of the release products (116) and must be considered to predominate. Estimated values of $2\times10^{-4}$ to 0.1 V/m have been used in the $E\times B$ instability calculations, with the understanding that specific values cannot be assigned. The true electric field magnitudes probably fall somewhere in the middle of the range selected.

Digital computer solutions for instability growth rates have been obtained for instability wavelengths of 5, 10, 20, 30, and 40 m at altitudes between 85 and 110 km. Electrostatic field intensities logarithmically spaced between $2\times10^{-4}$ and 0.1 V/m have been used in all cases. The instability growth rate for the fastest-growing instability wavelength also has been calculated for these conditions (except the maximum electrostatic field intensity for this case is 0.05 V/m). In addition, the threshold value of electrostatic field intensity for instability wavelengths of 5, 10, 20, and 40 m has been calculated for altitudes within the 85-110 km interval, and the minimum instability wavelength for electrostatic field intensities of $2\times10^{-4}$ to 0.05 V/m have been determined in the same interval. The results appear in Figs. 22-29.

Perhaps the outstanding feature in all these illustrations is the strong tendency for instabilities to be most favored in the 100-105 km altitude region. Thus, as suggested by the data described in the first section of Part II, it would be expected that plasma clouds in this interval would display a greater variety of instability modes than at lower altitudes.

The predominance of the decameter radar data were acquired at a radar wavelength of about 20 m. Assuming that the radiation was incident obliquely on the plasma cloud, then phase reinforcement of the backscattered energy would require a lowest-order mode of plasma-density variation of somewhat longer wavelength, possibly 30 to 40 m. Figures 22 and 23 indicate that instabilities of these wavelengths are possible at all altitudes above 87.5 km (the lowest height at which a release was made) for an electric field intensity of $10^{-3}$ V/m or greater. This value is well within the range which can

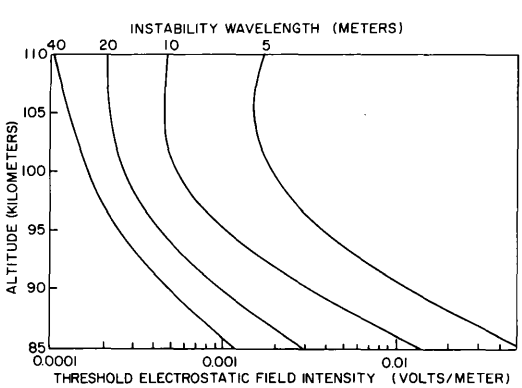


Fig. 22 - Threshold electrostatic field intensity vs altitude for $E\times B$ instability of wavelengths from 5 to 40 m

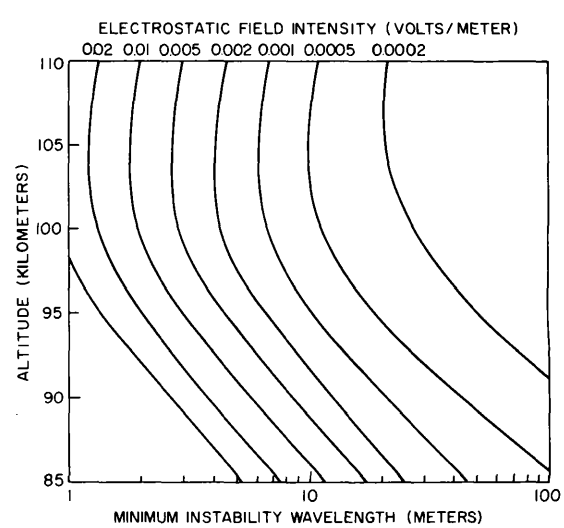


Fig. 23 - Minimum $E\times B$ instability wavelength vs altitude for electrostatic field intensities of 0.0002 to 0.02 V/m

be accounted for by normal ionospheric winds. Instabilities of 3 to 4 m wavelength, which would be required to explain similar behavior in the meter-wave radar data (if such behavior had been detected), would have been supported only if electric fields of 0.05 V/m had existed. Electric fields of this intensity have been observed at auroral latitudes, but not in the temperate zone of concern in this investigation. It is noted, however, that in one 94-km release, evidence of a plasma instability coincident with one in the decameter-wave data was recorded on the meter-wave radar signal. This evidence is not cited here as conclusive, however, because it has not been repeated (it is discussed briefly in the Appendix). If it does indeed represent a manifestation of the $\mathbf{E} \times \mathbf{B}$ instability with perhaps a wavelength of 3 to 4 m (these values would correspond to the same geometry as that which would permit the decameter-wave radar to detect 30- to 40-m wavelength irregularities), then Fig. 22 indicates that a local electric field of about 0.01 V/m must have existed. This value is probably slightly too high to be associated with normal-E-layer processes and can only be explained by a more severe turbulence than is ordinarily encountered. That this evidence of meter-wavelength plasma instability was acquired only once in many releases is testament to the likelihood that it arose from an uncommon source. However, this testimony is not conclusive — instabilities of the proper wavelength may have existed in other cases but simply were too small in density to be detected.

Figure 24 contains a collection of curves for the logarithmically spaced values of electric field which indicate the e-folding growth time of the fastest-growing instability at each altitude within the 85-110 km interval. Growth rates for the $10^{-3}$ to $10^{-2}$ V/m interval considered as likely for the lower-E-layer range from as short as 0.03 sec to longer than 100 sec. As indicated in the first section of Part II the decameter-wave data indicate that instability growth times of a few tenths of a second are typical; these values fall nicely within the midrange of the likely values on Fig. 24.

Figures 25-29 contain curves similar to Fig. 24 and show the growth times for instability wavelengths of 40, 30, 20, 10, and 5 m, respectively. It should be noted that Figs. 27-29 do not contain curves for some of the smaller values of electric field strength, and that some of the curves which appear on them do not extend over the full altitude interval. This circumstance results from the threshold effect indicated on Figs. 22 and 23.

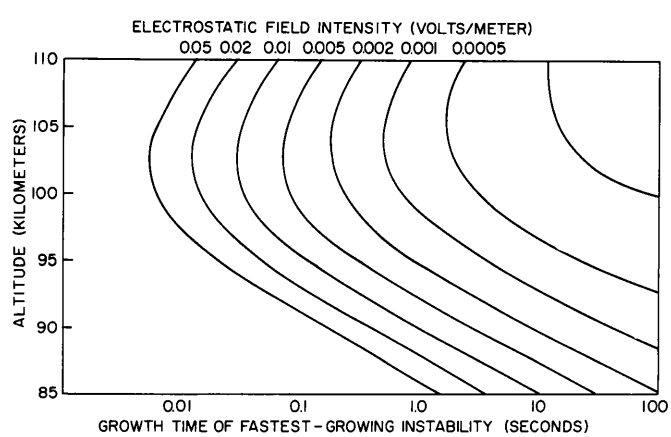


Fig. 24 - Growth time of fastest-growing $\mathbf{E} \times \mathbf{B}$ instability wavelength vs altitude for electrostatic field intensities between 0.0005 and 0.05 V/m

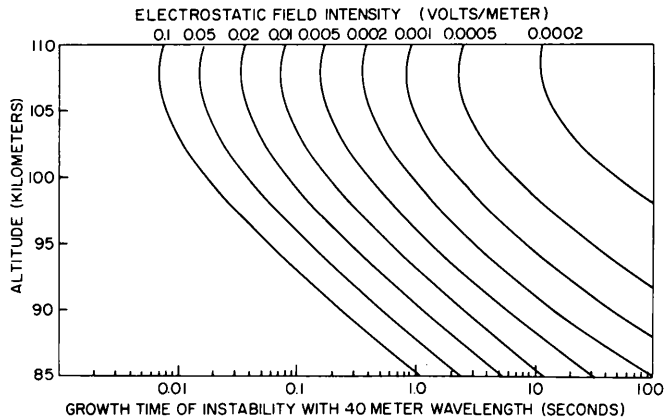


Fig. 25 - Growth time of 40-m-wavelength $E \times B$ instability vs altitude for electrostatic field intensities between 0.0002 and 0.1 V/m

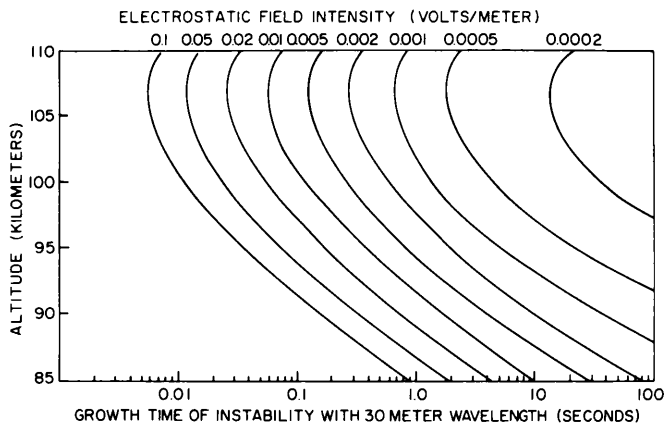


Fig. 26 - Growth time of 30-m-wavelength $E \times B$ instability vs altitude for electrostatic field intensities between 0.0002 and 0.1 V/m

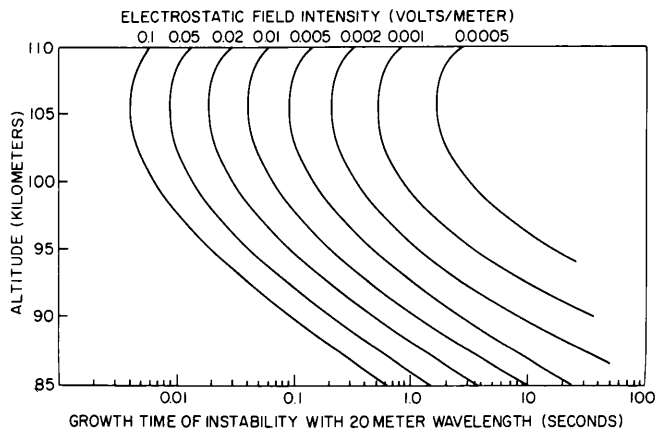


Fig. 27 - Growth time of 20-m-wavelength $E \times B$ instability vs altitude for electrostatic field intensities between 0.0005 and 0.1 V/m

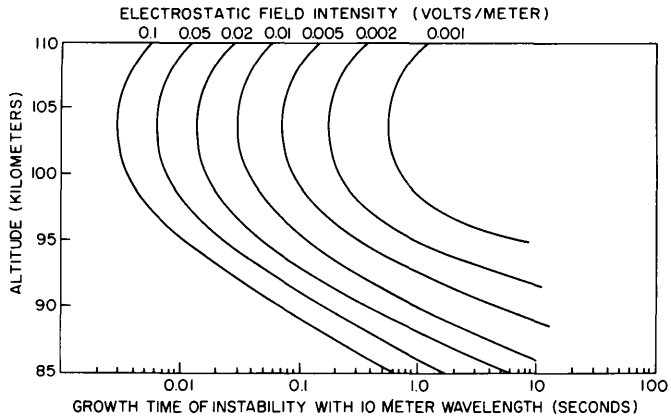


Fig. 28 - Growth time of 10-m-wavelength $E \times B$ instability vs altitude for electrostatic field intensities between 0.001 and 0.1 V/m

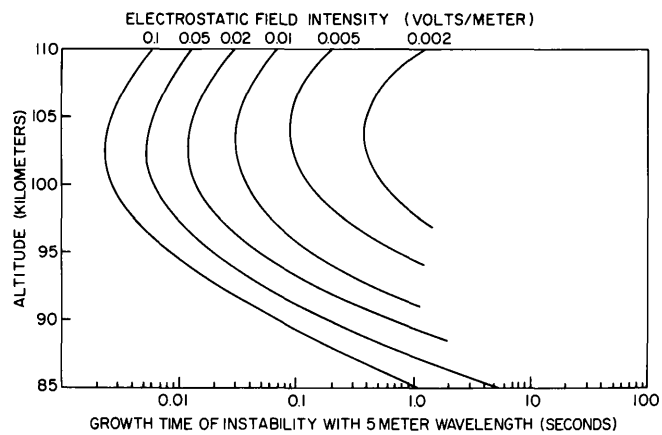


Fig. 29 - Growth time of 5-m-wavelength $E \times B$ instability vs altitude for electrostatic field intensities between 0.002 and 0.1 V/m

Figure 30 is a scatter plot of the measured growth times observed in the five releases whose instability-associated spectrally discrete components were adequately resolvable. Shown as open circles in Fig. 30 are the e-fold growth times of individual components. Those with left-pointing arrows attached to them are data which fell at or below the time-resolution limit of the analysis filters; in these cases, the symbols are placed at this limit to represent an upper bound to the actual growth times. The filled squares are mean growth times calculated for each altitude from the observed data, with the points weighted in proportion to their amplitudes. Thus a high-amplitude spectral component is given more weight than a small one. The dashed line is included to indicate, on an approximate least-squares basis, the general tendency of mean growth time to decrease with altitude. This tendency is of the same sense as that displayed in calculations described above, but has a more gradual slope. Most values fall between 0.4 and 1.4 sec and are consistent with electric field values of 0.02 to 0.002 V/m.

Figure 31 is a scatter plot of the $1/e$-lifetimes of the spectrally discrete components observed on decameter radar for the same five releases. Some data which appear on

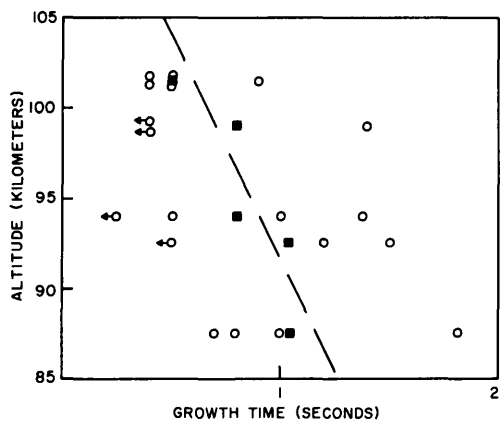


Fig. 30 - Growth times of spectrally discrete features observed in five cesium releases

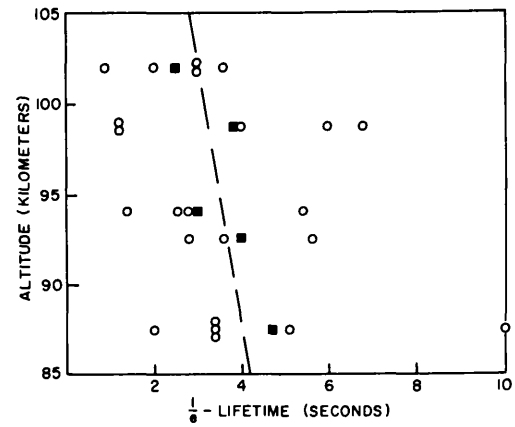


Fig. 31 - Lifetimes of spectrally discrete features observed in five cesium releases

Fig. 10 have no counterparts on Fig. 9; their growth rates were not measurable due to radar clutter which partially obscured them. Mean lifetimes of 2 to 4 sec are predominant. It is believed that the normally irregular behavior of the lower E region, whether or not it may properly be described as turbulent, is responsible for this circumstance. The values certainly are compatible with those described above in the second section of Part II as determined by other measurements.

## A Possible Interpretation of Phase IV Behavior in Terms of the Nonlinear $E \times B$ Instability, and Implications for Sporadic E

The plasma cloud behavior in Phase III demonstrates that the $E \times B$ instability does indeed develop, under suitable conditions, in the lower E layer. The remaining step, and certainly the most critical one, is to associate this behavior with the formation of sporadic-E layers. By virtue of its hundreds-of-meters scale in this investigation, which can be attributed to the limited effect that a few moles of cesium can be expected to create in the atmosphere, a definitive association cannot be drawn with tens-of-kilometers scale, blanketing sporadic E. However, in view of the tens-of-meters scale of the fine structure in sporadic E which has been discerned in radiofrequency measurements, and which has been previously described in the second section of Part I, it is evident that events which occur in the cesium plasma clouds are directly related to the smaller-scale aspects of sporadic E. Indeed, it is believed that diffuse, nonblanketing sporadic E may well consist of a large number of scattering entities of the type which are created by the $E \times B$ instability described above. The intense blanketing species of sporadic E may be an exaggerated version of this multiscatterer structure, with each element dependent on its own local electric field and local plasma density gradient. And, under these circumstances, the essential condition for formation of an extensive blanketing layer may simply be the requirement that an electrostatic field above the threshold value must exist everywhere within an atmospheric volume in which irregularity structure (which may be associated with neutral turbulence, or with nonlinear laminar flow) of the appropriate gradient scale exists. In view of the fact that radiofrequency backscatter from naturally occurring sporadic E displays a coherent spectral structure, it is likely that some degree of order exists in the scattering volume, and hence the latter association may be more likely.

The growth rates and lifetimes of the instabilities described in the first section of Part II, and this chapter, do not bear a direct relationship to the equivalent parameters of sporadic E. These observed parameters are supposed to correspond to the small-amplitude linear regime of instability development, and it is expected that under the conditions in which formation of a persistent scattering structure is favored, a saturation effect is likely. The behavior exhibited by the example of Phase IV development discussed in the above mentioned section is presented as evidence of just such behavior. In that example, three unique features are discerned:

1. The signature duration is nearly twice that of any other release, and many times the duration of a typical release.

2. The direct backscattered echo exhibits pronounced cyclical behavior in both spectral dispersion and in intensity.

3. A persistent, sporadic-E-like reflecting surface is formed which is spectrally discrete.

The cyclical behavior of this signature is characterized by the appearance of spectrally discrete intense components of the type associated with Phase III, interspersed with intervals of spectral broadening and flattening, with a total period of about 50 sec. This behavior is consistent with a growth phase in which the decameter radar may detect a single coherent mode of the instability, followed by a saturation phase in which mode-mode coupling causes distortion of the modal structure and a consequent contamination of the radar signal's spectral content. It is of particular importance to note that, in addition, the motions associated with this evolution take place in a plane perpendicular to the geomagnetic field and in a manner which is symmetric relative to the geomagnetic field direction. This fact is consistent with both the behavior of midlatitude sporadic E and the geometrical features of the $\mathbf{E} \times \mathbf{B}$ instability.

The indications of nonlinear limiting upon instability development described above may be corroborated by a nonlinear analysis of the $\mathbf{E} \times \mathbf{B}$ instability. Sato, Tsuda, and Maeda (104,108,117), Sato and Tsuda (105,118), and Tsuda, Sato, and Matsushita (112) have carried out an analysis of the $\mathbf{E} \times \mathbf{B}$ instability in which both the linear and nonlinear (one- and two-dimensional) regimes have been investigated in circumstances which are appropriate to the lower E layer. Concentrating on sporadic E scattering irregularities which are field-aligned, and which are characterized by wavelengths transverse to the geomagnetic field of a few hundred meters and less, they have found that normal ionospheric conditions allow irregularities of as much as 50% enhancement in electron density to persist for tens of minutes. These authors have made very nearly the same approximations as are described above in the first section of Part III, except that they have treated a horizontally stratified medium. This seeming incompatibility with the cylindrically symmetric case treated in the immediately preceding subsection is of little consequence if the results are used only for an order-of-magnitude comparison with observed temporal and spatial scales.

A criticism which has been made of the work in Refs. 104-106, 108, 112, 117, and 118 is that their postulated unperturbed background electron density is required to obey boundary conditions which are appropriate to a contained laboratory plasma, but not to the ionosphere (106). While this criticism is a matter of controversy, it should be mentioned that the plasma clouds studied in this investigation probably *do* obey boundary conditions of that type. (Whether either the results of this investigation or the nonlinear $\mathbf{E} \times \mathbf{B}$ instability analysis may be applied to the normal ionosphere must rest on the sensitivity of their behavior to these boundary conditions. The similarity of the plasma cloud observations described here to sporadic E indicates that, in at least the former case, no likely sensitivity exists.)

In both the linear and nonlinear instability analyses, atmospheric parameters were used (105,108) which are essentially identical to those assumed in this investigation. However, the value of electrostatic field which was used is at the lower limit of values considered here as most likely. The effect of introducing up to ten times the value used by Sato and Tsuda (105,108) in their treatment would be a speedup in the expected temporal behavior by a factor as great as ten and a decrease in threshold wavelength from their minimum of 25 m. With this provision, the results of the one-dimensional nonlinear analysis for growth rate and instability size are compatible with those acquired in the subsection above. It should be noted that the linear instability analysis in that subsection is one dimensional — it treats wave propagation only in the azimuthal direction. Thus the only essential difference between the two approaches is in selection of the direction of propagation. Since Sato and Tsuda (105,108) selected the most favorable slab geometry for instability growth, their results can be expected to be comparable to those for the most favorable position on the cylindrical plasma boundary treated in the above subsection of this report. All the results described and illustrated in that subsection are for just this position.

Two results of the nonlinear analysis are of interest. Sato and Tsuda continued their one-dimensional nonlinear instability analysis (with a limited number of modes, encompassing wavelengths of 20 to 200 m) until mode-mode coupling caused a saturation effect. The individual Fourier components ceased to grow monotonically after a period of about 30 sec (which could be equivalent to a time as short as 3 sec for the higher electric field values treated in this investigation), whereupon instability growth was limited at 30% to 50% over the unperturbed state. It is of a great deal of interest to note that in the strong plasma turbulence which resulted there occurred a continuous cascade of energy from the longest-wavelength modes through the spectrum to that short-wavelength extreme at which collisional diffusion caused their dissipation. Hence the picture that emerges is one of a growth phase dominated by a few discrete modes, followed by a saturation (and decay, if only limited energy is available) phase in which a broad spectrum of modes may exist. This picture is consistent with the observed data if they are conceived as a series of discrete spectral components whose few seconds of lifetime correspond to the growth of the instabilities, succeeded by spectrally diffuse decaying components which correspond to the mode-coupling saturation and decay of the instabilities.

Secondly, it is noted that in the ordered growth process described by these authors, some modes begin to grow only after a lapse in time of up to 30 sec (which, of course, would be compressed in the higher-field case). This circumstance is most pronounced in the shorter-wavelength modes which actually *decrease* from their assumed initial amplitude for several seconds. (This behavior arises from the fact that, in the case treated by these authors, these shorter-wavelength modes are not actually unstable, but gain energy only after they are fed it in the cascade process by longer-wavelength modes.) Indeed, it is illustrated in one example (105) that a given mode may display an interrupted growth period in which it grows at one rate for a few seconds, begins to decay as it transfers energy to higher harmonics, then begins to grow once more at an accelerated rate. Thus it is possible to envision that the radar data, which may reflect the behavior only of certain modes, display distinct growing spectral features only during certain periods of instability growth. They may also show evidence of interrupted growth, or of repeated growth and decay. Much of the radar data contain examples in which the development of *some* spectral components is delayed by several tens of seconds, and hence may be indicative of these processes.

To summarize the comparison of the one-dimensional nonlinear instability analysis in Refs. 104-106, 108, 112, 117, and 118 with the decameter radar data, the following points are of importance:

1. The analysis indicates that growth periods of 3 to 30 sec for decameter-scale irregularities may be expected, during which a few dominant modes grow coherently. This result is compatible with the growth rates and spectral discreteness of the specular signatures obtained in Phase III of the cesium plasma cloud evolution.

2. The analysis indicates that some instability wavelengths, particularly those which are shorter than the dominant modes, display an interrupted or delayed growth phase in which more, rapid, short-term growth is displayed. The delay may be several tens of seconds after the dominant mode begins to grow. This result is compatible with the delayed appearance of some spectral features in Phase III of the cesium plasma cloud evolution, and with the fact that some of these features display more rapid growth than the 3-sec value cited above.

3. The analysis indicates that after the growth period, a state of plasma turbulence is created in which mode-mode coupling destroys the phase-coherence which the growing modes display and distorts the modal structure as energy is interchanged randomly among modes. The overall tendency is for energy to cascade continuously downward from long wavelengths into the short-wavelength dissipation regime. In the absence of a continuous energy input, then, an ultimate decay of the plasma turbulence is predicted. This result is consistent with the spectral broadening and decay displayed by the discrete spectral features of the decameter radar data.

The two-dimensional extension of this nonlinear instability treatment provides the essential link with sporadic E. Sato and Tsuda (118) and Tsuda, Sato, and Matsushita (112) have extended the nonlinear analysis in such a way as to assess not only the interaction of the growing modes among themselves but also their interactions with the background density inhomogeneity which permits the initial instability growth to proceed. The extension to two dimensions permits spatial Fourier transformation with the additional complexity necessary to accommodate this added interaction. The above authors use the same physical model and boundary conditions as in the one-dimensional theory, and hence preserve the close correspondence to the cesium plasma cloud case (except for the geometry, which remains a horizontally stratified one).

The two-dimensional analysis confirms the initial growth rates cited above and yields two other important results. In the first place, it indicates that in the growth phase a localized spatially coherent density irregularity is formed. This result is of importance because it tends to explain the highly monochromatic character of the decameter radar echo's spectral features in Phase III. Secondly, this analysis confirms that after saturation takes place there occurs a decay phase in which the turbulent, and hence spatially noncoherent, modal structure decays toward the initial condition. It also suggests that a cyclical process of growth, saturation, and decay can be expected, with saturation occurring at about 75 sec (which could be as low as 7.5 sec for the cesium plasma cloud case), followed by a decay phase of undetermined duration. The conditions are then favorable for renewed instability growth, which would restart the cycle. The physical explanation of this behavior is that the saturation which occurs in the two-dimensional treatment is not strictly a result of modal coupling, as in the one-dimensional case, but results partially from deformation of the background density structure. This deformation occurs in such a manner as to partially cancel the driving electrostatic field and hence to weaken the tendency for instability growth. In this altered environment, the energy cascade from longer (and hence more unstable) to shorter (and hence less unstable, or even nominally stable) wavelengths causes the instability to disappear and reestablishes the initial configuration, whereupon the process begins once more.

These results are of great significance for interpretation of the behavior of cesium plasma clouds in Phase IV, when a cyclical growth and decay process in the discrete spectral features discerned by decameter radar is accompanied by formation of a

sporadic-E-like reflecting layer. The 50-sec period displayed by these data, as well as their spectral appearance, are indisputably consistent with the results of the two-dimensional nonlinear instability analysis. Although this cyclical behavior cannot now be causally related to the formation of sporadic E *beyond doubt*, there can be no dispute that it must be admitted as a prominent candidate.*

## CONCLUSIONS AND RECOMMENDATIONS

### Behavior of Plasma Clouds in the Lower E Layer

It has been found that explosively emitted cesium plasma clouds in the 85-105 km altitude region display four phases of evolution:

Phase I is a blast-wave phase, of 4 to 8 sec duration, in which an ellipsoidal bubble of some hundreds of meters dimensions is formed with its major axis aligned with the geomagnetic field.

Phase II is a period of ordered diffusion, of up to several tens-of-seconds duration, in which the cesium plasma cloud acts as a single-scatterer to decameter-wavelength radar illumination.

Phase III is a period of highly irregular behavior in which intense nearly monochromatic spectral features appear and decay with growth times of a few tenths of seconds and lifetimes of a few seconds. This phase may last several minutes; its occurrence is not restricted to explosively emitted plasma clouds, but also has been discerned in a deflagratively emitted barium release.

Phase IV is a period of up to tens of minutes in which cyclic growth and decay of distinct spectral features and modulations of spectral dispersion are accompanied by formation of a sporadic-E-like reflecting layer.

It also has been found that the statistics of decameter radar echoes from a plasma cloud are lognormal, and hence that it evolves as an ordered entity in which each scattering center is related temporally and spatially to other regions in the cloud. This fact, together with the spectral behavior exhibited in Phase III, is presented as evidence for plasma instabilities in the cesium (and barium) clouds.

### $\mathbf{E} \times \mathbf{B}$ Instability

A survey of possible instability mechanisms showed that a dissipative plasma instability, in which crossed electric and magnetic fields interact with a properly oriented plasma density gradient, is a prominent candidate for explanation of the growth rates, wavelengths, and spectral characteristics of the plasma clouds in Phase III. Application of this instability mechanism in a cylindrically symmetric, linear, perturbation analysis showed that the observed values of these parameters are remarkably consistent with such an instability in the 85-110 km altitude region for reasonable, estimated, electric field intensities. The results of this analysis were presented in detail, with predicted growth rates and thresholds for instability wavelengths of 5 to 40 m and electric field intensities of $2 \times 10^{-4}$ to 0.01 V/m in the 85-110 km altitude interval.

*Because the ionosphere is an uncontrolled environment, it cannot be conclusively demonstrated, short of many repetitions, that this behavior is solely responsible for formation of the release products into a sporadic-E-like reflecting surface.

Further remarkable confirmation of the $\mathbf{E} \times \mathbf{B}$ instability as a probable explanation for the plasma cloud behavior was found in comparison with a nonlinear instability analysis. This analysis, in addition to corroborating the instability wavelengths and growth rates observed and predicted above, provided an explanation for the delayed appearance, and seemingly interrupted growth, which characterized the plasma cloud data. It also predicted a nonlinear saturation effect in which modal intercoupling caused a distortion of the spectral structure of the turbulence, and which was found to explain the spectral broadening and noncoherence which appeared at the time of decay of Phase III spectral features in the decameter radar data.

Finally, a second more-sophisticated version of the nonlinear instability analysis predicted a cyclical growth, saturation, and decay process in the plasma instability evolution, which corresponded to the Phase IV behavior of the plasma cloud. This correspondence, together with the appearance in Phase IV of a sporadic-E-like reflecting layer, was interpreted as strong evidence for the validity of the $\mathbf{E} \times \mathbf{B}$ instability as a cause for temperate latitude sporadic E.

## Recommendations for Further Investigations

The 85-95 km interval is attractive for investigations directed at measuring the characteristics of specific modes, including growth rates, lifetimes, and apparent sizes. It is believed that three advancements can be made in investigations conducted in this altitude interval:

1. The use of an advanced radar and spectral analysis combination can achieve greater time resolution without serious degradation of the spectral and spatial resolution which are necessary to preserve a high signal-to-noise ratio. This possibility can be achieved only with a high-power radar of the coherent-pulse-doppler type, or with an equivalent pulse-compression radar.

2. The use of several radar frequencies simultaneously, together with improved time resolution, may permit instabilities of different wavelengths, and hence with different growth rates, to be observed. Because the instability growth rates predicted in the section on "Application of the $\mathbf{E} \times \mathbf{B}$ Instability" do not vary rapidly with wavelength, these radar frequencies must be distributed widely in, say, the band from 5 to 50 MHz.

3. The location of radar transmitting and/or receiving stations at positions *not* symmetrically oriented relative to the magnetic field (as opposed to the present investigation) will permit the postulated symmetry of the instability mechanism to be confirmed or negated.

The 100-110 km altitude interval has not been studied thoroughly. The linear instability analysis in the above mentioned section indicates that it is the most favorable region for the $\mathbf{E} \times \mathbf{B}$ instability to operate, and indeed the two cases in which a sporadic-E-like reflecting layer was formed both involved releases in this region. It is believed that a repetition of the cyclical Phase IV behavior, which has been found to coincide with formation of such a layer, is essential if the $\mathbf{E} \times \mathbf{B}$ instability is ever to be causally associated with sporadic E. Thus, it is recommended that the emphasis of future experiments of this type be placed on the region above 100 km and that an attempt be made to achieve such a repetition. It is noted that if the repetitive nonlinear saturation and decay described in the subsection on the interpretation of Phase IV behavior is effective, its success in any given instance may rely on there being enough *persistent* ionization to endure many cycles of this process. Future experiments might well be directed toward finding longer-lived ions or toward emplacing larger payloads in the region of interest.

Finally, some future work should be directed toward evaluating the role of neutral winds in sporadic E. Because it is likely that "sequential" sporadic E (the type of broadly peaked layer which is observed to form at 120-140 km altitude and to descend gradually to about 110 km before becoming indistinguishable) is explained by the wind-shear theory, it might be possible to emplace a long-lived plasma cloud at an appropriate position in the neutral wind structure and observe its subsequent descent and mergence with the lower E layer. Secondly, a suitable plasma cloud release, emplaced in the 90-110 km region just as a (natural) wind-shear-conveyed layer of ions reaches the same height, might serve the double purpose of triggering the formation of sporadic E, involving both packages of ions, and permitting the growth rates and instability wavelengths characteristic of this formation to be compared with the $\mathbf{E} \times \mathbf{B}$ theory.

## ACKNOWLEDGMENTS

The author is grateful for the stimulation and guidance given generously by Dr. Peter M. Livingston of the Department of Applied Physics, the Catholic University of America. He also wishes to acknowledge the cooperation of personnel in the Radar Techniques Branch and the Radar Geophysics Branch of the Radar Division, Naval Research Laboratory, who assisted in the operation of the radars, and of Mr. E. D. Boyer of the U.S. Army Ballistic Research Laboratory, Aberdeen Proving Grounds, who conducted the gun firings. Range support services were furnished by NASA Wallops Station, Virginia. Some financial support was provided by the Naval Electronic Systems Command, Department of the Navy.

## REFERENCES


1. Boyer, E.D., and MacAllister, L.C., "Seven-Inch Harp Gun-Launched Vertical Probe System: Initial Development," U.S. Army Materiel Command, Ballistic Research Laboratories, Memo. Rept. 1770, July, 1966

2. Marmo, F.F., Aschenbrand, L.M., and Pressman, J., "Artificial Electron Clouds - I: Summary Report on the Creation of Artificial Electron Clouds in the Upper Atmosphere," Planet. Space Sci., 1:227-237 (1959)

3. Marmo, F.F., Pressman, J., and Aschenbrand, L.M., "Artificial Electron Clouds - II: General Considerations," Planet. Space Sci., 1:291-305 (1959)

4. Marmo, F.F., Aschenbrand, L.M., and Pressman, J., "Artificial Electron Clouds - III: Release of Atomic Potassium at 121 km," Planet. Space Sci., 1:306-318 (1959)

5. Pressman, J., Marmo, F.F., and Aschenbrand, L.M., "Artificial Electron Clouds - IV: Thermal Ionization Study, Night Time Cesium Release at 101 km," Planet. Space Sci., 2:17-25 (1959)

6. Marmo, F.F., Pressman, J., Manring, E.R., and Aschenbrand, L., "Artificial Electron Clouds - V: Morning Twilight Study, Release of Cesium and Sodium at 128 and 116 km," Planet. Space Sci., 2:174-186 (1960)

7. Pressman, J., Marmo, F.F., and Aschenbrand, L.M., "Artificial Electron Clouds - VI: Low Altitude Study, Release of Cesium at 69, 82 and 91 km," Planet. Space Sci., 2:228-237 (1960)

8. Rosenberg, N.W. (ed.), "Project Firefly 1960, Vol. I," Air Force Cambridge Research Laboratories, Geophysics Research Directorate, Tech. Rept. AFCRL-256(I), 1961

9. Rosenberg, N.W. (ed.), "Project Firefly 1962-1963," Air Force Cambridge Research Laboratories, Environmental Research Papers No. 15, Tech. Rept. AFCRL-64-364, 1964

10. Gallagher, P.B., and Barnes, R.A., "Radio-Frequency Backscatter of Artificial Electron Clouds," J. Geophys. Res., 68:2987-3010 (1963)

11. Wright, J.W., "The Lifetime and Movement of Artificially Produced Electron Clouds Observed with Spaced Ionosondes," J. Geophys. Res., 68:3011-3020 (1963)

12. Edwards, H.D., Cooksey, M.M., Justus, C.G., Fuller, R.N., Albritton, D.L., and Rosenberg, N.W., "Upper-Atmosphere Wind Measurements Determined from Twelve Rocket Experiments," J. Geophys. Res., 68:3021-3032 (1963)

13. Groves, G.V., "Initial Expansion to Ambient Pressure of Chemical Explosive Releases in the Upper Atmosphere," J. Geophys. Res., 68:3033-3047 (1963)

14. Zimmerman, S.P., and Champion, K.S.W., "Transport Processes in the Upper Atmosphere," J. Geophys. Res., 68:3049-3056 (1963)

15. Rosenberg, N.W., "Chemical Releases in the Upper Atmosphere (Project Firefly), A Summary Report," J. Geophys. Res., 68:3057-3063 (1963)

16. Stewart, B., Encyclopedia Britannica (ninth ed.), 1882

17. Davis, T.N., Stolarik, J.D., and Heppener, J.P., "Rocket Measurements of Mid-Latitude Sq Currents," pp. 453-465 in R. L. Smith-Rose, ed., "Space Research VI," Washington, D.C.:Spartan Books, 1966

18. Burrows, K., and Hall, S.H., "Rocket Measurements of the Geomagnetic Field Above Woomera, South Australia," J. Geophys. Res., 70:2149-2158 (1965)

19. Smith, L.G., "Rocket Observations of Sporadic E and Related Features of the E Region," Radiosci., 1:178-186 (1966)

20. Bowhill, S.A., "A Rocket Experiment on the Structure of Sporadic E," Radiosci., 1:187-190 (1966)

21. Goodwin, G.L., "Some Aspects of Direct Backscatter Echoes from Sporadic E," J. Atmos. and Terres. Phys., 27:777-793 (1965)

22. Booker, H., "A Theory of Scattering by Nonisotropic Irregularities with Applications to Radar Reflections from the Aurora," J. Atmos. and Terres. Phys., 8:204-221 (1956)

23. Booker, H.G., "Radio Scattering in the Lower Ionosphere," J. Geophys. Res., 64: 2164-2177 (1959)

24. Tao, K., "A Theoretical Study of Sporadic-E Structure in the Light of Radio Measurements," pp. 235-257 in E. K. Smith, Jr., and S. Matsushita, "Ionospheric Sporadic E," New York:Pergamon, 1962

25. Austin, G.L., and Manson, A.H., "On the Nature of the Irregularities that Produce Partial Reflections of Radio Waves from the Lower Ionosphere (70-100 km)," Radiosci., 4:35-40 (1969)

26. Dungey, J.W., "The Influence of the Geomagnetic Field on Turbulence in the Ionosphere," J. Atmos. and Terres. Phys., 8:39-42 (1956)

27. Whitehead, J.D., "The Formation of the Sporadic-E Layer in the Temperate Zones," J. Atmos. and Terres. Phys., 20:49-58 (1961)

28. Axford, W.I., "The Formation and Vertical Movement of Dense Ionized Layers in the Ionosphere due to Neutral Wind Shears," J. Geophys. Res., 68:769-779 (1963)

29. Hines, C.O., "Internal Atmospheric Gravity Waves at Ionospheric Heights," Can. J. Phys., 38:1441-1481 (1960)

30. Axford, W.I., "Note on a Mechanism for the Vertical Transport of Ionization in the Ionosphere," Can. J. Phys., 39:1393-1396 (1961)

31. Rosenberg, N.W., and Justus, C.G., "Space and Time Correlations of Ionospheric Winds," Radiosci., 1:149-155 (1966)

32. Kochanski, A., "Atmospheric Motions from Sodium Cloud Drifts," J. Geophys. Res., 69:3651-3662 (1964)

33. Rosenberg, N.W., "Statistical Analysis of Ionospheric Winds-II," J. Atmos. and Terres. Phys., 30:907-917 (1968)

34. Spizzichino, A., and Revah, I., "Systematic Analysis of Wind Profiles Obtained by Meteor Observation," in Conf. Proc. of the Second Seminar on the Cause and Structure of Temperate Latitude Sporadic-E, 1968 (unpublished)

35. Heisler, L.H., and Whitehead, J.D., "Rapid Variations in the Sporadic-E Region," J. Atmos. and Terres. Phys., 24:753-764 (1962)

36. Ovezgel'dyyev, O., and Vasil'yeva, Ye. K., "One Theory of the Formation of $E_s$ in Middle Latitudes," Geomag. and Aeron., 4:321-322 (1964)

37. Ovezgel'dyyev, O., and Korsunova, L.P., "The Sporadic E-layer of the Ionosphere and Daily Variations of the Earth's Magnetic Field," Geomag. and Aeron., 4:322-324 (1964)

38. Rosenberg, N.W., Edwards, H.D., and Wright, J.W., "Ionospheric Winds: Motions into Night and Sporadic-E Correlations," NASA Tech. Note D-2114, 1963

39. Rosenberg, N.W., and Edwards, H.D., "Observations of Ionospheric Wind Patterns Through the Night," J. Geophys. Res., 69:2819-2826 (1964)

40. Smith, L.G., "Results of a Sequence of Measurements of Nighttime Sporadic-E," in Conf. Proc. of the Second Seminar on the Cause and Structure of Temperate Latitude Sporadic-E, 1968 (unpublished)

41. Hines, C.O., "The Formation of Midlatitude Sporadic E Layers," J. Geophys. Res., 69:1018-1019 (1964)

42. Wright, J.W., Murphy, C.H., and Bull, G.V., "Profiles of Winds in the Lower Thermosphere by the Gun-Launched Probe Technique and their Relation to Ionospheric Sporadic E," pp. 113-122, in R. L. Smith-Rose, ed., "Space Research VII," Amsterdam:North-Holland, 1967

43. Wright, J.W., Murphy, C.H., and Bull, G.V., "Sporadic E and the Wind Structure of the E Region," J. Geophys. Res., 72:1443-1460 (1967)

44. Wright, J.W., "Sporadic E as an Indicator of Wind Structure in the Lower Ionosphere and the Influx of Meteors," J. Geophys. Res., 72:4821-4829 (1967)

45. Murphy, C.H., and Bull, G.V., "Nighttime Variation of Ionospheric Winds Over Barbados, West Indies," J. Geophys. Res., 72:4831-4837 (1967)

46. Bowen, P.J., Norman, K., Willmore, A.P., Baguette, J.M., Murtin, F., and Storey, L.R.O., "Rocket Studies of Sporadic-E Ionization and Ionospheric Winds," Planet. Space Sci., 12:1173-1177 (1964)

47. Murphy, C.H., Bull, G.V., and Edwards, H.D., "Ionospheric Winds Measured by Gun-Launched Projectiles," J. Geophys. Res., 71:4535-4544 (1966)

48. Layzer, D., "Generalization and Critique of the Wind-Shear Theory of Sporadic E," J. Geophys. Res., 69:1853-1860 (1964)

49. Whitehead, J.D., "Survey of Sporadic E Processes," pp. 89-99 in R. L. Smith-Rose, ed., "Space Research VII," Amsterdam:North-Holland, 1967

50. Axford, W.I., and Cunnold, D.M., "The Wind-Shear Theory of Temperate Zone Sporadic E," Radiosci., 1:191-198 (1966)

51. Gleeson, L.J., "Positive Ion Layers in the E-Region of the Ionosphere," Planet. Space Sci., 15:27-37 (1967)

52. Axford, W.I., "The Wind Shear Theory of the Formation of Temperate Zone Sporadic E Layers," pp. 126-134 in R. L. Smith-Rose, ed., "Space Research VII," Amsterdam:North-Holland, 1967

53. Gleeson, L.J., and Axford, W.I., "Electron and Ion Temperature Variations in Temperate Zone Sporadic-E Layers," Planet. Space Sci., 15:123-136 (1967)

54. Hooke, W.H., "Electron, Ion and Neutral-Gas Temperatures in Temperate Latitude Sporadic-E Layers," Planet. Space Sci., 17:737-748 (1969)

55. Chimonas, G., and Axford, W.I., "Vertical Movement of Temperate-Zone Sporadic E Layers," J. Geophys. Res., 73:111-117 (1968)

56. Kato, S., Reddy, C.A., and Matsushita, S., "Formation of Sporadic-E Layer Due to Wind Shear in the Presence of Electrostatic Field," in Conf. Proc. of the Second Seminar on the Cause and Structure of Temperate Latitude Sporadic-E, 1968 (unpublished)

57. MacLeod, M.A., "Sporadic-E Theory. I. Collision-Geomagnetic Equilibrium," J. Atm. Sci., 23:96-109 (1966)

58. Sagalyn, R.C., Smiddy, M., and Sullivan, W.P., "Experimental Investigation of the Nighttime E Region," pp. 448-463 in R. L. Smith-Rose, ed., "Space Research VII," Amsterdam:North-Holland, 1967

59. Aubry, M., Blanc, M., Clauvel, R., Taieb, C., Bowen, P.J., Norman, K., Willmore, A.P., Sayers, J., and Wager, J.H., "Some Rocket Results on Sporadic E," Radiosci., 1:170-177 (1966)

60. Dorling, E.B., Norman, K., and Willmore, A.P., "Rocket Studies of Sporadic-E Ionization," Planet. Space Sci., 17:1207-1211 (1969)

61. Bedinger, J.F., Knaflich, H., Manring, E., and Layzer, D., "Upper-Atmosphere Winds and Their Interpretation-I. Evidence for Strong Nonlinearity of the Horizontal Flow Above 80 km," Planet. Space Sci., 16:159-193 (1968)

62. Layzer, D., and Bedinger, J.F., "Upper-Atmosphere Winds and Their Interpretation - II. Turbulence in the Lower E-Region," Planet. Space Sci., 17:1891-1911 (1969)

63. Bedinger, J.F., and Knaflich, H.B., "Observed Characteristics of Ionospheric Winds," Radiosci., 1:156-168 (1966)

64. Bedinger, J.F., and Smith, L.G., "Measured Wind Shears and Electron Densities," pp. 100-112 in R. L. Smith-Rose, ed., "Space Research VII," Amsterdam:North-Holland, 1967

65. Bedinger, J.F., and Constantinides, E., "Time Dependent Relation of Electron Density Profiles and Wind Profiles in the E-Region," in Conf. Proc. of the Second Seminar on the Cause and Structure of Temperate Latitude Sporadic-E, 1968 (unpublished)

66. Layzer, D., "A Theory of Midlatitude Sporadic-E," in Conf. Proc. of the Second Seminar on the Cause and Structure of Temperate Latitude Sporadic-E, 1968 (unpublished)

67. Kato, S., "Theoretical Basis of the Formation of Sporadic E Due to Wind Motion in the Ionosphere," Radiosci., 1:226-234 (1966)

68. Gershman, B.N., Grigor'yev, G.I., and Ignat'yev, Yu.A., "Contribution to the Theory of the Sporadic E-Layer," Geomag. and Aeron., 8:57-61 (1968)

69. Donahue, T.M., "Ionospheric Composition and Reactions," Science, 159:489-498 (1968)

70. Narcisi, R.S., "Ion Composition Measurements and Related Ionospheric Processes in the D and Lower E Regions," Ann. de Geophys., 22:224-234 (1966)

71. Narcisi, R.S., Bailey, A.D., and Della Lucca, L., "Composition Measurements of Sporadic E in the Nighttime Lower Ionosphere," p. 123 in R. L. Smith-Rose, ed., "Space Research VII," Amsterdam:North-Holland, 1967

72. Bates, D.R., and Massey, H.S.W., "The Basic Reactions in the Upper Atmosphere. II. The Theory of Recombination in the Ionized Layers," Proc. Roy. Soc. (London), A192:1 (1947)

73. Kasner, W.H., Rogers, W.A., and Biondi, M.A., "Electron-Ion Recombination Coefficients in Nitrogen and in Oxygen," Phys. Rev. Letters, 7:321-323 (1961)

74. Biondi, M.A., "Laboratory Measurements of Electron-Ion Recombination Coefficients," pp. 154-164 in R. L. Smith-Rose, ed., "Space Research VII," Amsterdam: North-Holland, 1967

75. Young, J.M., Johnson, C.Y., and Holmes, J.C., "Positive Ion Composition of a Temperate-Latitude Sporadic E Layer as Observed During a Rocket Flight," J. Geophys. Res., 72:1473-1479 (1967)

76. Narcisi, R.S., "Processes Associated with Metal-Ion Layers in the E Region of the Ionosphere," pp. 360-369 in A.P. Mitra, L.G. Jacchia, and W.S. Newman, eds., "Space Research VIII," Amsterdam:North-Holland, 1968

77. Istomin, V.G., "Ions of Extra-Terrestrial Origin in the Earth Ionosphere," pp. 209-220 in W. Priester, ed., "Space Research III," Amsterdam:North-Holland; New York:Interscience, 1963

78. Ferguson, E.E., and Fehsenfeld, F.C., "Some Aspects of the Metal Ion Chemistry of the Earth's Atmosphere," J. Geophys. Res., 73:6215-6223 (1968)

79. Rosenberg, N.W., and Golomb, D., "Generation and Properties of High Altitude Chemical Plasma Clouds," pp. 395-408 in "Progress in Astronautics and Aeronautics, Volume 12," New York:Academic Press, 1963

80. Brode, H.L., "Blast Wave From a Spherical Charge," Phys. Fluids, 2:217-229 (1959)

81. Rosenberg, N.W., "Chemical Releases at High Altitudes," Science, 152:1017-1027 (1966)

82. Donahue, T.M., "The Problem of Sodium Distribution," pp. 165-171 in R. L. Smith-Rose, ed., "Space Research VII," Amsterdam:North-Holland, 1967

83. Greenhow, J.S., and Neufeld, E.L., "Measurements of Turbulence in the 80- to 100-km Region from the Radio Echo Observations of Meteors," J. Geophys. Res., 64:2129-2133 (1959)

84. Greenhow, J.S., "Eddy Diffusion and Its Effect on Meteor Trails," J. Geophys. Res., 64:2208-2209 (1959)

85. Justus, C.G., "The Spectrum and Scales of Upper Atmospheric Turbulence," J. Geophys. Res., 72:1933-1940 (1967)

86. Blamont, J.E., and Barat, J., "Introduction d'un Modéle Pour la Structure des Mouvements de l'Atmosphere entre 85 et 110 km d'Altitude," Ann. de Geophys., 23:173-195 (1967)

87. Kolmogoroff, A., "The Local Structure of Turbulence in Incompressible Viscous Fluid for Very Large Reynolds' Numbers," Compt. Rend. Acad. Sci. URSS, 30:301-305 (1941)

88. Kolmogoroff, A.N., "Dissipation of Energy in the Locally Isotropic Turbulence," Compt. Rend. Acad. Sci. URSS, 32:16-18 (1941)

89. Aitchison, J., and Brown, J.A.C., "The Lognormal Distribution," Cambridge: University Press, 1966 (originally published in 1957)

90. Cramer, H., "Mathematical Methods of Statistics," pp. 219-220, Princeton: Princeton University Press, 1946

91. Chapman, S., "The Electrical Conductivity of the Ionosphere: A Review," Nuovo Cimento. Suppl., 4:1385-1412 (1956)

92. Thrane, E.V., and Piggott, W.R., "The Collision Frequency in the E- and D-Regions of the Ionosphere," J. Atmos. and Terres. Phys., 28:721-737 (1966)

93. Farley, D.T., Jr., "A Plasma Instability Resulting in Field-Aligned Irregularities in the Ionosphere," J. Geophys. Res., 68:6083-6097 (1963)

94. Davis, J.R., and Moore, J.C., "Decameter and Meter Wavelength Radar Studies of Artificial Plasma Clouds in the Lower Ionosphere. 1: Thermodynamic Properties of the Atmosphere Discerned from Blast Wave Measurements," J. Geophys. Res., 75:171-182 (1970)

95. Taylor, G., "The Instability of Liquid Surfaces when Accelerated in a Direction Perpendicular to their Planes. I," Proc. Roy. Soc. (London), A201:192-196 (1950)

96. Kruskal, M., and Schwarzschild, M., "Some Instabilities of a Completely Ionized Plasma," Proc. Roy. Soc. (London), A223:348-360 (1954)

97. Furth, H.P., Killeen, J., and Rosenbluth, M.N., "Finite-Resistivity Instabilities of a Sheet Pinch," Phys. Fluids, 6:459-484 (1963)

98. Kadomtsev, B.B., and Nedospasov, A.V., "Instability of the Positive Column in a Magnetic Field and the 'Anomalous' Diffusion Effect," J. Nucl. Energy, Part C (Plasma Phys.), 1:230-235 (1960)

99. Hoh, F.C., "Screw Instability of a Plasma Column," Phys. Fluids, 5:22-28 (1962)

100. Timofeev, A.V., "The Instability of a Gas Discharge in a Magnetic Field with no Longitudinal Current," Sov. Phys. Dokl., 8:890-892 (1964)

101. Self, S.A., "Ion Waves, Drift Waves, and Instability in a Weakly Ionized Magnetoplasma," SUIPR Report #265, Institute for Plasma Research, Stanford University, 1968

102. Simon, A., "Instability of a Partially Ionized Plasma in Crossed Electric and Magnetic Fields," Phys. Fluids, 6:382-388 (1963)

103. Hoh, F.C., "Instability of Penning-Type Discharges," Phys. Fluids, 6:1184-1191 (1963)

104. Tsuda, T., Sato, T., and Maeda, K., "Formation of Sporadic E Layers at Temperate Latitudes due to Vertical Gradients of Charge Density," Radiosci., 1:212-225 (1966)

105. Sato, T., and Tsuda, T., "Computer Study of Nonlinear Cross-Field Instability," Phys. Fluids, 10:1262-1268 (1967)

106. Whitehead, J.D., "Instabilities in a Gradient of Ionization and Sporadic-E," J. Atmos. and Terres. Phys., 29:1285-1297 (1967)

107. Whitehead, J.D., "Low Frequency Plasma Instabilities in the Ionosphere," J. Atmos. and Terres. Phys., 30:1563-1579 (1968)

108. Sato, T., Tsuda, T., and Maeda, K., "Fully Developed Turbulent Irregularities in the Ionosphere Due to Cross-Field Plasma Instability," Radiosci., 3:529-534 (1968)

109. Sato, T., "Brillouin Scattering in Plasmas as Applied to Ionospheric Irregularities," J. Geophys. Res., 73:2941-2949 (1968)

110. Kato, S., and Matsushita, S., "Space Charge Waves and Ionospheric Irregularities," J. Atmos. and Terres. Phys., 30:857-869 (1968)

111. Reid, G.C., "The Formation of Small-Scale Irregularities in the Ionosphere," J. Geophys. Res., 73:1627-1640 (1968)

112. Tsuda, T., Sato, T., and Matsushita, S., "Ionospheric Irregularities and the Cross-Field Plasma Instability," J. Geophys. Res., 74:2923-2932 (1969)

113. Chimonas, G., "Wind-Driven Instability in the Lower E Region," J. Geophys. Res., 74:4091-4098 (1969)

114. Rao, P.B., and Russell, W.H., "The Formation of Field-Aligned Striations in the Plasma Clouds Due to Cross-Field Instability: A Linear Analysis," Spencer Laboratory, Raytheon Company, 1969 (unpublished)

115. Megill, L.R., and Carleton, N.P., "Excitation by Local Electric Fields in the Aurora and Airglow," J. Geophys. Res., 69:101-122 (1964)

116. Haerendel, G., and Scholer, M., "Ambipolar Diffusion of a Plasma Cloud in a Magnetic Field," pp. 509-514 in R.L. Smith-Rose, ed., "Space Research VII," Amsterdam:North-Holland, 1967

117. Tsuda, T., Sato, T., and Maeda, K., "Ionospheric Irregularities and the Cross-Field Plasma Instability. Part 1. One-Dimensional Model," in Conf. Proc. of the Second Seminar on the Cause and Structure of Temperate Latitude Sporadic-E, 1968 (unpublished)

118. Sato, T., and Tsuda, T., "Ionospheric Irregularities and the Cross-Field Plasma Instability. Part 2. Two-Dimensional Model," in Conf. Proc. of the Second Seminar on the Cause and Structure of Temperate Latitude Sporadic-E, 1968 (unpublished)

## Appendix

## ADDITIONAL PLASMA CLOUD DATA

### INTRODUCTION

It is the purpose of this appendix to present further examples of the decameter-wavelength radar data (plus one example of meter-wavelength data) obtained for other plasma cloud releases than those discussed in the first section of Part II. All data from all releases have not been given complete analysis, but the examples illustrated in this appendix are adequate to corroborate the important features which were described in that section of the report.

The data are presented in chronological order of the releases, and an attempt is made in each case to describe the aspects which bear upon the phenomenological model described in the above mentioned section

### BARIUM RELEASE, OCTOBER 4, 1967

This plasma cloud was created at an altitude of 102 km by a deflagratively emitted 6-kg payload of barium and cupric oxide, and hence is atypical of the release mechanism used for the other fourteen releases. Figure A1 contains unthresholded and thresholded photographs of the release signature, in an intensity-modulated doppler shift vs time format. The signature lasts less than 1 min and exhibits a maximum spectral bandwidth of more than 15 Hz. This latter feature is its principal distinction in comparison with the explosively emitted plasma clouds. The lower photograph shows two or three examples of the intense "highlights" representing the discrete spectral features which characterize Phase III, the instability growth phase of plasma cloud evolution. Figure A2 is a computer-analyzed version of the same data, rotated counterclockwise by 90°, which displays these features more prominently. It is apparent in Figs. A1 and A2 that several (ten to fifteen) such features occur in the cloud's lifetime, with two dominant ones in the 2319:30 to 2319:40 GMT period. Figure A3 is a collection of amplitude spectra (horizontal cuts through Fig. A2) at 3 sec separation and with a 0.3-Hz resolution bandwidth. The presence of several spectrally discrete components is apparent in all photographs after the beginning of the signature at 2319:10 GMT, with typical lifetimes of 3 to 6 sec.

### CESIUM RELEASE, APRIL 12, 1968

This release was explosively emitted by a 2-kg payload at an altitude of 95.5 km and lasted about 100 sec. Figure A4 is a collection of unthresholded and thresholded photographs in doppler shift vs time format. The upper two photographs have small-amplitude radar clutter bands near 0 Hz for their entire duration. The prominent features of the signature are most evident in the middle photograph. The release at 1822:45 GMT is followed by a bright, downward-curved trace for about 20 sec. This trace, whose spectral narrowness is apparent in the bottom photograph, is indicative of the Phase II single-scattering behavior. At about 1823:00 GMT the spectrum becomes diffuse, with some highlights, and broadens to more than 5 Hz. No attempt was made to measure growth rates or lifetimes of features in this signature due to the clutter contamination. Figure A5 is a cumulative signal amplitude distribution for this signature, displaying excellent fidelity to lognormal character. Comparison with the cumulative probability distribution

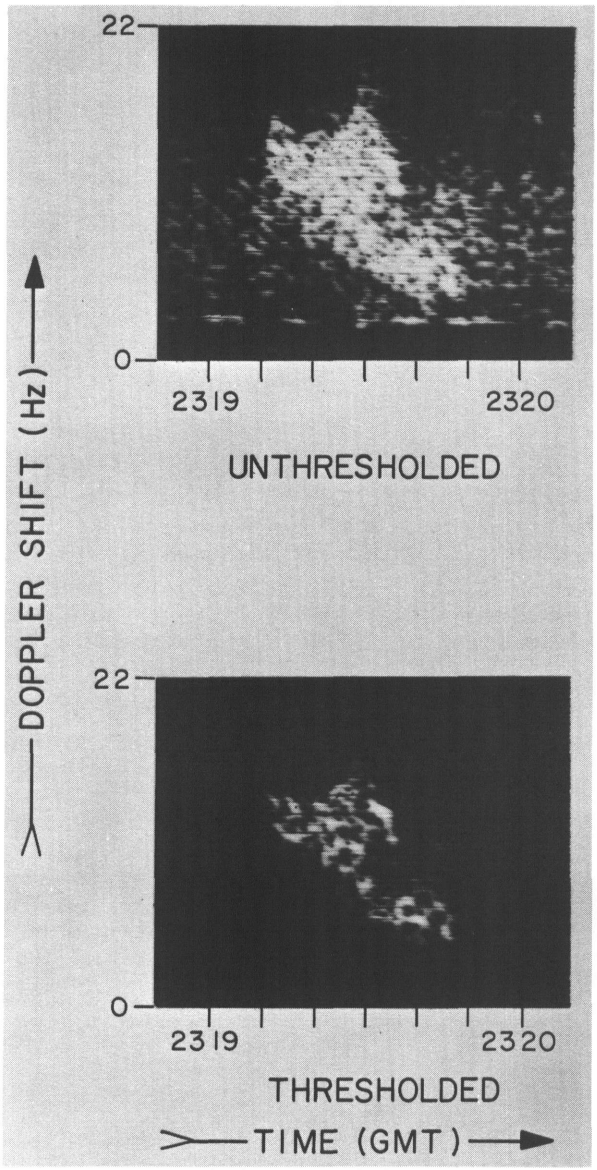


Fig. A1 - Doppler shift vs time displays for barium release, Oct. 4, 1967

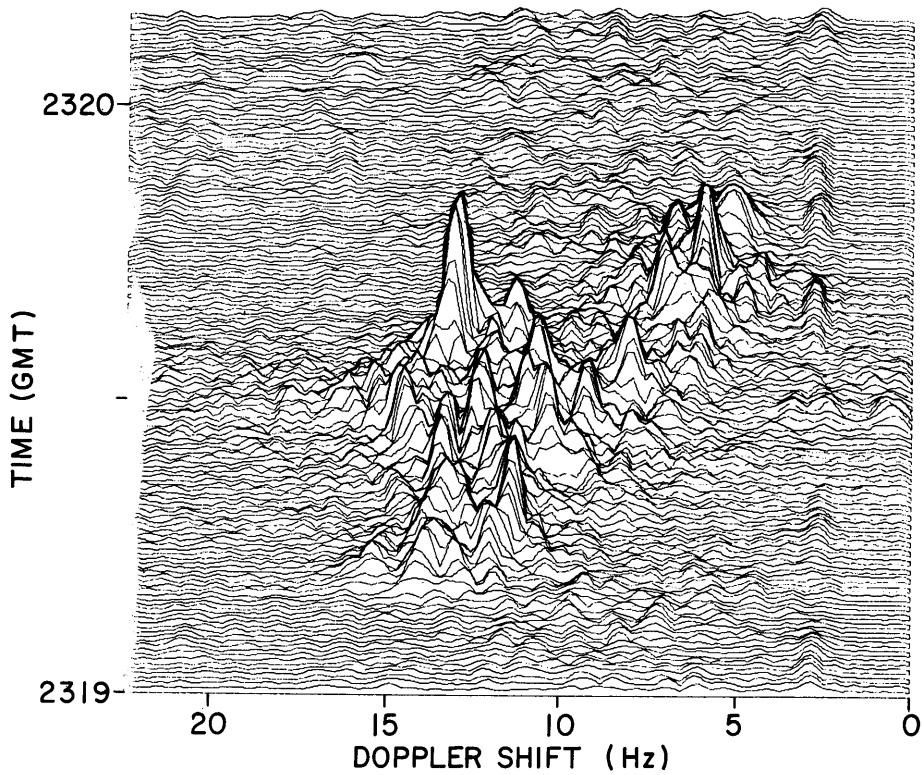


Fig. A2 - Time plot of computer-analyzed signal intensity vs doppler shift for barium release, Oct. 4, 1967

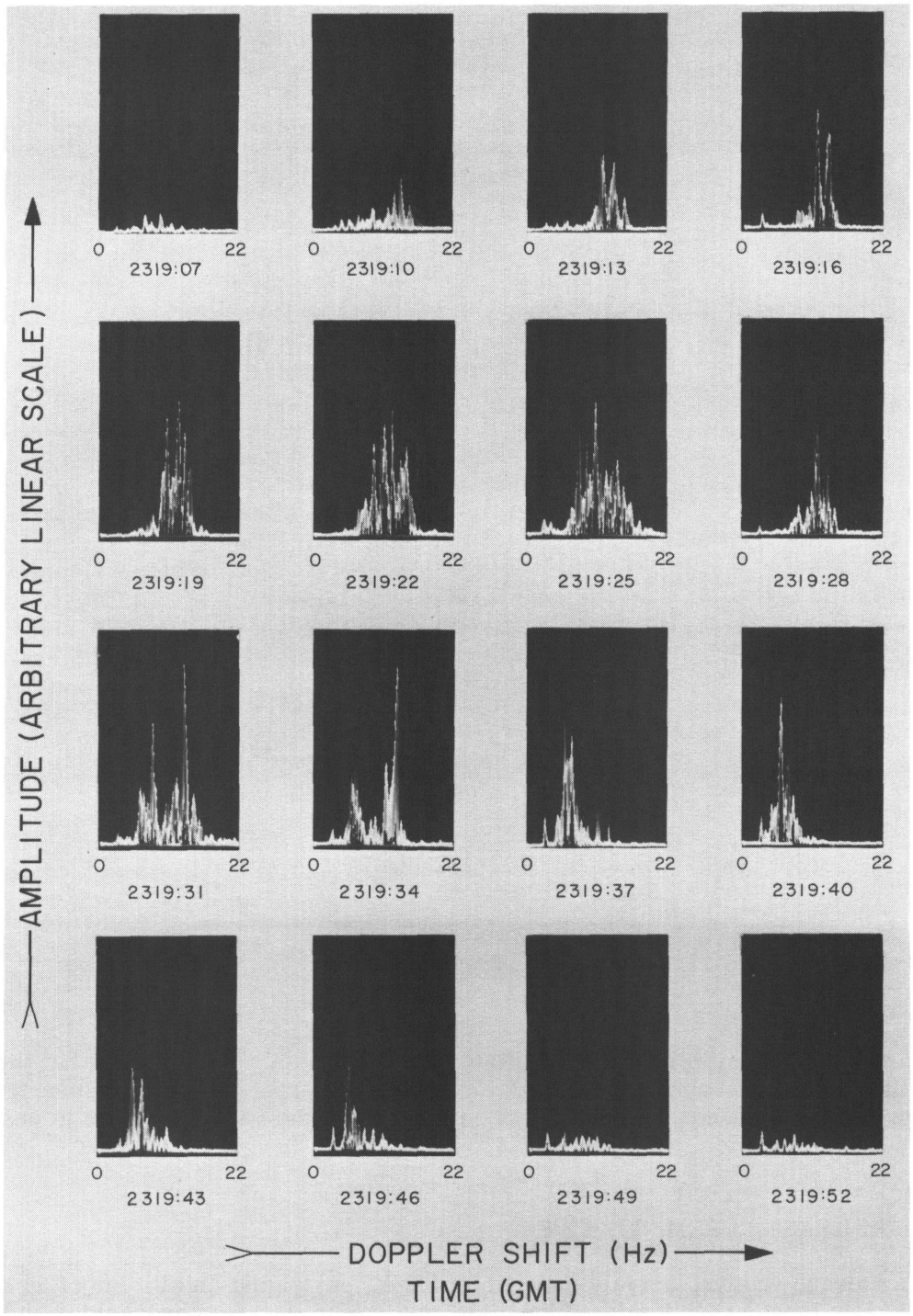


Fig. A3 - Amplitude spectra for barium release, Oct. 4, 1967

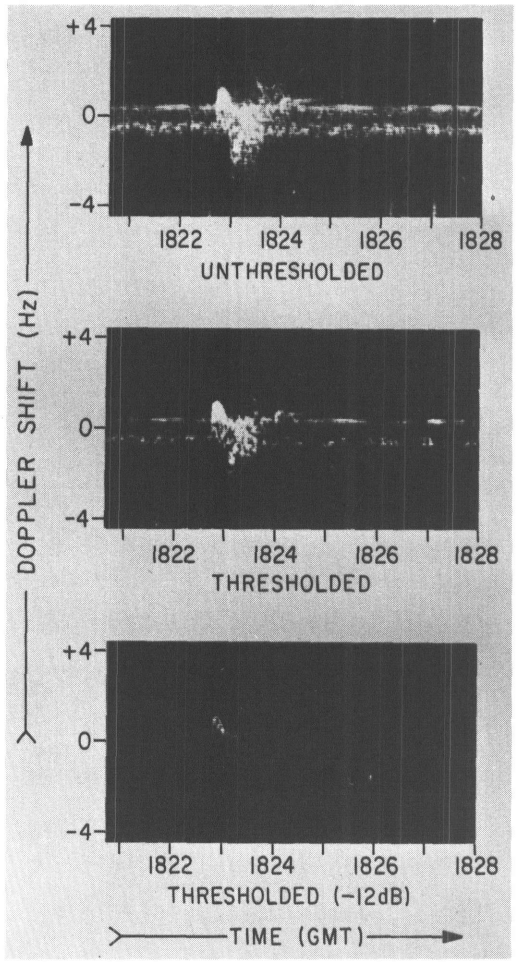


Fig. A4 - Doppler shift vs time for cesium release, Apr. 12, 1968

shown in the section on "Plasma Cloud Radar Echo Statistics" illustrates that the waviness of the distribution about lognormalcy is very similar in extent and appearance, and thus is probably a consequence of slight nonlinearity in the radar receiver at certain levels.

## CESIUM RELEASE, APRIL 17, 1968

This release was explosively emitted by a 2-kg payload at an altitude of 94 km and lasted slightly longer than 1 min. Figure A6 is a collection of unthresholded and thresholded photographs in doppler shift vs time format. A vertical bar occurs at the time of release, 2044:40 GMT. A light horizontal band at 4 Hz and a zigzag band, which wobbles back and forth in the upper part of the top photograph until 2045:10 GMT, then descends through the cloud signature and reaches 0 Hz at 2045:40 GMT, are the result of small interfering targets and can be ignored. The specular features of this signature are evident in the middle and lower photographs. Figure A7 is a computer-analyzed version of these data, with a vertical clutter band at 0 Hz, which shows the four or five discrete

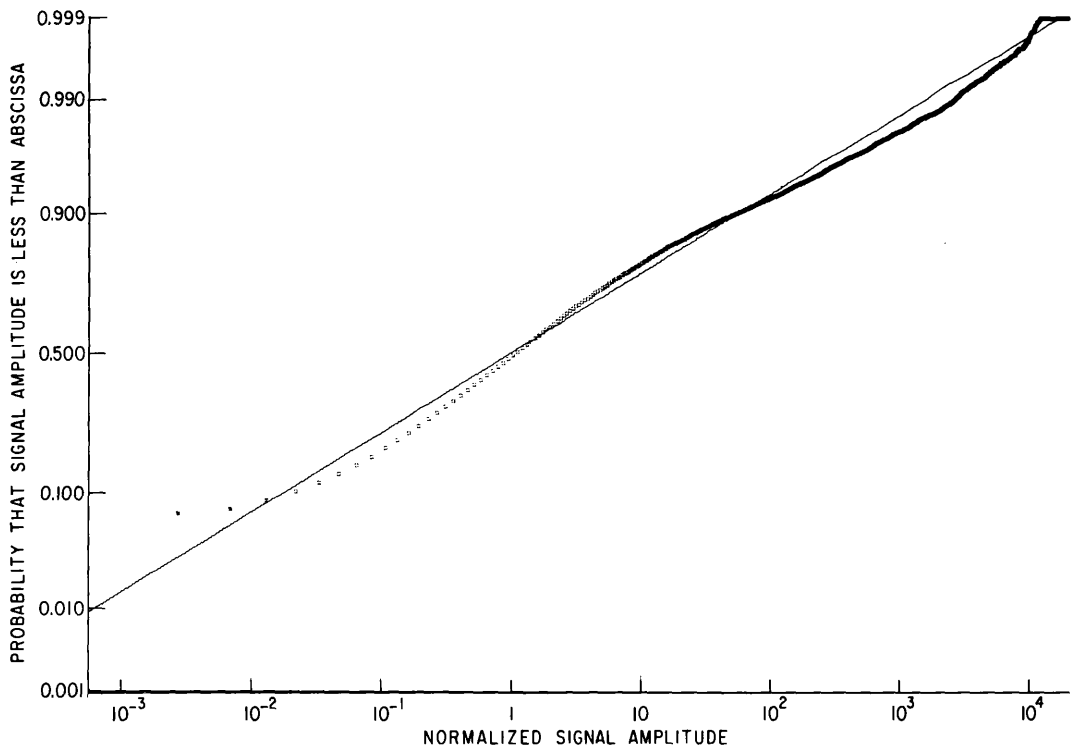


Fig. A5 - Cumulative amplitude distribution of signal components for cesium release, Apr. 12, 1968

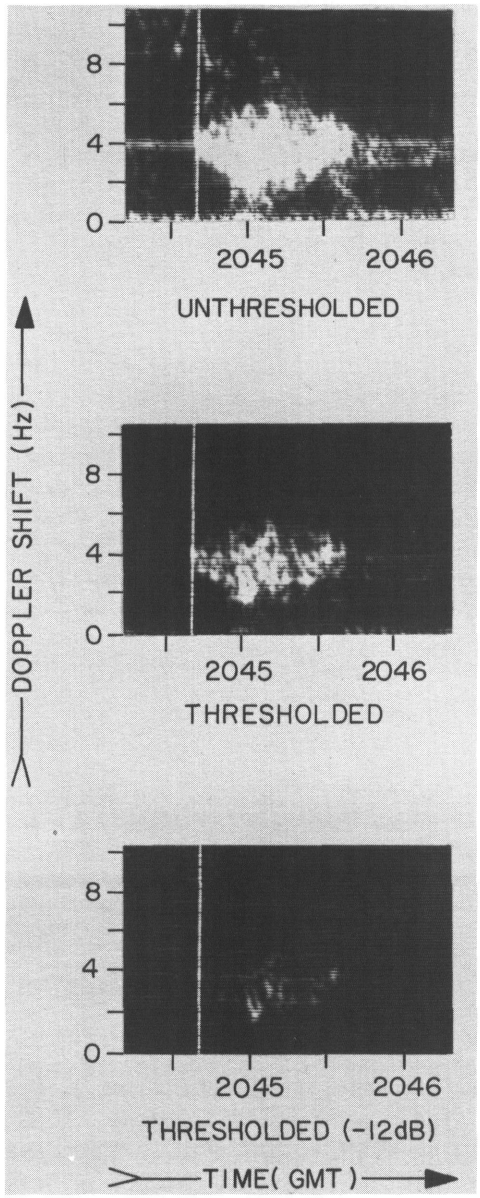


Fig. A6 - Doppler shift vs time for cesium release, Apr. 17, 1968

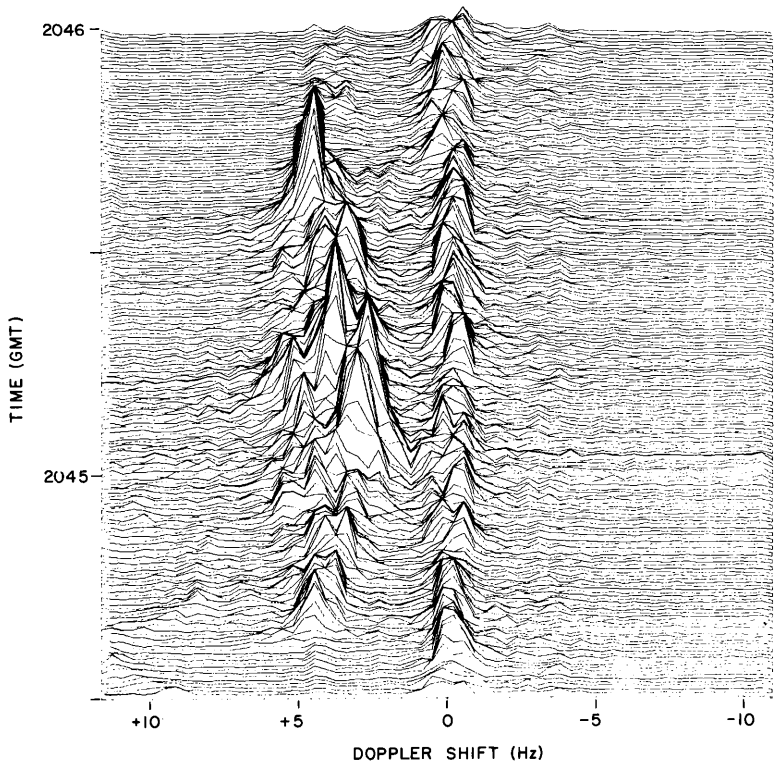


Fig. A7 - Time plot of computer-analyzed signal amplitude vs doppler shift for cesium release, Apr. 17, 1968

specular components more clearly. Figure A8 contains a collection of amplitude spectra. (Notice that in none of Figs. A6-A8 are the doppler shift scales exactly the same, although all include the +2- to +6-Hz interval where the plasma cloud signature appears.) The photograph at 2044:42 GMT exhibits the single-scattering Phase II echo which disappears immediately in this release, yielding to a gradually diffusing spectrum. Discrete spectral features begin to appear at 2045:00 GMT, with two extremely large ones lasting for 6 to 9 sec each. Several others, smaller but of comparable lifetime, appear until 2045:42 GMT, when the signature finally begins to disappear. Figure A9 is a plot of apparent radar cross section vs time for this signature. All the features, about five in number, which extend above $10^4$ $m^2$ are due to these spectrally discrete components. These components individually display apparent radar cross sections of greater magnitude than the $10^4$ $m^2$ quiescent plasma cloud.

Figure A10 contains photographs of the signature acquired on meter-wave radar. The upper photograph contains a bright zigzag line which corresponds to the rising projectile, and which disappears at 2044:00 GMT as the vehicle leaves the range interval for which the photograph was taken. The wobbly line across the top of this photograph is a contaminant. The lower photograph, at a different range, shows the zigzag projectile signature growing in intensity as the vehicle enters the range interval, and a very bright band at 2044:40 GMT corresponding to the burst. This photograph was taken with higher signal processor sensitivity than the upper one, so all wobbly lines, which represent contaminants, are much more intense. The left-hand scale is labeled "relative" doppler shift because the meter-wave radar was not phase-locked to the signal processor and

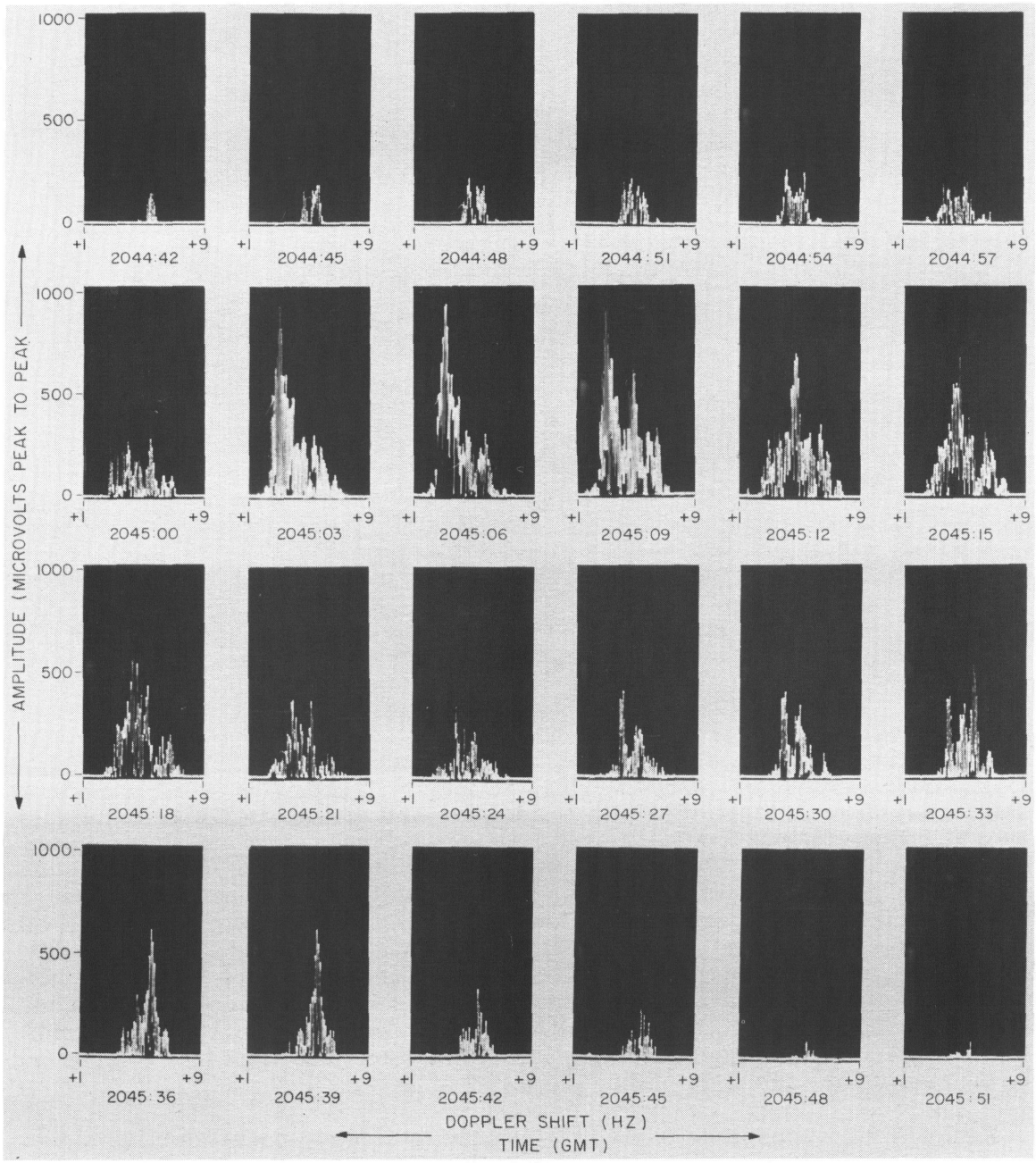


Fig. A8 - Amplitude spectra for cesium release, Apr. 17, 1968

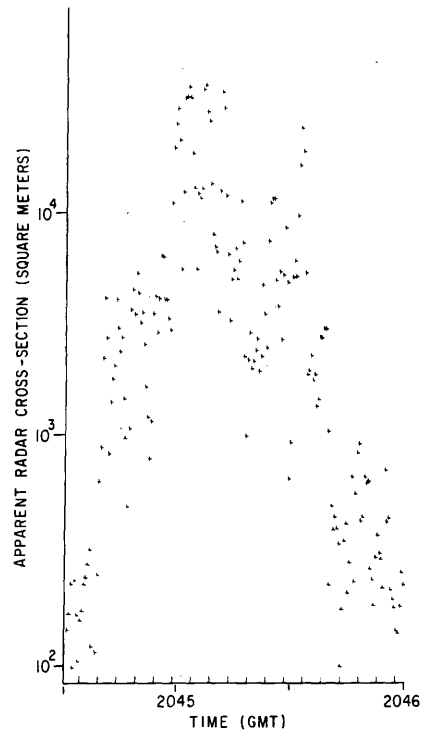


Fig. A9 - Apparent radar cross section vs time for cesium release, Apr. 17, 1968

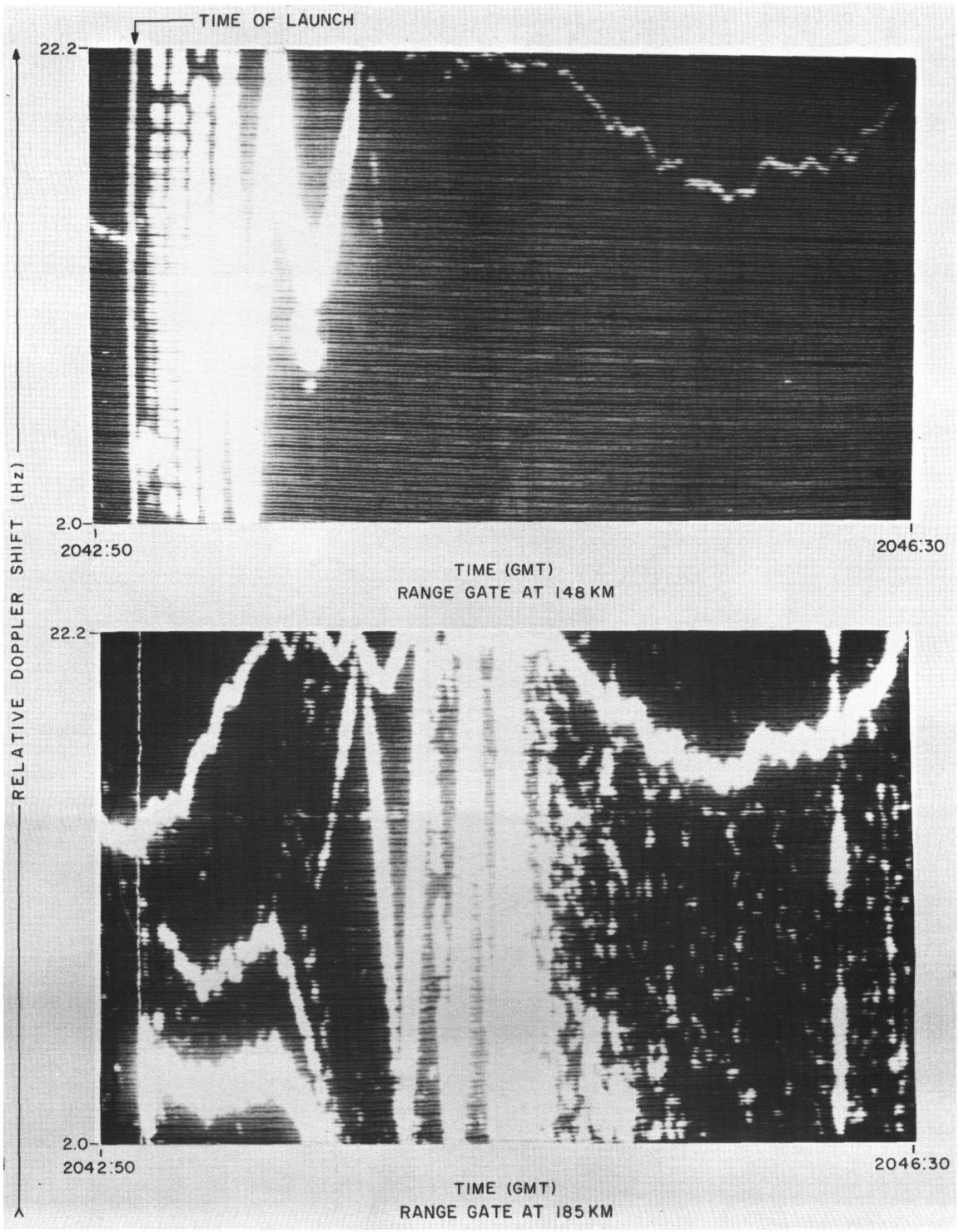


Fig. A10 - Doppler shift vs time of meter-wave signal for cesium release, Apr. 17, 1968

hence did not permit absolute doppler shift to be measured. The 2.0- to 22.2-Hz frequency range shown represents nearly the entire available unambiguous spectral extent (22.5 Hz), and of course the zigzag appearance of the projectile echo illustrates the passage of the target through several doppler ambiguities. The important features of the lower photograph are:

1. As is typical of meter-wave data, the signature at burst is quite large and dissipates rapidly after a few seconds.

2. The general noise level in the entire spectrum is raised, indicating that even after the blast echo there remain low-level incoherent signal components.

3. At about 2045:00 GMT there appear, between 2.0 and 5.0 Hz, two or three bright blobs. These traces represent coherent echoing entities, and can be seen by comparison with Figs. A6-A8 to correspond to the appearance of large discrete spectral components in the decameter-wave data. These blobs persist until about 2045:15 GMT, which corresponds to the time at which the two largest discrete components in Figs. A6-A8 disappear.

Figure A11 contains amplitude spectra of the meter-wave data, with a resolution bandwidth of 0.3 Hz. The first photograph contains an undulating spectrum which is the echo from the still-accelerating projectile in the last 3 sec before burst. The blast wave appears in the next three photographs, with spectral components filling the entire available spectrum. The highly peaked portion to the extreme left in these photographs is probably the echo from the nearly stationary contact surface in the later stages of the blast phase (Phase I). By 2044:49 GMT the meter-wave echo has nearly disappeared. This datum is repeated at a 12-dB-higher signal processor sensitivity, and all subsequent photographs correspond to this higher level. Notice that in all photographs after this increase in sensitivity there exists a high-amplitude spike near the right-hand edge, which moves in toward the central region as time proceeds. This component is a contaminant and corresponds to the wobbly line which appears in Fig. A10 near the tops of the photographs. The objects of interest in Fig. A11 are the several spectral components between 0 and 5 Hz which appear at 2045:01 GMT and disappear at 2045:13 GMT. These relatively discrete components occur in the same interval as the large spectral features of the decameter data. It is difficult to identify individual members of this spectrum, but lifetimes of 3 to 6 sec appear likely for each of them.

## CESIUM RELEASE NO. 1, SEPTEMBER 11, 1968

This release was explosively emitted by a 2-kg payload at an altitude of 92.7 km and lasted about 40 sec. Figure A12 is a pair of unthresholded and thresholded doppler shift vs time photographs of this signature, with a band of radar clutter between 0 and -1 Hz. The vertical traces at 2114, 2115:30, and 2116 GMT in the upper photographs are meteor echoes. The five blobs which appear between 0 and about 1.5 Hz in the lower photograph are the specular features. Figure A13 is a collection of amplitude spectra for this release. The first photograph in Fig. A13 shows a single, relatively narrow, spectral component which represents the clutter echo. Components at this doppler shift appear, generally with somewhat lower amplitude, in all photographs and should be ignored. The second photograph shows, in addition to the clutter echo, a pair of spectral components. One of these is a remnant of Phase I/Phase II single-scattering, and the other (to the far right) is a growing discrete spectral feature. Several other such features are seen to grow and decay in the succeeding photographs, with two or three separate components identifiable at many times. The last one to occur is probably the most easily resolved, even though it is not the largest. This feature just begins to rise in the photograph taken at 2115:12, reaches a peak at 2115:15, and descends into the clutter by 2115:18 GMT.

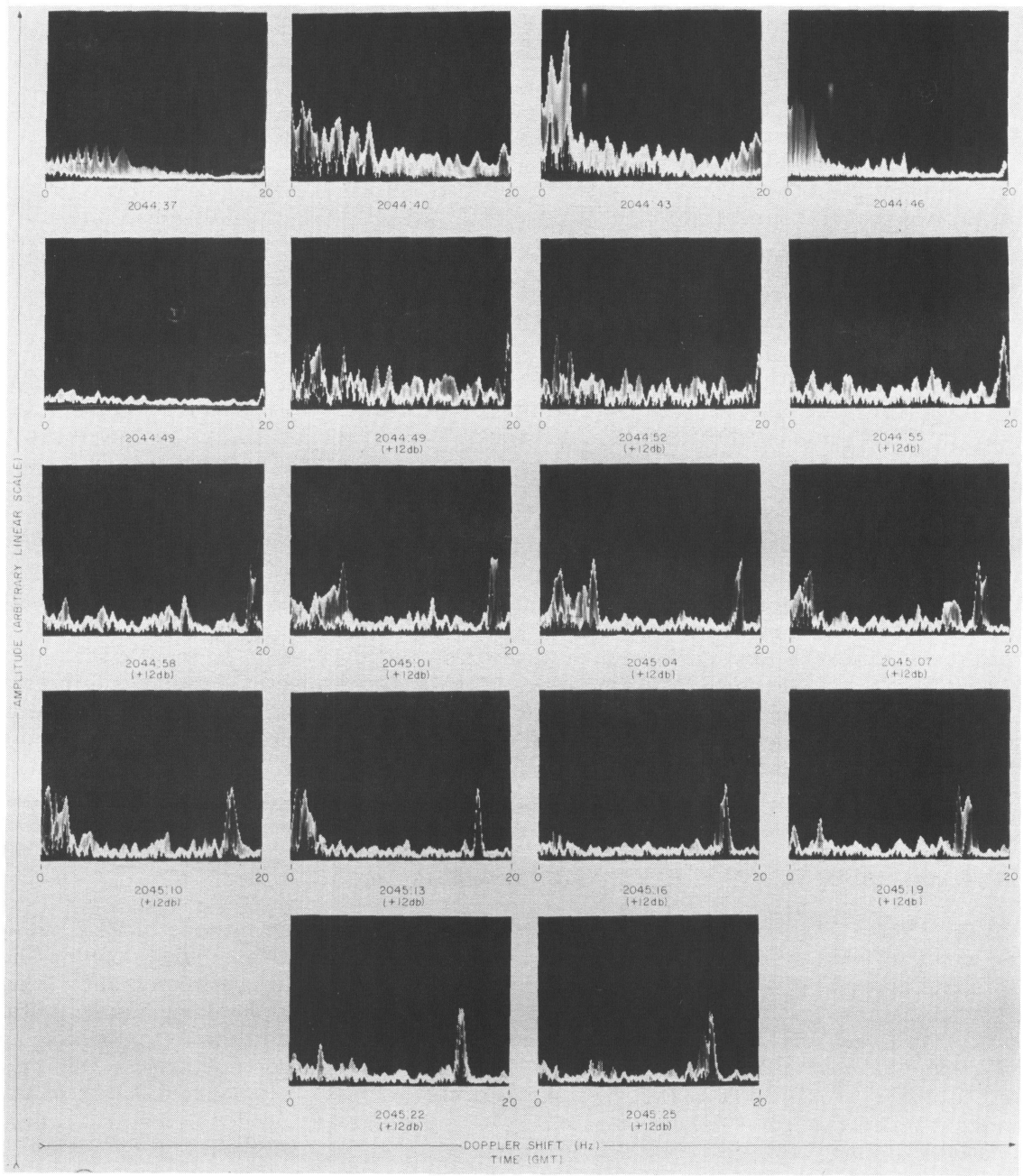


Fig. A11 - Amplitude spectra of meter-wave signal for cesium release, Apr. 17, 1968

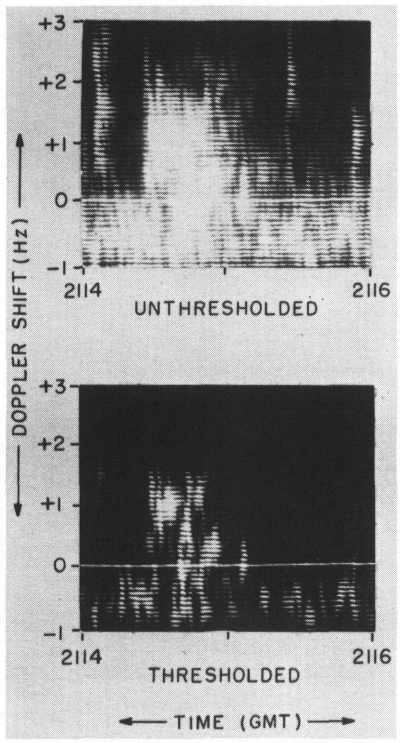


Fig. A12 - Doppler shift vs time for cesium release No. 1, Sept. 11, 1968

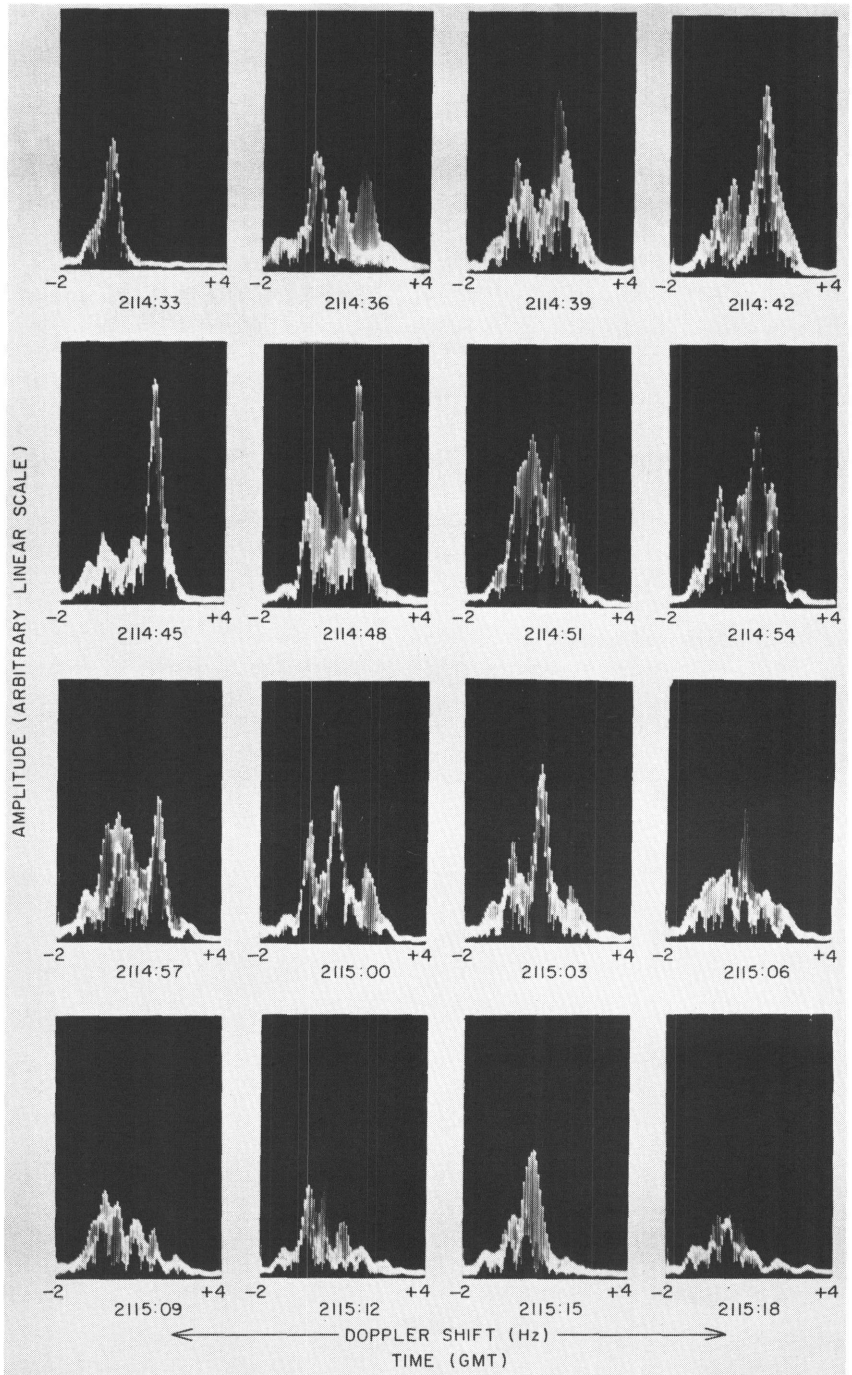


Fig. A13 - Amplitude spectra for cesium release No. 1, Sept. 11, 1968

## CESIUM RELEASE NO. 2, SEPTEMBER 11, 1968

This release was explosively emitted by a 2-kg payload at 93.3 km and lasted about 6 min. Figure A14 is a doppler shift vs time photograph of the signature, which displays distinct evidence of modulation in spectral bandwidth, intensity, and apparent doppler shift with a period of about 90 sec. Figure A15 is a computer-analyzed version of these data which shows the amplitude modulation more distinctly and also exhibits the occurrence of irregular spectral behavior which characterizes Phase III of plasma cloud evolution. Although only three cycles of the long-period modulation occur in this case, its similarity to the example of Phase IV behavior discussed in the first section of Part II is compelling. No earth-backscatter echo was acquired for this release, however, and it is likely that the cloud lifetime was too short at this relatively low altitude for a sporadic-E-like layer to be formed in spite of every likelihood that the mechanism was operating. It is noted that this release occurred very near local sunset, and the weakening solar illumination probably did not provide ionization at the rate necessary to compensate for diffusion and chemical loss processes.

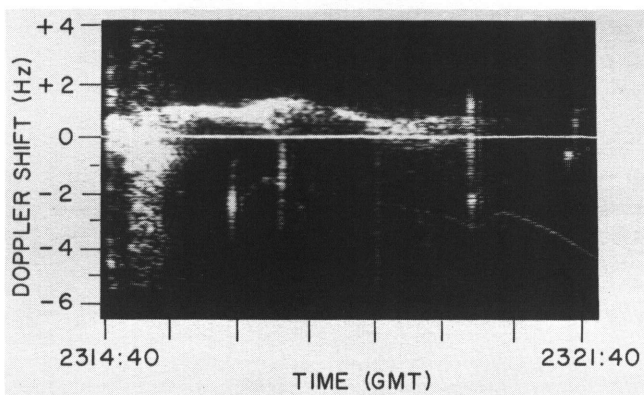


Fig. A14 - Doppler shift vs time for cesium release No. 2, Sept. 11, 1968

Figure A16 is a plot of apparent radar cross section vs time showing the 90-sec amplitude modulation in the presence of an irregular short-term behavior. Some of the sharp peaks on Fig. A16 are readily attributed to meteor echoes, which are identifiable on Figs. A14 and A15 as vertical bars of short duration. Figure A17 is an autocorrelation function computed for the data on this release. The 90-sec periodicity is evident but may be exaggerated due to the brevity of the sample (90 sec in lag is one-fifth the total sample length). A cumulative amplitude distribution for this release appeared as Fig. 15 of the section on "Plasma Cloud Radar Echo Statistics."

## CESIUM RELEASE NO. 3, SEPTEMBER 11, 1968

The data for this release appear in Figs. 5-7.

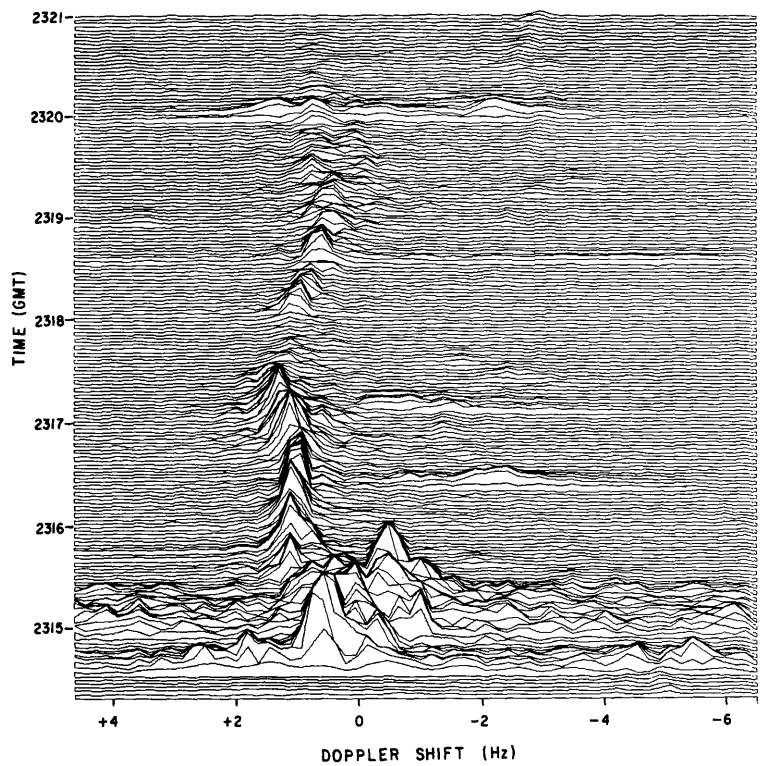


Fig. A15 - Time plot of computer-analyzed signal amplitude vs doppler shift for cesium release No. 2, Sept. 11, 1968

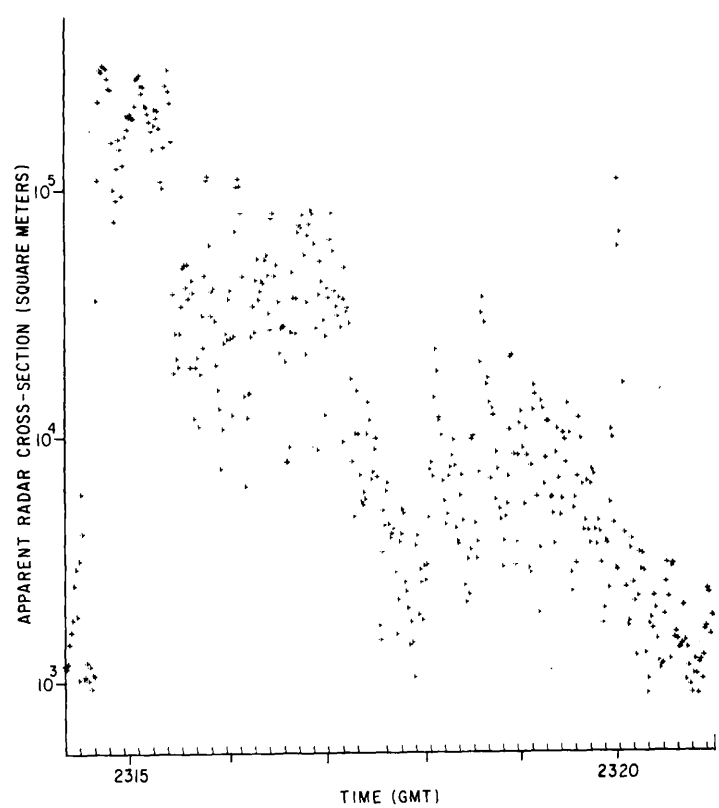


Fig. A16 - Apparent radar cross section vs time for cesium release No. 2, Sept. 11, 1968

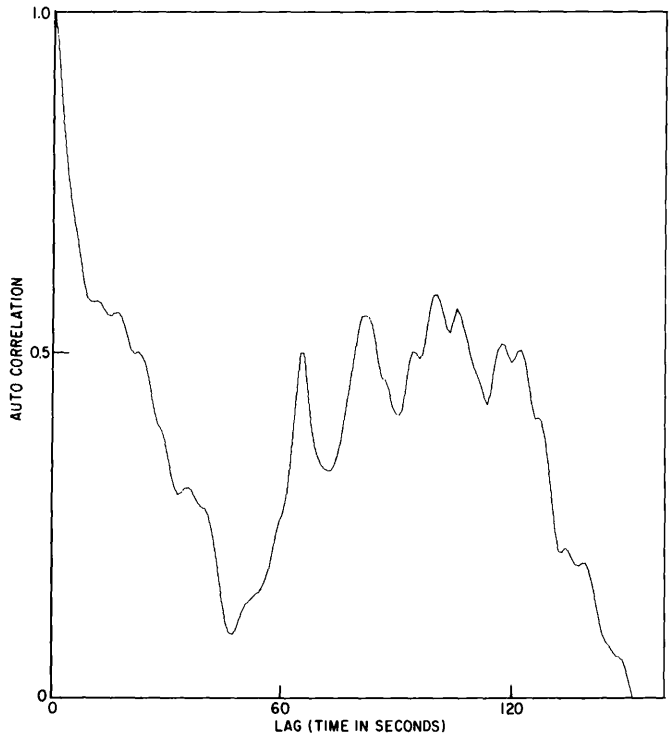


Fig. A17 - Cumulative amplitude distribution of signal components for cesium release No. 2, Sept. 11, 1968

## CESIUM RELEASE NO. 1, FEBRUARY 14, 1969

This release was explosively emitted by a 2-kg payload at an altitude of 99.1 km in total darkness. The signature lasted nearly 4 min and displayed a sudden disappearance immediately after Phase II, followed by reappearance a few seconds later and subsequent Phase III behavior. Figure A18 is a doppler shift vs time photograph of this release. The irregular wobbly lines are interfering targets and should be ignored. The vertical bar at about 0507:10 GMT is the blast-wave (Phase I) signature, followed by a wedge-shaped trace which represents the Phase II echo. Notice that this trace is symmetric about a frequency slightly below 0 Hz. The signature in this early interval represents a combined signal from targets decelerating in a direction toward the radar (the upper segment) and decelerating in a direction away from the radar (the lower segment). Hence the expanding plasma bubble is probably partially transparent, and both the receding and approaching surfaces are detected.

The signal disappears completely at the end of Phase II and reappears at a different apparent velocity. This new apparent velocity is probably the drift velocity of the cloud, while the former point of symmetry was probably a residual of the projectile motion. Notice that the second portion of the signature is ragged in appearance and quite irregular. Figure A19 is a computer-analyzed version of these data showing the irregular spectral behavior more clearly. The many discrete components at this high altitude, and several interfering targets, made it impossible to measure growth rates, lifetimes, and decay rates of these components. A plot of apparent radar cross section for this release appeared earlier as Fig. 4.

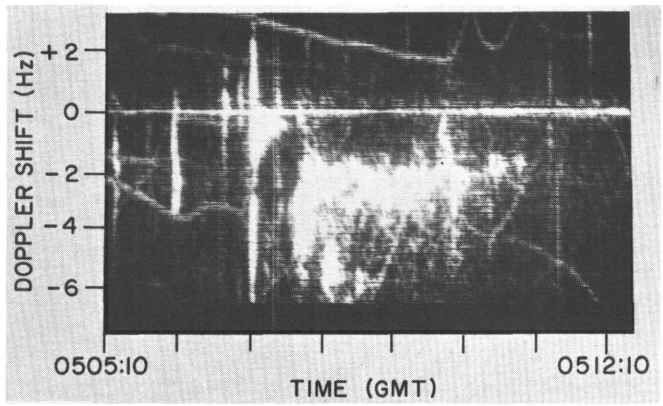


Fig. A18 - Doppler shift vs time for cesium release No. 1, Feb. 14, 1969

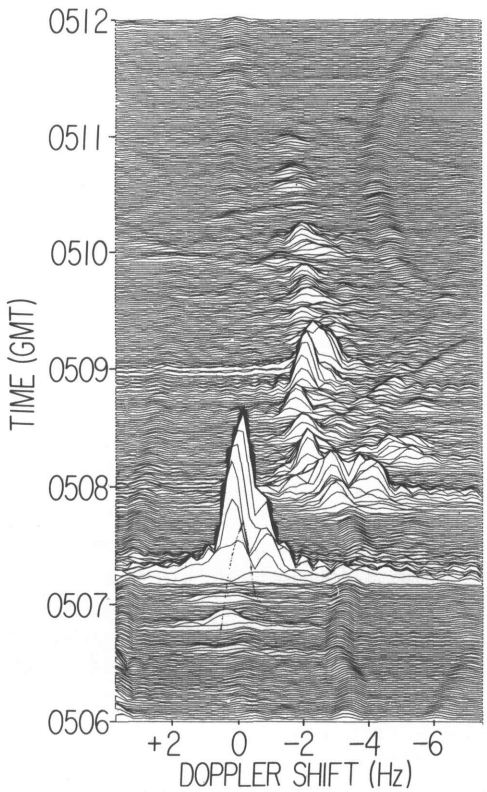


Fig. A19 - Time plot of computer-analyzed signal amplitude vs doppler shift for cesium release No. 1, Feb. 14, 1969

## CESIUM RELEASE NO. 2, FEBRUARY 14, 1969

This release was explosively emitted by a 2-kg payload at an altitude of 96.8 km, also in total darkness, and lasted about 2-1/2 min. Examples of its appearance were included as Fig. 3 to illustrate Phase II behavior. Figure A20, which is a slightly different doppler shift vs time display of these data, shows the irregular Phase III behavior more clearly. (The doppler shift axis on Fig. A20 is ambiguous, and the scale value labeled +10 actually represents -10 Hz.) A narrow band of clutter appears at the bottom of Fig. A20, as well as an intense horizontal bar at +7.5 Hz which is a spurious signal. The Phase III behavior which begins at 0708:00 GMT is once again characterized by a ragged diffuse spectrum studded by small highlights. Figure A21 is a computer-analyzed version of these data showing the ridge-like component which corresponds to Phase II, plus the irregular Phase III components. It can be noted that there are fewer, more distinct, discrete spectral features in this signature than in the previous higher-altitude case. Figure A22 is a cumulative amplitude distribution for these data, displaying the usual close conformity to lognormal characteristics and slight deviations from the straight line similar to previous examples.

## CESIUM RELEASE NO. 3, FEBRUARY 14, 1969

The data for this release appear in Figs. 8-14 in the first section of Part II of this report.

## CESIUM RELEASE, JUNE 3, 1969

This release was explosively emitted by a 2-kg payload at an altitude of 102 km and lasted more than 20 min. It exhibited the common irregular spectrum characteristic of Phase III and longer-term modulations characteristic of Phase IV. No sporadic-E-like reflecting layer could be identified with a high confidence level, however, due to inadvertent nonlinearity in the radar receiver. An illustration of its spectral appearance will appear in the last section of this Appendix below, in comparison with examples of all the other long-duration signatures.

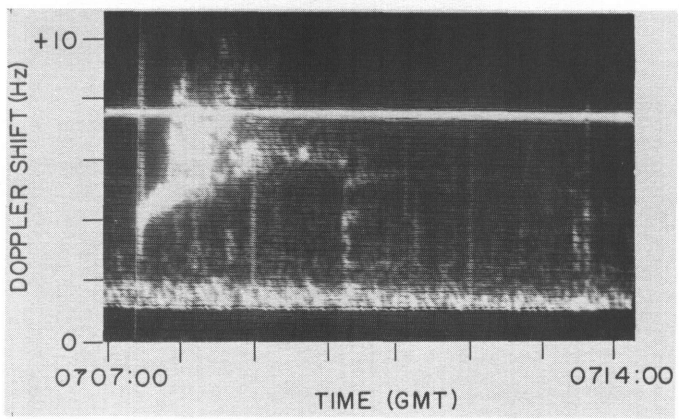


Fig. A20 - Doppler shift vs time for cesium release No. 2, Feb. 14, 1969

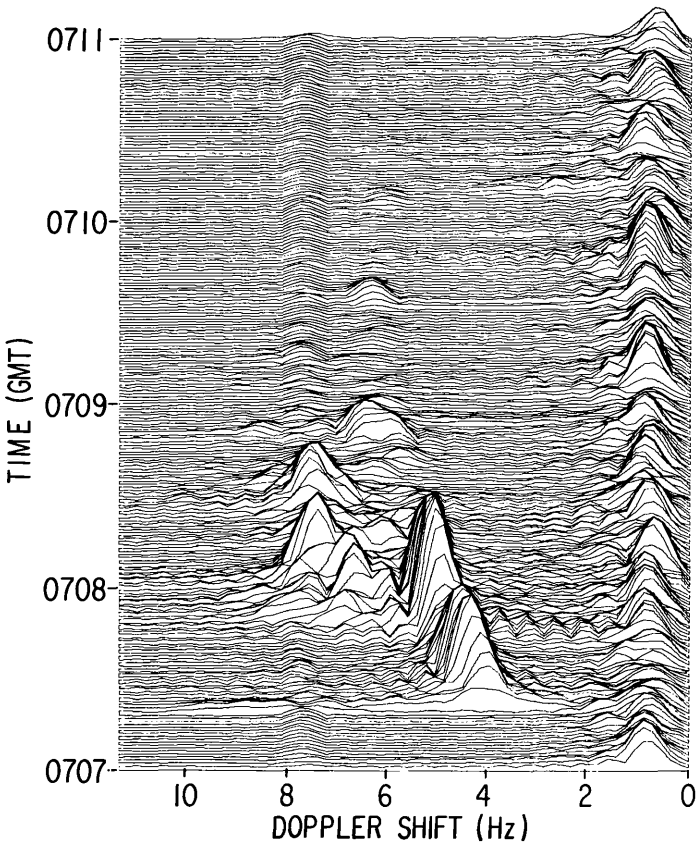


Fig. A21 - Time plot of computer-analyzed signal amplitude vs doppler shift for cesium release No. 2, Feb. 14, 1969

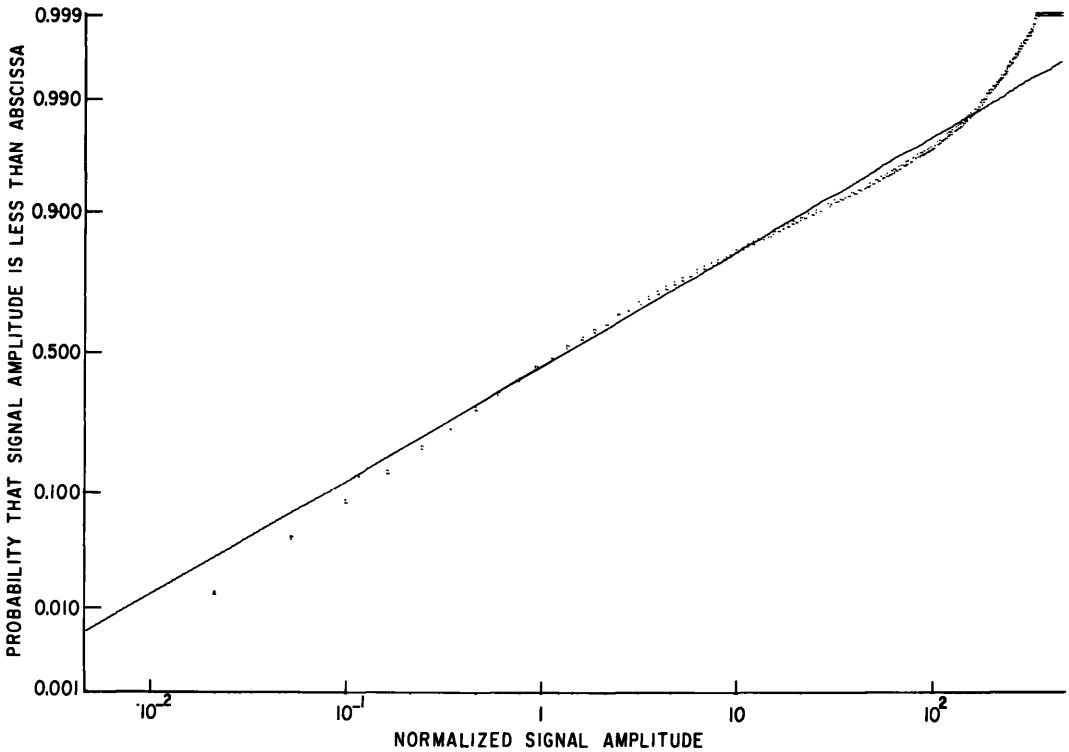


**Fig. A22 - Cumulative amplitude distribution of signal components for cesium release No. 2, Feb. 14, 1969**

## CESIUM RELEASE, JULY 18, 1969

This release was explosively emitted by a 2-kg payload at an altitude of 95.5 km and lasted nearly 1/2 hr. It was characterized by an unusually narrow spectral dispersion with extreme modulations in intensity.

Figure A23 is a computer-analyzed illustration of doppler shift vs time, with amplitude as the virtual third axis. It is evident from the very beginning that many discrete spectral components, characteristic of Phase III behavior, appear throughout the cloud's lifetime. There is also an evident long-period modulation, with a period of about 100 sec, which is most evident on the right-hand portion of Fig. A23. Figure A24 is a plot of radar cross section vs time which illustrates this somewhat irregular long-period modulation. It should be noted in Fig. A24 that short-term irregular behavior does not become pronounced until about 1720 GMT, and then it appears to display less frequent excursions than in other examples. The long-term modulation is irregular in period, with periods of 40 to 120 sec, but is very strong.

## CESIUM RELEASE, JULY 23, 1969

This release was explosively emitted by a 2-kg payload at an altitude of 99.1 km and lasted more than 3 min. Figure A25 contains three doppler shift vs time photographs of the signature showing several intense spectral features superimposed on the irregular cloud echo spectrum. Figure A26 is a computer-analyzed version of these data showing the two or three extremely-high-amplitude components, and several smaller ones. Figure A27 is a collection of amplitude spectra for the first 50 sec of this release; the prerelease condition is shown in the first photograph, the blast-wave phase (Phase I) in the second and third photographs, and the appearance of several spectral components of 3- to 6-sec lifetimes (Phase III) thereafter. The signature lasted considerably longer, but no truly distinctive examples of intense spectrally discrete components appeared.

## CESIUM RELEASE, JULY 25, 1969

This release was explosively emitted by a 2-kg payload at an altitude of 92.4 km and lasted about 40 sec. Figure A28 is a collection of three doppler shift vs time photographs in which three distinct spectral features are apparent. Figure A29 is a computer-analyzed version of these data. A comparison of Figs. A28 and A29 with Figs. 5 and 6 (which correspond to a release at 87.5 km) and with Fig. A12 (which corresponds to a release at 92.7 km) reveals a notable similarity in number, appearance, intensity, and relative position (in velocity/time space) of these features. There seems to be a consistent tendency, at these lower altitudes, for a single initial spectral component to be followed, after 10 sec or so, by a pair of components separated by less than 1 Hz. That this behavior occurred in the three lowest releases, and was qualitatively similar in all of them, may indicate a preferred manner of evolution (i.e., a preferred modal coupling in the nonlinear regime). The theory is not adequately developed to permit a causal relationship to be specified, of course.

Figure A30 contains amplitude spectra for this release, with discrete features appearing between 1018:31 (coincident with the latter part of the blast wave) and 1018:58 GMT.

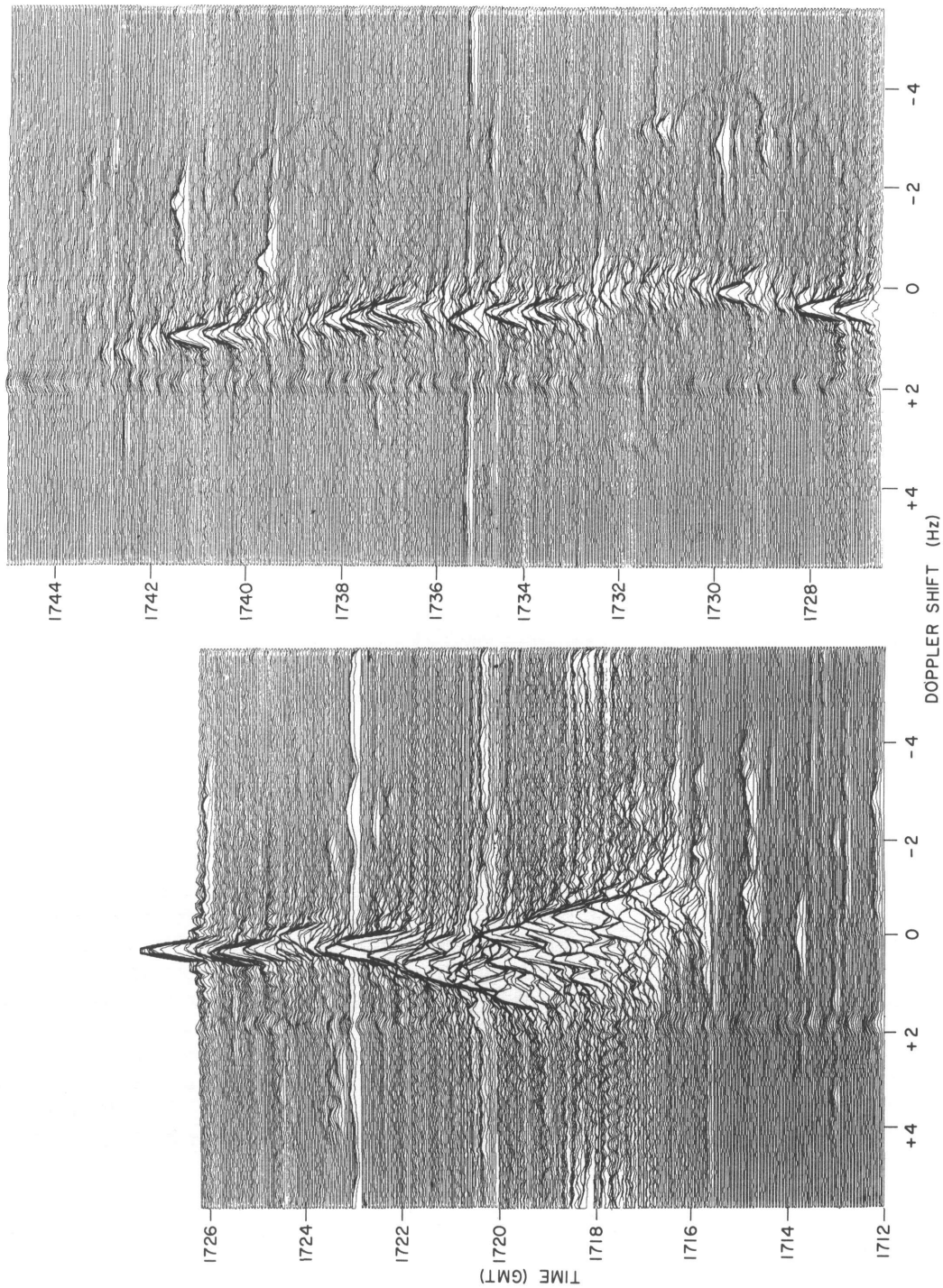


Fig. A23 - Time plot of computer-analyzed signal amplitude vs doppler shift for cesium release, July 18, 1969

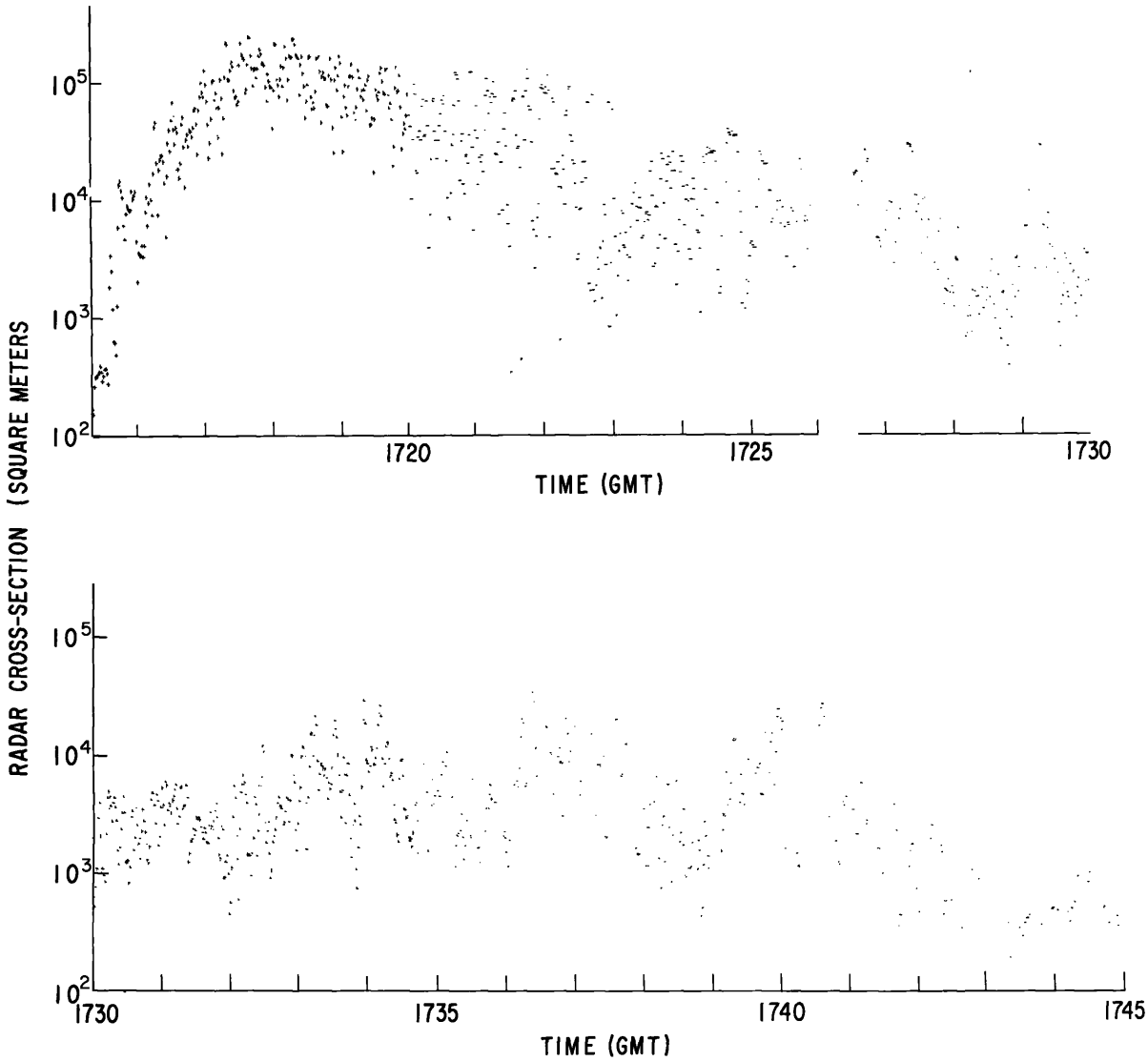


Fig. A24 - Apparent radar cross section vs time for cesium release, July 18, 1969

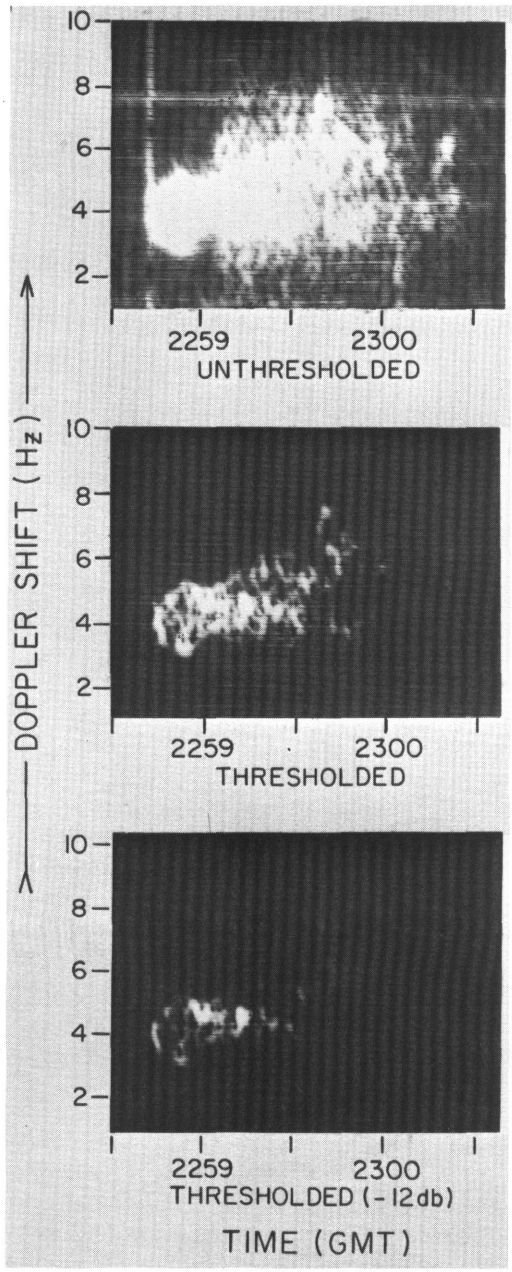


**Fig. A25 - Doppler shift vs time for cesium release, July 23, 1969**

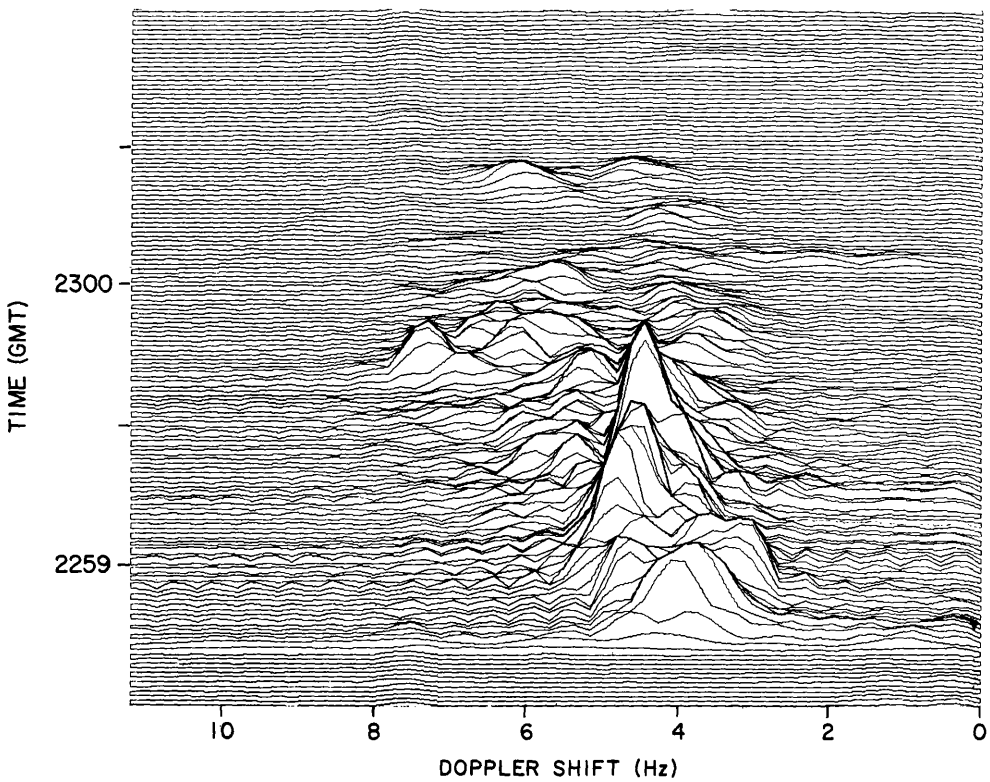


Fig. A26 - Time plot of computer-analyzed signal amplitude vs doppler shift for cesium release, July 23, 1969

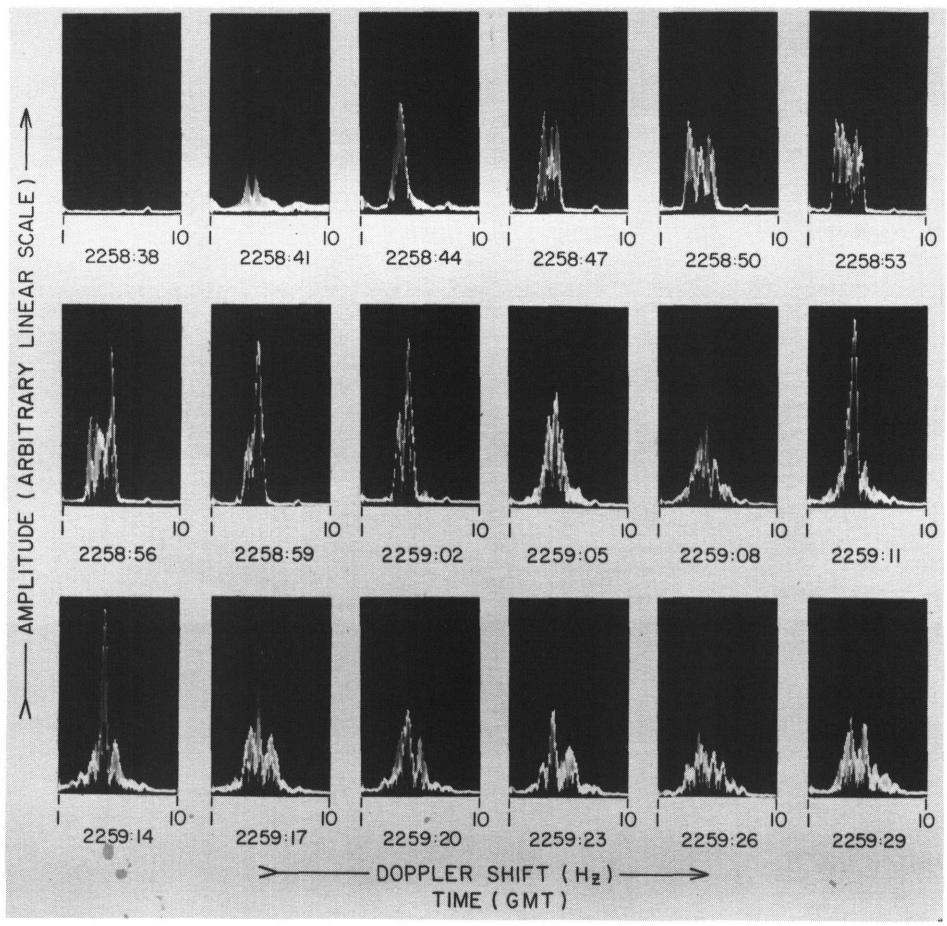


Fig. A27 - Amplitude spectra for cesium release, July 23, 1969

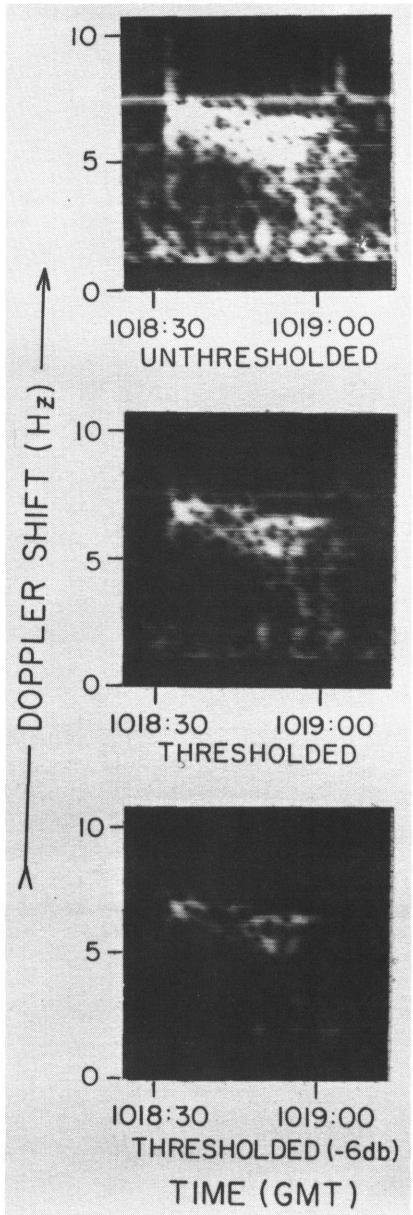


Fig. A28 - Doppler shift vs time for cesium release, July 25, 1969

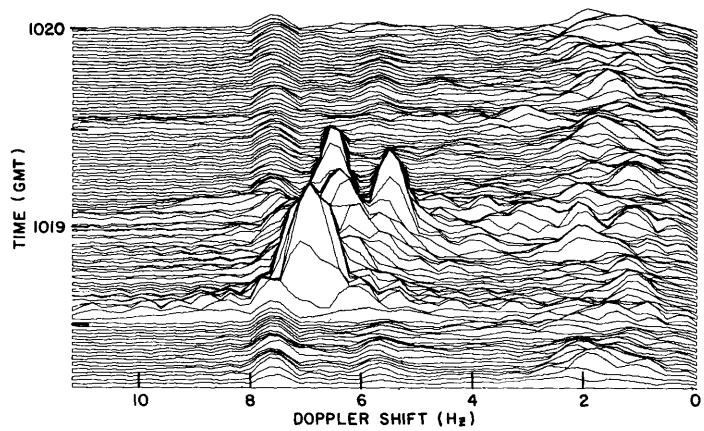


Fig. A29 - Time plot of computer-analyzed signal amplitude vs doppler shift for cesium release, July 25, 1969

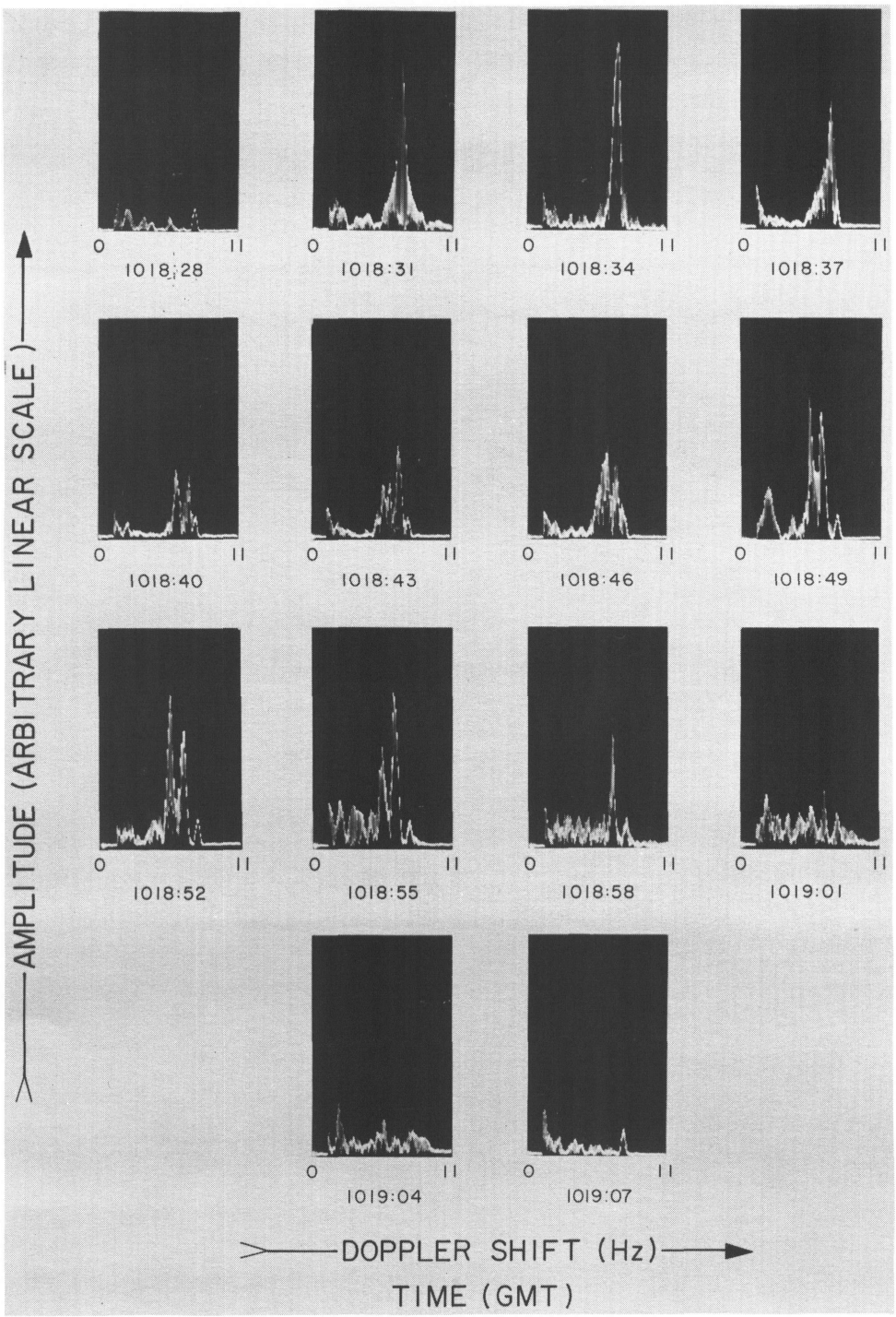


Fig. A30 - Amplitude spectra for cesium release, July 25, 1969

## PHASE IV BEHAVIOR OF LONG-DURATION SIGNATURES

The two 18-kg releases (Aug. 28 and 29, 1969) were similar in many respects to the other long-duration releases. Figure A31 contains six doppler shift vs time photographs of these events, distributed on the page relative to their burst heights. To the right of each photograph is an identifying label.

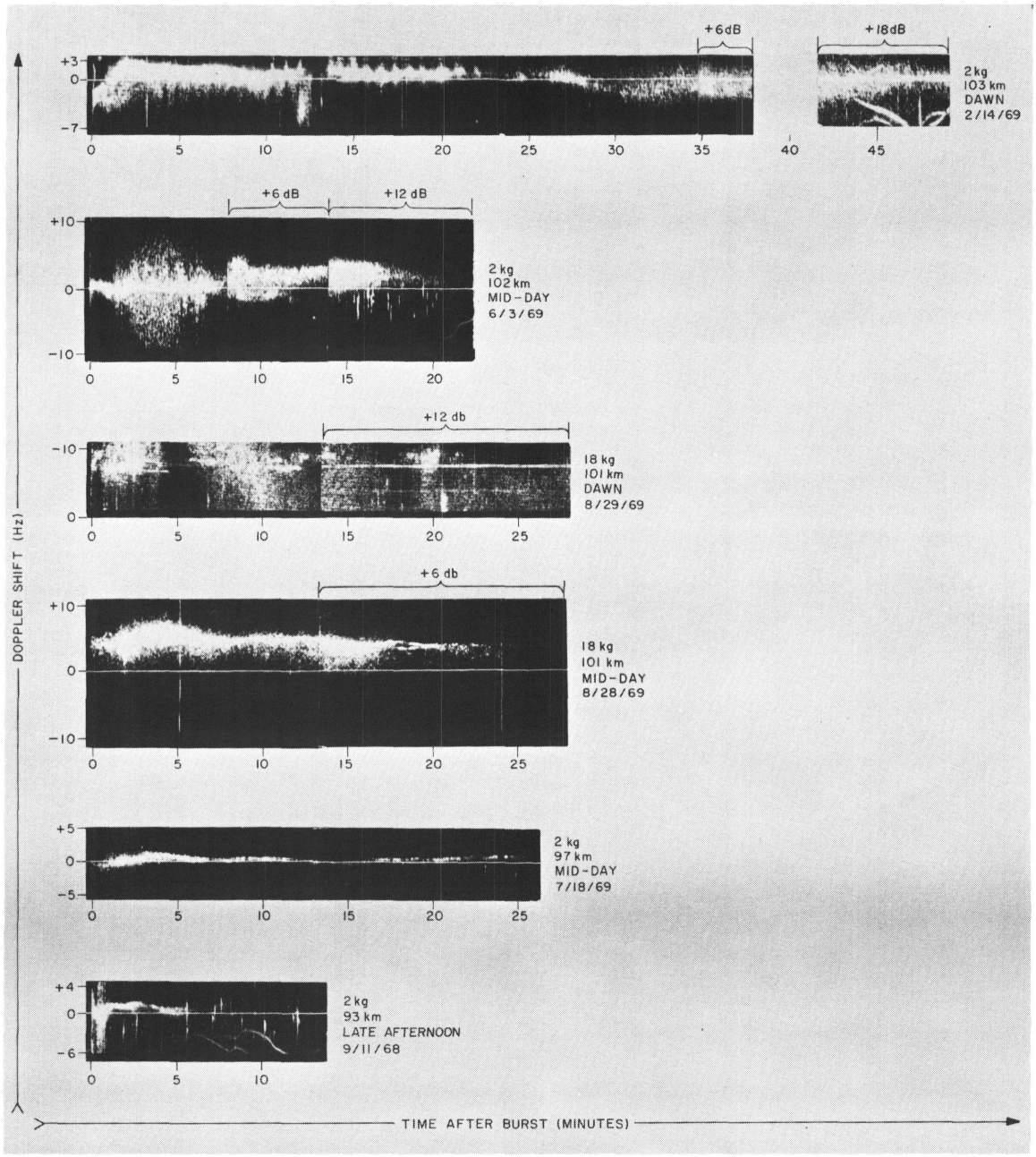


Fig. A31 - Doppler shift vs time for the six longest-duration cesium releases. Because this illustration was composed from preliminary data, the altitudes shown are not correct; the 6/3/69 release should fall below those for 8/28 and 8/29/69, which were at 102 and 103 km, respectively.

There seems to be no consistent tendency for periodicity to vary with altitude. The Feb. 14, 1969 release displayed 50-sec periodicity, but the Aug. 29, 1969 release (also at dawn and at about 103 km) exhibited a pronounced 6-min periodicity. It should be noted that the dawn releases are consistently more diffuse and studded with spectral features of greater definition than the others. This fact may indicate that the rapidly changing ionospheric chemi-ionic balance at dawn is favorable for the occurrence of instabilities.

There appears to be a tendency for spectral dispersion to increase with altitude, as mentioned in the first section of Part II, but this tendency does not affect either the amplitude modulations (which are strong in both of the lowest releases) or the tendency for discrete spectral features to occur.

The Aug. 28, 1969 release resulted in the formation of a sporadic-E-like reflecting layer. It appeared between 12 and 18 min after release (as in the Feb. 14, 1969 release), but remained for only about 5 min. Its appearance was accompanied by amplitude and spectral modulations of about 1-min periodicity, but these modulations were not nearly so pronounced as in the case of the Feb. 14, 1969 release. Figure A32 contains apparent radar cross section plots for the copolarized and the cross-polarized receiver channels. Modulation of about 10 dB in depth, coincident in phase, is apparent in the plots throughout the cloud's lifetime.

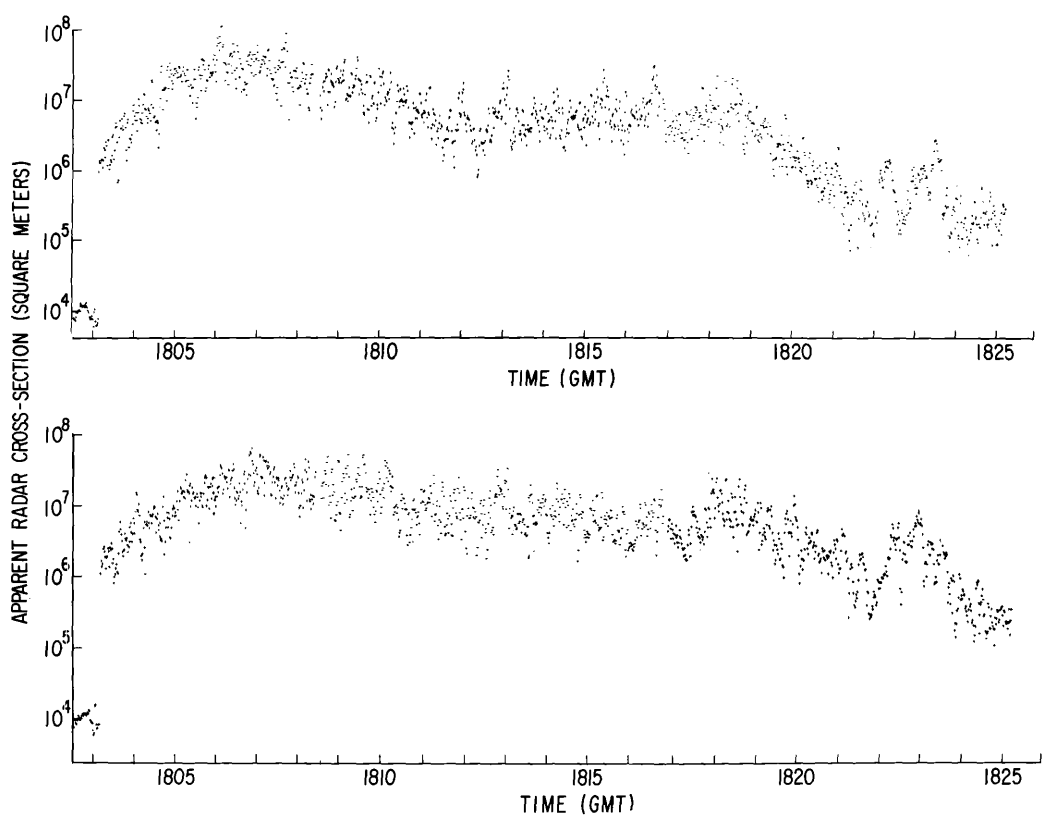


Fig. A32 - Apparent radar cross section vs time for copolarized (above) and cross-polarized (below) signal from cesium release, Aug. 28, 1969

Figure A33 is a computer-analyzed doppler shift vs time display of the earth-backscatter echo from the Aug. 28, 1969 release. It is apparent that the earth echo, which arises at 1815:20 GMT and lasts for about 5 min, does not correspond in this case to a single spectral component. (The vertical band at +4 Hz is spurious, and the irregular, horizontal bands at 1814 and 1820 GMT are meteor effects.) There exist three interfering components, in fact, and it is concluded that in this case the plasma cloud formed into several sublayers instead of one dominant one. This circumstance may explain both the short duration of the sporadic-E-like layer in this release and the smoother appearance of the radar cross section plot in Fig. A32.

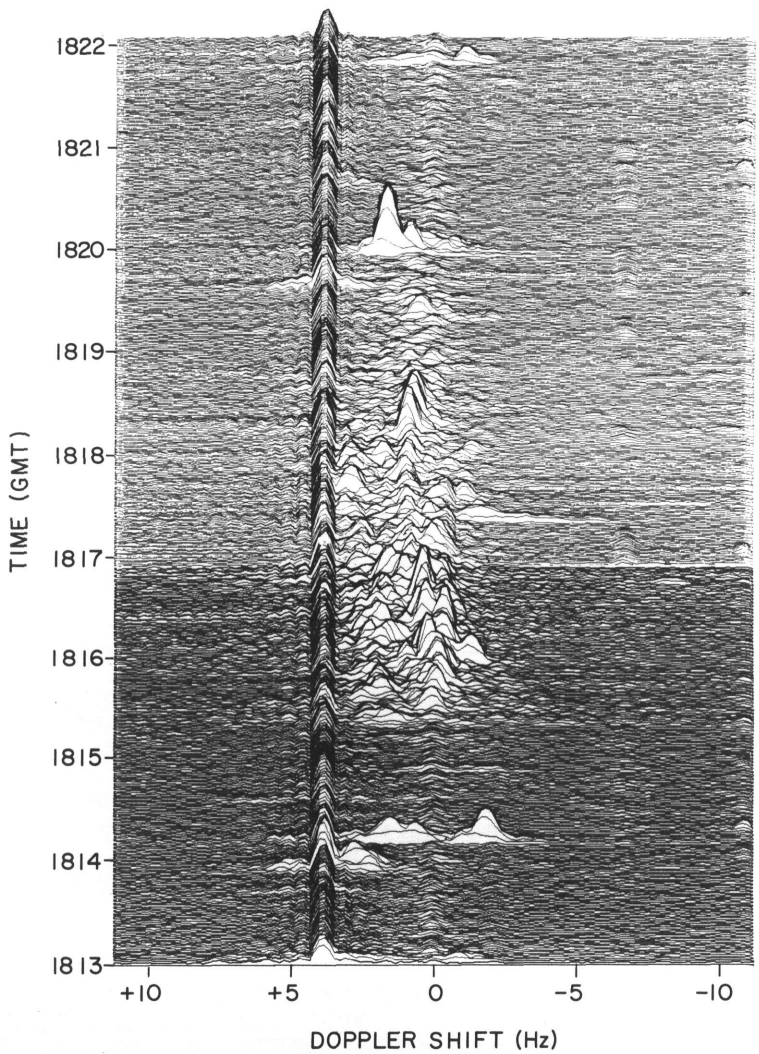


Fig. A33 - Time plot of computer-analyzed signal amplitude vs doppler shift for earth-backscattered signal from cesium release, Aug. 28, 1969

Security Classification

**DOCUMENT CONTROL DATA - R & D**

*(Security classification of title, body of abstract and indexing annotation must be entered when the overall report is classified)*

| | |
|---|---|
| 1. ORIGINATING ACTIVITY *(Corporate author)*<br>Naval Research Laboratory<br>Washington, D.C. 20390 | 2a. REPORT SECURITY CLASSIFICATION<br>Unclassified<br>2b. GROUP |

3. REPORT TITLE

INSTABILITIES OBSERVED IN LOWER-E-LAYER ALKALI-PLASMA-CLOUD RELEASES AND THEIR IMPLICATIONS REGARDING SPORADIC E

4. DESCRIPTIVE NOTES *(Type of report and inclusive dates)*
This is an interim report on one phase of a continuing problem.

5. AUTHOR(S) *(First name, middle initial, last name)*

John R. Davis

| | | |
|---|---|---|
| 6. REPORT DATE<br>July 28, 1970 | 7a. TOTAL NO. OF PAGES<br>110 | 7b. NO. OF REFS<br>118 |
| 8a. CONTRACT OR GRANT NO.<br>R02-23.501<br>b. PROJECT NO.<br>FB 2835-70-X-0014<br>c.<br>d. | 9a. ORIGINATOR'S REPORT NUMBER(S)<br>NRL Report 7105<br>9b. OTHER REPORT NO(S) *(Any other numbers that may be assigned this report)* | |

10. DISTRIBUTION STATEMENT

This document has been approved for public release and sale, its distribution is unlimited.

| | |
|---|---|
| 11. SUPPLEMENTARY NOTES | 12. SPONSORING MILITARY ACTIVITY<br>Department of the Air Force, Washington, D.C. and Department of the Navy (Naval Electronic Systems Command), Washington, D.C. 20360 |

13. ABSTRACT

This report describes a study of gun- and rocket-emplaced alkali plasma clouds in the 85-105 km altitude region of the ionosphere. The object of the investigation is to study the small-scale (tens-of-meters), short-term (fractions-of-seconds) irregular motion of the magnetofluid in the lower E layer. Motions on this spatial and temporal scale are known to be responsible for radiofrequency scattering at E-layer heights, and it has been suspected that they are important in the appearance and evolution of the sporadic-E layer. The resolution which is necessary to discern motions on the scale indicated was afforded by decameter- and meter-wavelength coherent-pulse-doppler radar.

A survey of possible instability mechanisms which can explain the spatial and temporal scales of the irregular motion observed in Phase III of plasma cloud evolution leads to the conclusion that a dissipative instability involving crossed electric and magnetic fields in the presence of a properly oriented plasma density gradient is the most likely candidate. It is found that the observed tens-of-meters instability wavelengths and tenths-of-seconds growth times are predicted by this mechanism, and curves of these parameters are presented for various altitudes, electrostatic field intensities, and wavelengths. A more sophisticated, two-dimensional, nonlinear instability analysis predicts a cyclic growth-and-decay process for the instability in the lower E layer and is in remarkable agreement with the Phase IV plasma cloud behavior. This circumstance is interpreted as strong evidence that the instability is instrumental in the formation of temperatelatitude nonblanketing sporadic E.

DD FORM 1 NOV 65 1473 (PAGE 1)

S/N 0101-807-6801



Security Classification

Security Classification

| 14. KEY WORDS | LINK A ROLE | LINK A WT | LINK B ROLE | LINK B WT | LINK C ROLE | LINK C WT |
|---|---|---|---|---|---|---|
| Atmospheric physics | | | | | | |
| Ionosphere | | | | | | |
| Sporadic E layer | | | | | | |
| Ionospheric disturbances | | | | | | |
| Plasmas (physics) | | | | | | |
| Plasma dynamics | | | | | | |
| Radar cross section | | | | | | |
| Pulse doppler radar | | | | | | |
| Rocket launchers | | | | | | |
| Gun launchers | | | | | | |

DD FORM 1 NOV 65 1473 (BACK)
(PAGE 2)



Security Classification